UC Berkeley
UC Berkeley Electronic Theses and Dissertations

Title

Spatial and Temporal Dissemination of Listeria monocytogenes Across Multiple Mouse Models

Permalink

https://escholarship.org/uc/item/3nr1s4w7

Author

Chevee, Victoria

Publication Date

2024

Peer reviewed|Thesis/dissertation

eScholarship.org Powered by the California Digital Library
University of California

Spatial and Temporal Dissemination of *Listeria monocytogenes* Across Multiple Mouse Models

By

Victoria Chevée

A dissertation submitted in partial satisfaction of the

requirements for the degree of

Doctor of Philosophy

in

Molecular and Cell Biology

in the

Graduate Division

of the

University of California, Berkeley

Committee in charge:

Professor Daniel A. Portnoy, Chair
Professor Sarah A. Stanley
Professor Russell E. Vance
Professor Diana M. Bautista

Spring 2024

Abstract

Spatial and Temporal Dissemination of *Listeria monocytogenes*
Across Multiple Mouse Models

By

Victoria Chevée

Doctor of Philosophy in Molecular and Cell Biology

University of California, Berkeley

Professor Daniel A. Portnoy, Chair

Listeria monocytogenes (Lm) is a Gram positive, facultative intracellular pathogen that infects its hosts upon ingestion of contaminated foods. Exposure is generally innocuous or followed by mild self-limiting gastroenteritis, but in certain contexts it can lead to more severe outcomes. In immunocompromised individuals, Lm can infect the central nervous system (CNS) and cause permanent brain damage or even be lethal, while infections in pregnant women often lead to high bacteremia in the placenta and loss of the fetus. In addition to being a public health issue, Lm is also a model system used to establish fundamental understandings about microbiology and cell biology, and a tool used to develop cancer-immunotherapies. Dissecting the dynamics of pathogen dissemination in a variety of contexts allows for the identification of bottlenecks and trafficking pathways that could be targeted for therapies and tool development both with Lm and other microbes.

In our study we first assessed the dynamics of Lm colonization and replication within mouse brains using barcoded bacteria. Upon intravenous inoculation, the CNS was seeded from multiple independent invasion events from the blood which led to a polyclonal CNS, yet one clone usually dominated within the brain. Sequential infections and intracranial inoculations established that timing of colonization, rather that entry site or access to a certain niche within the brain, was the main driver of clonal dominance. Since Lm is a food-borne disease, we then designed a new model of oral inoculation-induced cerebral listeriosis using immunocompromised mice fed with a piece of bread soaked in bacteria and pre-treated with streptomycin. In this context, rare colonization events led to a highly infected yet monoclonal CNS. This stringent dissemination bottleneck likely arose from pathogen transit into the blood, rather than directly from the blood to the brain and did not limit bacterial replication within the brain tissue. Collectively, our findings provided an in-depth analysis of the *Lm* population dynamics that lead to cerebral listeriosis and established a framework for studying the bacterial spread with other neuropathogens.

In order to assess the host bottlenecks that affect pathogen dissemination to the brain, we next investigated the role of the innate immune receptor STING in bacterial trafficking. Our goal was to establish whether activation of STING would control bacterial replication and limit spread of Lm to the brain, or if STING activity would instead facilitate bacterial dissemination by recruiting monocytes into circulation and providing Lm with "Trojan horses". Upon oral inoculation, Lm accumulated more efficiently within the CNS of STING-deficient mice (*Goldenticket*, Gt) than wild-type mice, suggesting that STING activity was involved in controlling host-wide infection more than promoting bacterial dissemination. STING-derived Type 1 interferon was not involved in the heightened Gt susceptibility, but signaling via the STING C-terminal tail was involved in STING-depended Lm control. Oral infection of Rag1KO-*Gt* double mutant mice suggested that STING was involved in controlling early stages of infection rather than bacterial accumulation in the brain over time. Finally, we expanded our study to assess bacterial dissemination to the placenta in the context of STING-deficiency. Intravenous infection of pregnant mice led to mild protection of Gt placentas, while oral infection led to increased sensitivity in Gt mice. Collectively, our results provided a new understanding on the limited impact of STING-activity during bacterial dissemination to the brain and established a framework for further analysis of the intriguing role of STING during placenta infections.

We then investigated Lm infection as a beneficial therapy in the context of tumor-bearing mice using barcoded attenuated Lm. Our preliminary work assessed the impact of the route of inoculation on bacterial spread and established that Lm colonized tumors within 4 hours, but only to a limited degree following intravenous (IV) inoculation, then dramatically expended locally with little to no further dissemination between tissues. Intratumorally (IT) inoculated mice experienced Lm spread beyond the tumor quite efficiently, but again Lm migration between tissues was limited by 3 days post injection. Combination therapy with IV vaccination followed by IT challenge one week later, led to Lm spread into systemic tissues from the tumor during the first 4 hours post inoculation, but this was followed by a massive clearance event. In cases where bacteria persisted in the tumor microenvironment, bacterial burden was generally high with a mostly clonal population. This finding suggested that host pressures cleared most of the early colonizing Lm, but a few bacteria were able to evade clearance and persist over time. Overall, our work provided a more granular picture of the landscape of pressures faced by Lm during dissemination in tumor-bearing mice and helped better understand the mechanisms of tumor clearance in IV+IT combination immunotherapy.

DEDICATION

To my family

The one I've always had
The one I became a part of
And the one I hope to build

ACKNOWLEDGEMENTS

I would first like to thank you Dan for your mentorship throughout the last few years. Graduate school has not been easy, but I am overall really happy with my experience in your lab. You and I didn't always agree on what aspects of science are the most interesting, but I am deeply appreciative that you allowed me to pursue my own ideas and introduced me to other amazing people who could help guide me. You are incredibly knowledgeable and could always see the bigger picture; you often nudged me in the right direction, but never forced me to do anything, which is a pretty amazing mentoring quality of yours. You let me engage with other projects too, which was very fun and allowed me to learn lots of different things, including how to let go (see chapter 2). I am grateful that you let me be so independent scientifically and I am very proud of the final project we built together. You also have a great ability to give both negative feedback which pushed me to do better, and positive feedback which gave me confidence and really helped through the hard times; I hope I can do that as efficiently as you for my future mentees. Finally, I really liked that you once said *we should always air on the side of generosity within the scientific community*. I find it to be a very hopeful message for academia and hope to use this as a guiding principle in my career. I am just really proud that I got to train with you, thank you.

Prior to grad school, I'd like to thank the Eleftherianos lab; thank you Ioannis for taking a chance on me in undergrad when I was still just figuring out what I liked about biology. To the Schneider lab; thank you David for taking me into your lab and pairing me up with Avni. I learned so much during that time about how to collaborate, how to be organized (which both came in really handy in grad school), how to handle mice (which became the basis of all my grad school work), and most importantly how to think about health and disease in creative ways. Avni, Nicole, Michelle, and Katie, you were all amazing friends and colleagues. You made me feel welcomed and supported and super ready to take on a PhD!

At Cal I found a home in the Portnoy lab**.** From the early days of BBQing on the Barker lawn with Alex, Sam, Brittney, Eric, Bret, Freddy, Helia, Ying, Raf, John, and Andrea to the new days of cake and tea and cyclebar and running races and tennis with Mariya, Ted, Preethi, and Bere (and John, Andrea, Raf and Ying still). Thank you all for making the lab a place full of fun and joy. So many of you have become very close friends and I can't even imagine what grad school would have been like without you. I am grateful to have shared a chunk of life with you.

Karthik and Katherine, you are the best collaborators I could have ever hoped for. You made STAMP make sense when it was confusing and always were incredibly patient with me. But more than that, I left every single one of our conversations feeling happy. I'm so glad we got to work together for multiple years, you are both incredible investigators but also kind, thoughtful, and fun. Thank you for being an amazing part of my grad school experience. Thank you also Matt, for supporting me through this collaboration and for taking on a really active role when we put the paper together, I'm really happy with what we accomplished.

The Portnoy lab was also a wonderful place to learn how to be a better mentor. Special thanks to Leslie, you were a wonderful mentee, super hard working, excited to learn, and fun to be around. It's been so great getting to watch you grow into an independent investigator and I'm grateful that I was able to be a part of your journey. Thank you also to Talia, you took on the colony management job so gracefully, it's amazing; I have so much confidence in you and your abilities and I'm sure you'll be a great researcher one day.

The MCB community at large has also been a wonderful space to be a part of, both within my cohort and beyond. I've had so much fun playing summer Softball (nod to the most phenomenal co-captain Hannah), watching Follies, and dancing at MCBootie. All of these events made me feel incredibly connected and supported at Cal and made the difficult times that much more bearable. Elizabeth, Lisa, and Kayla, you were all wonderful housemates and going through rotations, awkward week, quals and all the ups and downs of grad school with you made it all less daunting. MCB also gave me the opportunity to improve my public speaking skills with GradSlam and to learn to teach effectively, which I really loved. Thank you, Kathleen Ryan for being an incredible teaching mentor and for inspiring me to be an effective communicator, and to Rita for being a wonderful co-GSI and friend.

To my Immunology and Pathogenesis cohort: Elizabeth, Shaina, Vic, Jesse (who was also an incredible collaborator), Tim, Stephanie, + Kayla, + Rita, +Sebi, +Marcus. You guys were an amazing group of people to go through this with. Having such a wonderful group of friends was really great through the thick of it. Special thanks to Alex, Livia, Eduard, and Katie, you were amazing mentors and taught me how to survive grad school and thrive in the lab. Special thanks also to Laurent, Sarah, Russell, Greg, Ellen, and Filipa for showing me much kindness and support over the years. You have all had incredibly beneficial impacts on my grad school experience and I am grateful to you all.

Finally, thank you to my family for always supporting me through the difficult times, for encouraging me to always reach for the best, and for sharing in the joys with even more *ferveur* than I could myself. Thank you to the Marchandos for taking me in and cheering me on every step of the way. And thank you to you Paul, for dealing with me through this ridiculously difficult time in our lives and for always being patient, kind, but also fun, and adventure seeking.

Thank you all.

TABLE OF CONTENT

CHAPTER 1. INTRODUCTION 1

1.1. Dynamics of infection and bottlenecks 2
1.2. Barcoding, the perfect tool to study bacterial dissemination 2
1.3. Listeriosis, a multifaceted disease and model system 4
1.3.1. Bacterial meningoencephalitis 4
1.3.2. Infection of the placenta 5
1.4. The role of STING in Lm infection *in vivo* 6
1.5. Lm as a tool for cancer immunotherapy 7

CHAPTER 2. TEMPORAL AND SPATIAL DYNAMICS OF LISTERIA MONOCYTOGENES CENTRAL NERVOUS SYSTEM INFECTION IN MICE 9

2.1. Summary of Results 10
2.2. Introduction 10
2.3. Results 12
2.3.1. Intravenous inoculation of Lm leads to multiple waves of CNS invasion 12
2.3.2. Circulating bacteria lead to multiple independent infections of the brain, brain stem and spinal cord 12
2.3.3. One Lm clone is dominant in the brain and highly abundant in the brain stem 15
2.3.4. All regions of the brain are susceptible to infection, but Lm clones display heterogenous patterns of regional segregation 16
2.3.5. Early invading Lm are the main drivers of clonal dominance in the brain 18
2.3.6. Food-borne infection of immunocompromised mice reproducibly leads to cerebral listeriosis. 19
2.3.7. Dynamics of food-borne Lm invasion of the CNS differ from the IV model 21
2.4. Discussion 23
2.5. Material and methods 25
2.6. Supplementary Figures 28
2.7. Unpublished work 33
2.7.1. Controlling for the effect of microbiota during oral infection with littermates 33
2.7.2. Assessing early brain damage with rotarod 34
2.7.3. Clonal dominance in orally infected Rag1KO mouse brain regions 36
2.7.4. Additional material and methods for unpublished work 37

CHAPTER 3. INVESTIGATING THE ROLE OF THE INNATE IMMUNE RECEPTOR STING DURING LM DISSEMINATION TO THE BRAIN AND THE PLACENTA 39

3.1. Summary of Results 40
3.2. Introduction 40
3.3. Results 41
3.3.1. Dynamics of infection across organs in STING deficient mice 41
3.3.2. Assessing which functions of STING are involved in bacterial control 43
3.3.3. Assessing the impact of STING deficiency in our newly developed model of food-borne induced cerebral listeriosis 45
3.3.4. Assessing the role of STING during pregnancy in mice 47
3.4. Discussion 48
3.5. Materials and Methods 50

CHAPTER 4. DYNAMICS OF L. MONOCYTOGENES DISSEMINATION IN TUMOR-BEARING MICE 52

4.1. Summary of results 53
4.2. Introduction 53
4.3. Results 55
4.3.1. Library generation and quality control 55

4.3.2. IV inoculation leads to low colonization of the tumor, high replication within the tumor, and little to no migration from systemic sites into the tumor *56*
4.3.3. IT inoculation leads to efficient migration from the tumor to systemic site, then limited further bacterial exchange between tissues *58*
4.3.4. IV and IT combination therapy led to early Lm spread out of the tumor, then massive clearance events host-wide, but bacteria that persisted in tumors became mostly monoclonal *60*
4.4. Discussion 61
4.5. Material and Methods 63
4.6. Supplementary figures 66
CHAPTER 5. CONCLUDING REMARKS AND FUTURE DIRECTIONS 69
5.1. Conclusions and summary of results 70
5.2. Remaining questions and avenues for future work 71
CHAPTER 6. REFERENCES 74

LIST OF FIGURES

CHAPTER 2

Figure 2.1: Intravenous inoculation of *Lm* leads to multiple waves of CNS invasion……..14
Figure 2.2: One Lm clone is dominant in the brain and highly abundant in the brain stem……16
Figure 2.3: All regions of the brain are susceptible to infection, but *Lm* clones display heterogenous patterns of regional segregation……17
Figure 2.4: Early invading Lm are the main drivers of clonal dominance in the brain……..19
Figure 2.5: Food-borne infection of immunocompromised mice reproducibly leads to cerebral listeriosis...21
Figure 2.6: Dynamics of food-borne Lm invasion of the CNS differ from the IV model……22

Supplementary Figure S2.1: *Intravenous infections of C57BL/6J mice intravenously infected with $1x10^4$ CFU of Lm*……..28
Supplementary Figure S2.2: *Dissection of brain regions 3 days post intravenous infection*……..29
Supplementary Figure S2.3: *Oral infection of mice with $1x10^9$ CFU of Lm*……..31

Figure 2.7: The microbiota does not drive the difference in development of cerebral listeriosis between store bought C57BL6/J mice and Rag1KO mice bred in house……34
Figure 2.8: Rotarod did not allow for identification of early signs of cerebral listeriosis……..36
Figure 2.9: The CNS of orally infected Rag1KO mice at late stages of infection is monoclonal……37

CHAPTER 3

Figure 3.1: Tissue colonization dynamics in Sting-deficient mice……43
Figure 3.2: Assessing which functions of Sting are involved in cerebral infection……45
Figure 3.3: Cerebral infections at later stages of infection. ……46
Figure 3.4: Placentas of Sting deficient mice are not protected from infection……48

CHAPTER 4

Figure 4.1: Quality control of the newly generated barcoded library in ΔactA Lm……56
Figure 4.2: Intravenous inoculation with barcoded ΔactA Lm. ……58
Figure 4.3: Intratumoral inoculation with barcoded ΔactA Lm. ……59
Figure 4.4: Combination therapy with intravenous and intratumoral inoculation of barcoded ΔactA Lm……61

Supplemental Figure S4.1: *Frequency of barcodes in mice from the IV only group*……66
Supplemental Figure S4.2: *Frequency of barcodes in mice from the IT only group*……67
Supplemental Figure S4.3: *Frequency of barcodes in mice from the IV + IT combination therapy group...68*

CHAPTER 1. INTRODUCTION

1.1. Dynamics of infection and bottlenecks

2023 marked the 75th anniversary of the World Health Organization. During this time global advances in vaccine delivery, access to medicine, and both prevention and response to health emergencies have dramatically improved, leading to the elimination of multiple infectious diseases worldwide. Yet, 2023 also saw the resurgence of a record-breaking number of infectious diseases and millions of lives are still lost to pathogens yearly.[1] With the rise of antimicrobial-resistant bacteria world-wide[2], microbiologists are looking for novel therapeutic avenues that move away from targeting specific pathogenic effectors.

One particular area of microbiology thus focuses on understanding the host factors that naturally curb disease progression. Upon inoculation, pathogens will generally disseminate and reach niches within the host that are permissible for replication. The availability of such niches, as well as the pressures from host immune responses, the physiological accessibility to a niche, and a pathogen's internal capacity to survive and replicate all reflect barriers that can affect an infection's success. These barriers are referred to as "bottlenecks"[3,4]. Bottlenecks can be identified by tampering with the ability of a pathogen to surmount the barrier, or with the ability of a host to raise said barrier, and then assessing bacterial burden over time in different tissues. However, these approaches provide limited information regarding bacterial population structure[3].

Here is an example to illustrate this point: if a mouse has high bacterial burden in the intestines immediately following infection with an enteric pathogen, and high bacterial burden is found in the liver 3 days following infection, it is possible that all the bacteria from the inoculum easily crossed the intestinal barrier and disseminated to the liver directly. However it is also possible that bacteria from the inoculum were severely restricted by barriers such as the commensal microbes using up required nutrients, direct antagonism by gut microbes, or immune effectors that responded quickly and limited systemic spread.[5,6] In this context, a few bacteria may still be able to overcome the initial bottlenecks and grow efficiently in the liver, leading to a similar bacterial load, but a very different bacterial population in the liver than in our first scenario. A third option could be that bacteria from the inoculum efficiently passed through the first bottlenecks, but reached the spleen first for example, then stochastically spread to the liver which would lead to yet a different bacterial population structure than in the previous examples. Disentangling the contribution of these different bottlenecks and trafficking pathways can provide a better understanding of the within-host dynamics of infection, as well as identify pathogen exchange between tissues, assess population changes over time and provide new avenues for preventing disease progression.

1.2. Barcoding, a useful tool to study bacterial dissemination

In order to overcome the limitations of strictly assessing bacterial burden, multiple approaches have been developed to track spatiotemporal spread of bacteria *in vivo*. One option is to use an *in vivo* bioluminescence imaging system (IVIS). Here, bacteria are genetically engineered to express the light-producing luciferase enzyme. The generated signals can be

detected through the tissues of anesthetized animals using an ultra-sensitive charge-coupled device camera.[7] Using this system, bacterial spread can be followed non-invasively over time in single animals. This system was successfully used to assess bacterial dissemination to the bone marrow[8], the gall bladder[9], and the placenta[10] among others. Yet, this tool is limited by the relatively high limit of detection (a few thousand colony forming units (CFU)[8]) that is required to generate enough signal. Another option is to perform co-infection of hosts with bacteria tagged with anti-microbial resistance cassettes[11]. By infecting animals with non-clonal bacteria, the bacterial population structure can easily be assessed. This technique was skillfully leveraged to identify trafficking pathways in the context of pregnant mice[12], which will be further discussed in *section 1.3.1*. However, introducing mutations that require the expression of a product to identify bacteria can come at a fitness cost for the pathogen and is limited in the number of usable markers.

Sequence "barcodes" were thus developed to create libraries where markers would come at a low fitness cost to the bacteria and easily be scaled up. Multiple groups have developed such tools where short (20-40bp) DNA signatures would be inserted into a non-coding region of the bacterial chromosome. These barcoded strains have limited to no phenotypical differences in *in vitro* or *in vivo* growth rates and can thus be co-infected into hosts to study the spaciotemporal shifts in bacterial population without risking competition between non-equivalent tagged strains.[13–16] These libraries allowed for a broader understanding of pathogen dynamics but generally required quantification of each barcode by qPCR and thus were still limited to a minimal number of tags.

Since 2015, a barcoding system termed STAMP (Sequence Tag-based Analysis of Microbial Population)[3] was developed to overcome this lack of a systemic approach to assess barcode frequency. STAMP still relies on a small (~20-25bp) DNA tag inserted in a fitness-neutral site in the bacterial chromosome but leverages technological advances in high throughput sequencing to scale the barcoding system to libraries of a few hundred[3,4,17] to tens of thousands[18,19] strains. This approach is continually being further refined with systems such as STAMPR (STAMP in R), which better accounts for uneven expansion of subpopulations[20], and RESTAMP (Rate Estimates by STAMP), which better determines division and death rates[21].

Using these toolkits, allows for the detailed quantification of the forces that shape population changes over time such as the spread of barcodes between tissues and the bottlenecks that limit colonization and replication. A more detailed explanation of the metrics provided by STAMPR can be found in *Chapter 2*. This method has dramatically expanded our understanding of pathogen dynamics in a variety of contexts, such as infections with *Vibrio cholerae* [3], extraintestinal pathogenic *Escherichia coli* [17,22,23], and others [18,21,24–28]. Similarly, the dissemination of the model bacterial pathogen *Listeria monocytogenes* (Lm) has been extensively studied in mice. Indeed, comparative analysis of barcodes recovered from livers, gall bladders, and feces of infected mice revealed that a tight bottleneck limits pathogen dissemination into the gall bladder, but does not prevent bacterial replication within the organ. The gall bladder population is thus dominated by very few barcodes and this same barcode is later reproducibly found to be dominant in the feces, establishing the gall bladder as reservoir

for fecal shedding.[4] Further analysis established that bacterial effectors required for pathogenesis were also required for this bacterial population shift in the fecal pellets.[29] In addition, immune depletion studies showed that immune cells participate in restriction of replication in the liver and spleen, and studies in germ-free mice established that commensal bacterial affect colonization of the spleen but not the liver[4]. Together these analyses provide a more detailed and quantitative understanding of the spatiotemporal spread of Lm *in vivo*.

1.3. Listeriosis, a multifaceted disease and model system

Lm is a Gram-positive bacterial pathogen that can infect most mammals including humans and ruminants, and has long been used as a model organism for understanding host cell biology. Listeriosis causes disease upon ingestion of contaminated foods but is generally confined to a self-limiting gastroenteritis in healthy individuals. However, infection can be severe and lead to miscarriages. In the case of immunocompromised individuals - such as patients undergoing chemotherapy, transplant recipients, and people living with AIDS - as well as infants and the elderly, listeriosis can spread systemically and lead to sepsis and meningoencephalitis. Although this is a rare disease with 0.1-10 cases per million, it has a high mortality rate (20-30%)[30] making it the third most lethal foodborne infection in the U.S.[31]

Lm is also a facultative intracellular pathogen, and can be found both intracellularly and extracellularly within its hosts. Following invasion of a cell, Lm uses the virulence factor LLO, a pore-forming hemolysin, to escape the restricting vacuole and reach the cytosol. Then, it uses the virulence factor ActA to subvert host actin polymerization machinery and propel itself through the cytoplasm and into neighboring cells.[32] Lm is a highly genetically tractable bacterium, which was successfully leveraged to uncover mechanisms of cellular function. Indeed, studying the ability of ActA to polymerize actin 'comet' tails via existing host systems enabled the discovery of the molecular mechanism behind Arp2/3-dependant actin assembly.[33] As a pathogen that can teach us about host and other bacterial pathogens, as well as a multifaceted medical challenge, Lm is a perfect model organism.

1.3.1. Bacterial meningoencephalitis

Neuroinfectious diseases are devastating illnesses which require urgent medical attention and can lead to severe long-term complication or be fatal. They can be caused by a plethora of microbial agents such as bacteria, viruses, fungi, and parasites, but bacterial infections are particularly dangerous with 1:6 cases ending in fatality.[34] Infections can affect variable neural cell types causing broad cerebral damage and dysfunction of neural networks.[35]

Neural pathogens can use a variety of mechanisms to infect the central nervous system (CNS). First, several bacteria gain access to the blood and/or cerebral spinal fluid (CSF) then adhere to the endothelium of micro-blood vessels in the brain via interactions between bacterial effectors and host proteins. Overactive host inflammatory responses and in some cases virulence factors can also lead to disruption of the blood-brain-barrier (BBB) and promote the invasion of the CNS.[35] Second, phagocytes which contribute to pathogen clearance may be

co-opted to promote access to the brain parenchyma. Internalized microbes use these migratory immune cells as "Trojan horses" and take advantage of their ability to circulate through the host vasculature and cross the BBB to invade the CNS.[35] Third, pathogens can invade peripheral neurons and traffic directly to the CNS by spreading from neuron-to-neuron. RNA and DNA viruses are particularly adept at using this final method and get delivered directly into the brain parenchyma.[35]

With regards to cerebral listeriosis, there is evidence that supports Lm using all three of these mechanisms of dissemination. Indeed Lm had been found to infect inflammatory monocytes (CCR2+, Ly6C hi) and use the "Trojan horse" mechanism to reach the BBB.[36–38] It was even suggested that Lm can modulate infected monocytes' expression of cell surface proteins to limit CD8+ T cell-mediated killing of their migratory host.[39] Other studies have suggested that Lm can use intraneural trafficking to migrate directly from peripheral organs to the CNS within and along axons of peripheral nervous system. In support of this hypothesis, there is *in vitro* evidence that Lm can spread both between rat spinal cells[40] and along axons of fetal bovine brain cells[41], and *in vivo* evidence that snout infections can lead to brain invasion via the cranial-facial nerve in neonate mice.[42] In addition extracellular Lm can use the cell surface virulence factor InlF to bind the intermediate filament protein vimentin found on cell surfaces to promote its internalization at the BBB. Of note, the mechanisms of Lm spread to the CNS were studied using a wide variety of routes of infection. The relevance of each mechanism seems to be heightened depending on the route of infection, highlighting the importance of using experimental routes of infection that closely mimic natural exposure to Lm.

Even though our understanding of the mechanisms that enable bacterial dissemination to the brain have been extensively studied, our understanding of the relative contribution of these mechanisms and the dynamics of bacterial population changes following infection are not well understood and are discussed in depth in *chapter 2*.

1.3.2. Infection of the placenta

Contrary to cerebral listeriosis, which is a rare occurrence that mostly only affects immunocompromised individuals, Lm infections are 10-20 times more likely to happen in pregnant than in non-pregnant people.[43,44] Infections during pregnancy are severe and can cause miscarriage, stillbirth, preterm birth, or congenital neonatal infections. Many systemic infections can lead to fetal loss and most pathogens that can survive within host cells have the potential to infect the placenta and fetus from the blood.[45] One particularity of Lm infection compared to other systemic infections, is that mothers tend to show few symptoms of disease, which delays treatment and increases the risk of adverse effects.[46] During pregnancy, a state of immune tolerance is established to protect the fetus from the maternal immune system reaction to non-self. The placenta sits at the interface between the mother and fetus and both provides for (exchange of nutrients and waste) and protects (barrier function) the developing fetus.[46] Of note, placental structure is highly variable between organisms[47] so it is important to remember that findings are dependent on the model system used and the route of infection chosen.

Two main routes of infection have been proposed for Lm infection. The first, is direct invasion from the extracellular space (blood) and requires interaction of virulence factors and cell surface receptors. The second is by intracellular cell-to-cell spread following invasion at a distal site.[47] In both cases 3 sets of Lm virulence factors are involved. Internalins (InlA, InlB, InlP), which promote invasion into cells, have been shown to participate in placenta infections both *in vitro*[48,49] and *in vivo*[50] although results are variable depending on the model of infection. The pore forming toxin LLO, which is required for Lm to escape the vacuole and reach the cytosol upon internalization, and ActA, which is required for actin-based motility and cell-to-cell spread, have also been shown to participate in *in vivo* infections.[51,52] Interestingly, invasion of the placenta and fetus is not required to cause fetal injury. Studies have found that Lm infection can lead to "sterile fetal wastage" due to infection-induced inflammation.[53]

Indeed, fetal tolerance is maintained during pregnancy by multiple immune mechanisms and Lm infection can disrupt this immunological balance. During pregnancy homeostasis, ~70% of immune cells are Natural Killer cells (NK), while macrophages make up ~20% and T cells ~10-20%.[54,55] In particular, anti-inflammatory maternal regulatory T cells (Tregs) are critical for maintaining fetal tolerance.[53,56] Upon Lm infection, innate and adaptive immune responses are induced, overriding the maternal Treg suppressive state and leading to recruitment of inflammatory neutrophils, macrophages, and eventually CD8+ T cells.[47,57] In addition to direct damage by Lm to the placenta and the fetus, this increase in inflammation is thought to participate in harming the fetus and leading to Lm-induced miscarriages.[47]

Of note, the dissemination patterns of Lm during infection of a pregnant host have been assessed and further support infection of the mother as a driver for fetal loss. Indeed, using two strains of tagged Lm, Bakardjiev et al. showed that Lm first infects the mother and only rarely/inefficiently infects the placenta. As infection progresses Lm replicates in the placenta and traffics back to the maternal organs, then back again to the placenta, establishing the placenta as a reservoir for continuous infection of maternal organs.[12] This example further establishes tagging of bacteria as a complementary method to thoroughly understand the dynamics of infection in various models.

1.4. The role of STING in Lm infection *in vivo*

As mentioned in the previous sections, the immune response to Lm has been extensively studied over the past few decades[58,59]. Here, we focus on the role of the innate immune receptor STING (stimulator of interferon genes) and its role during infection.

Following cellular invasion and escape from the vacuole into the cytosol, the Lm-secreted secondary messenger cyclic-di-AMP is recognized by the cytosolic sensor STING[60]. STING is known to mediate a multitude of pathways including type 1 IFN production, NF-kB activation, STAT-6 dependent chemokine secretion, and autophagy. Secreted chemokines and cytokines attract and activate monocytes (CCR2+ Ly6Chi) and neutrophils at the infection focus. Although these cells can be co-opted for pathogen dissemination as described above (section

1.3.1), the primary role of these early cellular moderators is to contain the infection until the adaptive immune system (particularly CD8 T cells) can completely clear Lm within about one week after initial exposure. [58]

Although STING is activated during early stages of Lm infection, STING-deficient mice are not more sensitive to intravenous Lm infection than wild-type (WT) mice, suggesting that STING is minimally involved in the systemic response to listeriosis[60]. However, STING-deficient mice are more susceptible than WT mice to oral infection and this response is not dependent on Type 1 IFN response[61], which is one of the major outputs of STING activation. In addition, orally infected STING-deficient mice exhibit a reduced influx of inflammatory monocytes to the gastro-intestinal tract, suggesting that STING responses may play a major role specifically at the intestinal barrier.

This is of particular importance because the human STING gene (TMEM173) is polymorphic and a portion of the population carries an allele that makes STING defective in response to cyclic-di-nucleotides[62]. This was linked to possible predisposition to diseases, but the role of STING in bacterial dissemination to the brain and the placenta remains poorly understood.

1.5. Lm as a tool for cancer immunotherapy

Bacterial pathogens are generally considered detrimental to human health, but they can be manipulated and delivered in creative ways that turn them into vectors for therapies. In particular, benefits of conventional treatments in cancer research, such as surgery, radiotherapy, and chemotherapy are sometimes outweighed by their severe off-target effects, which highlights a need for novel therapies.[63] With the discovery that solid tumors may naturally harbor a microbiome[64–66], a body of research on bacteria-based cancer immunotherapies that would naturally home to the tumor microenvironment[67–69] has been growing in recent years.

Lm is one such pathogen that has been extensively studies for its potential as an efficient vector for immunotherapy. Multiple clinical trials have been undertaken with antigen-expressing Lm strains, but results have been mixed leading to a stalling in Lm-based anti-cancer research[70–73]. Recently Garcia-Castillo et al.[74] instead harnessed the ability of Lm to induce potent innate and adaptive immune responses to reactivate anti-tumor immune activity in an antigen-independent manner. They found that vaccination of tumor-bearing mice with intravenously (IV) inoculated Lm, followed by challenge with intratumoral (IT) inoculation of Lm promoted efficient tumor control in mice. This result was dependent on CD8 T cell-mediated killing of Lm-harboring immune cells, rather than direct killing of tumor cells. This discovery suggested that the presence of Lm in specific cell types in tumors, and their removal, could lead to a reversal of the immunosuppressive state in the tumor microenvironment (TME) and promote tumor clearance. This however was specific to combination IV/IT therapy and was not recapitulated upon IV only or IT only inoculations, even though all conditions led to some degree of bacterial persistence within the tumor.

Investigating the dissemination routes of Lm, the context for Lm persistence, and the bottlenecks faced by Lm within tumor-bearing hosts could provide a better understanding og the impact of Lm in the TME and its ability to promote efficient tumor clearance.

CHAPTER 2. TEMPORAL AND SPATIAL DYNAMICS OF LISTERIA MONOCYTOGENES CENTRAL NERVOUS SYSTEM INFECTION IN MICE

Sections of this chapter are published in:

Chevée V, Hullahalli K, Dailey KG, Güereca L, Zhang C, Waldor MK, Portnoy DA. Temporal and spatial dynamics of *Listeria monocytogenes* central nervous system infection in mice. Proc Natl Acad Sci U S A. 2024 Apr 23;121(17):e2320311121.

2.1. Summary of Results

Listeria monocytogenes is a bacterial pathogen that can cause life-threatening central nervous system (CNS) infections. While mechanisms by which *L. monocytogenes* and other pathogens traffic to the brain have been studied, a quantitative understanding of the underlying dynamics of colonization and replication within the brain is still lacking. In this study, we used barcoded *L. monocytogenes* to quantify the bottlenecks and dissemination patterns that lead to cerebral infection. Following intravenous inoculation, multiple independent invasion events seeded all parts of the CNS from the blood, however, only one clone usually became dominant in the brain. Sequential intravenous inoculations and intracranial inoculations suggested that clones that had a temporal advantage (i.e. seeded the CNS first), rather than a spatial advantage (i.e. invaded a particular brain region), were the main drivers of clonal dominance. In a new foodborne model of cerebral infection with immunocompromised mice, rare invasion events instead led to a highly infected yet monoclonal CNS. This restrictive bottleneck likely arose from pathogen transit into the blood, rather than directly from the blood to the brain. Collectively, our findings provide a detailed quantitative understanding of the *L. monocytogenes* population dynamics that lead to CNS infection and a framework for studying the dynamics of other cerebral infections.

Significance statement

Listeria monocytogenes is one of many pathogens that cause cerebral infections, mainly in immunocompromised individuals. In this study, we used a library of *L. monocytogenes* bacteria each labeled with a unique chromosomally encoded barcode to quantify bacterial dissemination and host bottlenecks during cerebral infection. Following intravenous inoculation, multiple clones sequentially invaded the central nervous system, but the first 1-3 clones that gained access to the brain became dominant. In contrast, after oral infection of immunocompromised mice, a single clone led to an overwhelming cerebral infection and profound neurological symptoms. Collectively these data provide a highly detailed map of pathogen dynamics in multiple models of cerebral listeriosis and a valuable framework to study other infections of the central nervous system.

2.2. Introduction

Central nervous system (CNS) infections are often fatal or leave affected individuals with severe and permanent brain damage. Many microorganisms can cause CNS infections and employ a variety of mechanisms to infect the CNS. For example, the protozoan intracellular pathogen *Toxoplasma gondii* infects leukocytes that deliver the pathogen to the brain. Many viruses, including Herpes Simplex Virus-1, West Nile virus, and Rabies virus migrate within axons of the peripheral nervous system and traffic directly into the CNS. In contrast, some bacteria such as *Streptococcus pneumoniae* transcytose across the blood-brain barrier (BBB) [35]. Despite understanding the routes by which certain pathogens enter the CNS, a quantitative understanding of the host bottlenecks and the patterns of pathogen colonization and replication that result in CNS infection is generally lacking.

Listeria monocytogenes (Lm) is a Gram-positive, facultative intracellular pathogen that can infect most mammals, including humans and ruminants. Upon ingestion of contaminated food, particularly by immunocompromised, infant, or elderly individuals, Lm can lead to sepsis and meningoencephalitis[75]. Although Listeriosis is a rare disease, it has a high mortality rate (20-30%)[31] and is reported as the third most lethal foodborne infection in the U.S. [30].

In the host, Lm can invade non-phagocytic cells or be phagocytosed, avoid autophagy, enter the cytosol, and spread from cell-to-cell using actin-based mobility [32]. These abilities are all critical for the three mechanisms of cerebral infection that have been proposed: Lm can infect inflammatory monocytes (Ly6C^{hi}, CCR2^{pos}) in the bone marrow and hijack these migratory immune cells to traverse the blood-brain barrier (BBB) and invade the CNS ("Trojan horse" hypothesis) [36–39]. Extracellular Lm can also directly invade endothelial cells at the BBB[76], and Lm can infect peripheral neurons and traffic along/within nerves to reach the CNS [40–42,77–79]. Regardless of the precise route(s) of entry however, a quantitative understanding of how individual Lm cells replicate and disseminate across the host during CNS infection is lacking.

Questions regarding the population dynamics of Lm within the host are challenging to answer when assessing bacterial burden alone. For example: Do only a few bacteria replicate in the brain following a rare invasion event and expand to fill the niche? Is the CNS broadly and consistently permissive to infection? Are clones from the CNS found in other tissues? Are there one or more tissues that act as reservoirs for CNS invasion? Addressing these questions will inform our understanding of pathogenesis beyond the characterization of specific virulence factors by providing a quantitative understanding of infection bottlenecks and patterns of pathogen replication and dissemination. Dissecting these underlying dynamics can provide new insights into factors that promote host susceptibility and suggest new avenues for therapies.

Barcoded pathogens can be used to decipher these dynamics of infection. Barcodes are unique short nucleotide sequences that generally do not impact fitness and are incorporated into the same neutral chromosomal site within each bacterium. Following deep sequencing of the barcode locus, computational methods can be used to quantify the infection bottlenecks by assessing the number of bacteria from the inoculum that give rise to the population in a tissue, known as the founding population (FP, also referred to as Ns) [19,80,81]. In addition, comparison of barcode frequencies between organs further quantifies patterns of dissemination. Barcoded pathogens have been used to shed light on our understanding of the infection dynamics of diverse pathogens, including *Vibrio cholerae* within the gut [3], intra-organ dissemination of extraintestinal pathogenic *Escherichia coli* [17], *Toxoplasma gondii* cerebral infections [82], and others [18,21,24–28]. Tagged- Lm have also been used to understand the dynamics of vertical transmission between mother and fetus [12] and to elucidate bacterial trafficking circuits outside of the CNS after oral infection [4,29,83].

Here, we quantify the dynamics of Lm cerebral infection using a library of bacteria with ~200 barcodes and the STAMPR analytic toolset [20]. Intravenous inoculations in mice with barcoded Lm revealed that the CNS is invaded in multiple, independent waves of infection from the blood over time. Within the brain, there was marked dominance of only 1-3 Lm clones.

Clonal dominance can be explained by timing of CNS colonization, where early arrivers become most prominent, rather than by colonization of a particularly permissive region of the brain. These dynamics were recapitulated in a new model of CNS infection using foodborne Lm in streptomycin-treated immunocompromised mice. Here, bacterial replication was again substantial in the brain, although foodborne infection yielded tighter bottlenecks in all organs, and the CNS was consistently monoclonal. Collectively, our findings provide a new understanding of the within-host pathogen dynamics that lead to cerebral listeriosis and a framework to study other CNS infections.

2.3. Results

2.3.1. Intravenous inoculation of Lm leads to multiple waves of CNS invasion

Intravenous (IV) infections are routinely used to study murine listeriosis. In this context of early high-level bacteremia, we monitored changes in bacterial burden and barcode frequency over 3 days post infection (DPI). Mice were infected IV with a relatively low yet lethal dose (10^4 CFU)[84] of a barcoded Lm library [4] and organs were harvested 1, 2, and 3 DPI. At 1 DPI, the Lm burden was already at ~10^6 CFU in the spleen and close to ~10^4 in the bone marrow, whereas the blood usually had titers that were several logs lower (~10^1), and the CNS rarely harbored any detectable Lm. The Lm burden increased by 100-10,000-fold in all organs over time (Fig. 1A) and the increased burden in the CNS was most prominent in the brain (Fig. S1A). The elevation in CNS bacterial burden over time could either be attributed to repeated influx of bacteria from other tissues within the host, or to a few bacteria that passed through a tight bottleneck and replicated within the CNS [3]. These two possibilities are distinguishable by assessing the abundances of different barcodes; if additional bacteria (with new barcodes) invaded the brain, FP values would increase over time. In contrast, if the increase in CFU was due to the replication of the original invading bacteria, the number of barcodes represented in the sample would remain the same and FP would be constant. We observed an increase in FP over time (Ns, Fig. 1B) indicating that during the first 3 days of infection multiple Lm clones invaded the CNS and suggesting that Lm migration into the CNS, in addition to *in situ* CNS Lm replication, may account for the increased pathogen burden in the CNS.

2.3.2. Circulating bacteria lead to multiple independent infections of the brain, brain stem and spinal cord

Comparisons of barcode distributions between tissues can provide insight into routes of pathogen dissemination. The genetic distance (GD) broadly assesses the similarity between two samples: a high GD (~0.8) indicates that two samples have dissimilar populations, while a low GD indicates they have similar populations. GD is calculated based on the similarity in abundances of barcodes between two samples. However, it is possible for pairs of samples with very different barcode distributions to have the same GD value: two similar samples that have low GD can either share many of their barcodes (Fig. 1Cw) or share few highly abundant barcodes (Fig. 1Cx). Likewise, two samples can have a high GD even if they share many barcodes, if there is also a marked expansion of a few barcodes in only one sample (Fig. 1Cy).

To assist in distinguishing between these possible scenarios, the STAMPR toolset also includes an additional metric known as RD ("resilient" genetic distance) that provides insight into the contribution of dominant clones to genetic similarity [20]. Quantifying the fraction of barcodes that are shared between two samples is achieved by log-normalizing the number of barcodes in each sample (FRD, "fractional" RD). For example, a high $FRD_{[A-B]}$ value indicates that the shared barcodes between sample A and sample B represent a large fraction of the total barcodes in sample B, and a low FRD_{B-A} indicates that these same shared barcodes represent only a small fraction of the barcodes in sample A (Fig. 1Cz). Of note, FRD is unaffected by the abundance of Lm bacteria with each barcode and is based solely on the number of barcodes shared [20].

We used GD and FRD to assess how Lm traffics into and within the CNS. The Lm clones in the brain were dissimilar to all other organs (high GD) at 3 DPI with the exception of the brain stem, where we observed moderate similarity (Fig. 1D). Correspondingly, FRD was moderate to low between the brain and brain stem/spinal cord (Fig. 1E), indicating that these CNS regions share relatively few of their barcodes with the brain. To examine whether these samples share very few barcodes simply due to poor colonization, we plotted FRD values as a function of CFU. We observed that tissues that share very few barcodes with the brain (low FRD) have a wide range of bacterial burden (Fig. S1B), confirming that the brain and brain stem/spinal have distinct bacterial populations and suggesting that they are infected independently. Despite the minimal overall genetic similarity between the brain and systemic sites (blood, bone marrow, spleen, and liver, Fig. 1D), the FRD[systemic organ-brain] was generally high

(Fig. 1E) regardless of CFU (Fig. S1C), indicating that a large fraction of the barcodes in the brain were shared with systemic sites. The discrepancy highlighted by GD and FRD in these samples is likely due to the uneven expansion of individual clones, leading to overall dissimilar populations with underlying populations of shared barcodes (similar to Fig. 1Cy). Notably, the fraction of barcodes shared with the blood was very high for all organs (Fig. 1F). Taken together, the observations of shared barcodes in the brain and blood (Fig. 1E and 1F) and an increase in diversity in the brain over time (Fig. 1B) strongly suggest that the CNS sustains multiple waves of infection over time from Lm circulating in the blood.

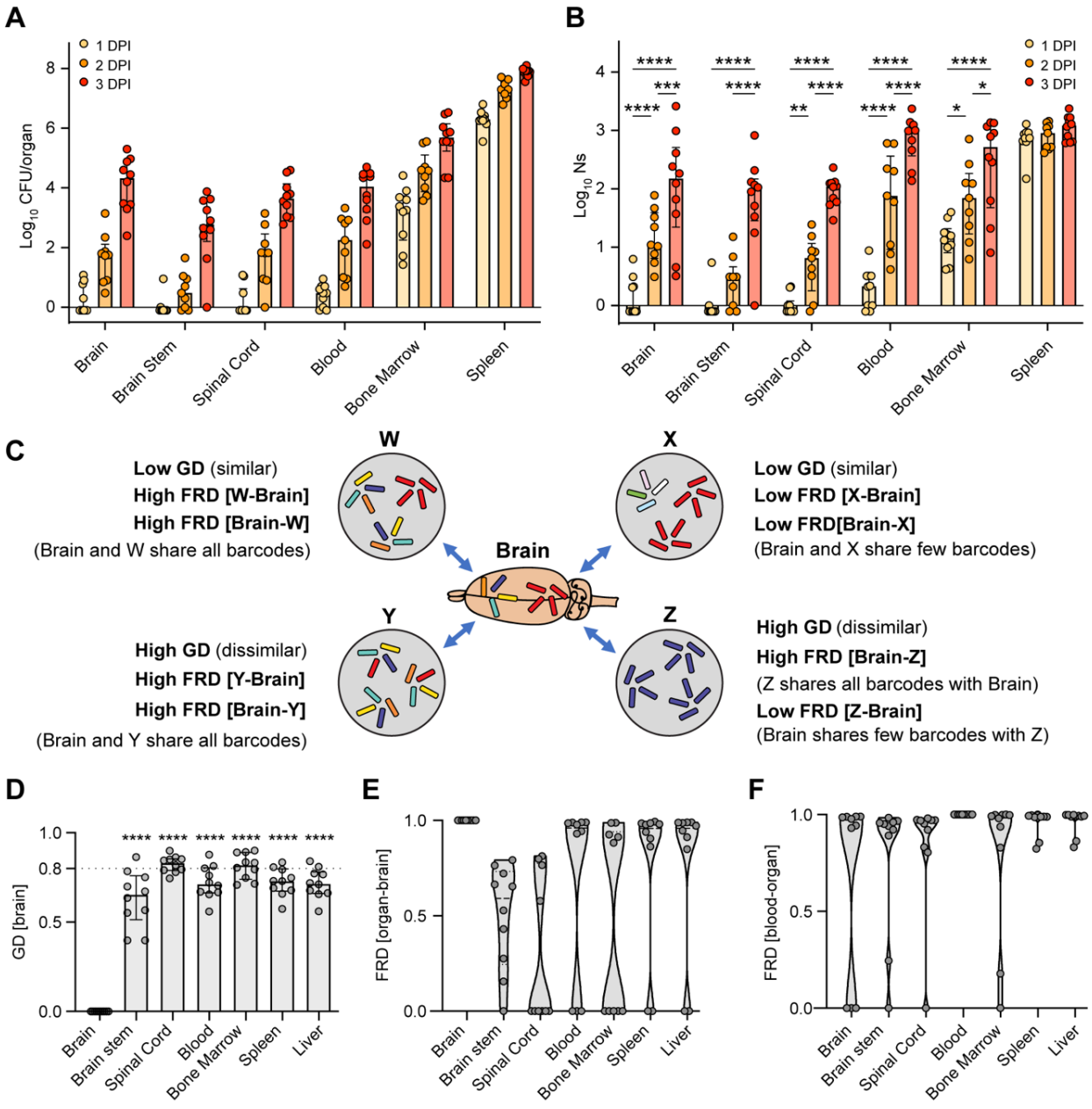


Figure 2.1: Intravenous inoculation of *L. monocytogenes* leads to multiple waves of CNS invasion. *(A-B)* Intravenous infection of C57BL/6J mice with 1x10^4 CFU and collection of organs at 1, 2, and, 3 days post infection (DPI). Bacterial burden (CFU, *A)* and founding population (Ns, *B*) per organ. Data are individual samples expressed as log-transformed values with median and interquartile range. Organs with no CFU are represented as -0.1CFU or Ns. *(C)* Graphical depiction of the genetic distance (GD) and the fraction of clones shared (FRD) between the bacterial populations of hypothetical organs (grey circles) and the brain. Each unique barcode is represented by a color. *(D)* GD between all organs and the brain at 3DPI. Data are individual samples with mean and SEM. The dotted line at 0.8 marks a "high" GD i.e. samples that are dissimilar. *(E)* Prevalence of barcodes from the brain in other organs (FRD[organ-brain]) and *(F)* prevalence of barcodes from various organs in the blood (FRD[blood-organ]) at 3DPI. Data are individual samples with violin plots and median. For all panels, data are combined from at least two independent experiments and 1 DPI N=10, 2 DPI N=9, 3 DPI N=10. Statistical significance was calculated using two-way ANOVA for *B,* and one-way ANOVA against the brain for *D*: ****p<0.0001; ***, p<0.001; **, p<0.01; *, p<0.1.

2.3.3. One Lm clone is dominant in the brain and highly abundant in the brain stem

The observed relatively high GD (dissimilar samples) and high FRD (many clones shared) between the brain and systemic sites (Fig. 1D and 1E) suggested that uneven clonal expansion may occur in the brain *in situ*. The presence of highly abundant barcodes can be analytically supported by comparing different metrics for estimating FP: Ns and Nb. Ns is the primary metric used to estimate FP in this work and is relatively resistant to uneven expansion of barcodes, relying instead only on their presence or absence. In contrast, Nb, another metric provided in the STAMPR toolset, determines FP by assessing differences in the frequencies of barcodes in a sample relative to the reference (which contains all ~200 barcodes). Nb is highly sensitive to uneven barcode abundances and decreases in the presence of disproportionally abundant barcodes (Fig. 2A). The ratio of Nb to Ns is therefore a useful metric to quantify uneven barcode distributions (Nb) relative to the overall diversity of the sample (Ns). At 1-2 DPI, Ns and Nb values were similar across the CNS, indicating that all bacterial clones had evenly expanded. In contrast, Ns was 50 times greater than Nb by 3 DPI, confirming the presence of disproportionately abundant clones in all parts of the CNS (Fig. 2B and S1D).

To corroborate our findings, we assessed the frequency of individual barcodes per organ in single mice. These analyses confirmed that the blood and spleen contained diverse clones starting at 1 DPI, while diversity increased in the CNS over time. However, after 1 DPI, one clone was predominant in the brain and particularly abundant in the brain stem of most mice (Fig. 2C and S1D). Notably, in the mice depicted in Fig. 2B at 2 and 3 DPI, a few clones also expanded in the spinal cord and the bone marrow but were distinct from the expanded clones in the brain and brain stem (Fig. 2C and S1D). Together, these observations support our previous assessment that multiple seeding events account for independent infection of the brain, brain stem, and spinal cord, and additionally indicate that the bone marrow is not a continuous reservoir for Lm clones that invade the CNS as the bacterial populations do not converge overtime.

Furthermore, the brain and brain stem often shared an abundant barcode suggesting that this clone had either a temporal or spatial advantage to establish a proliferative niche.

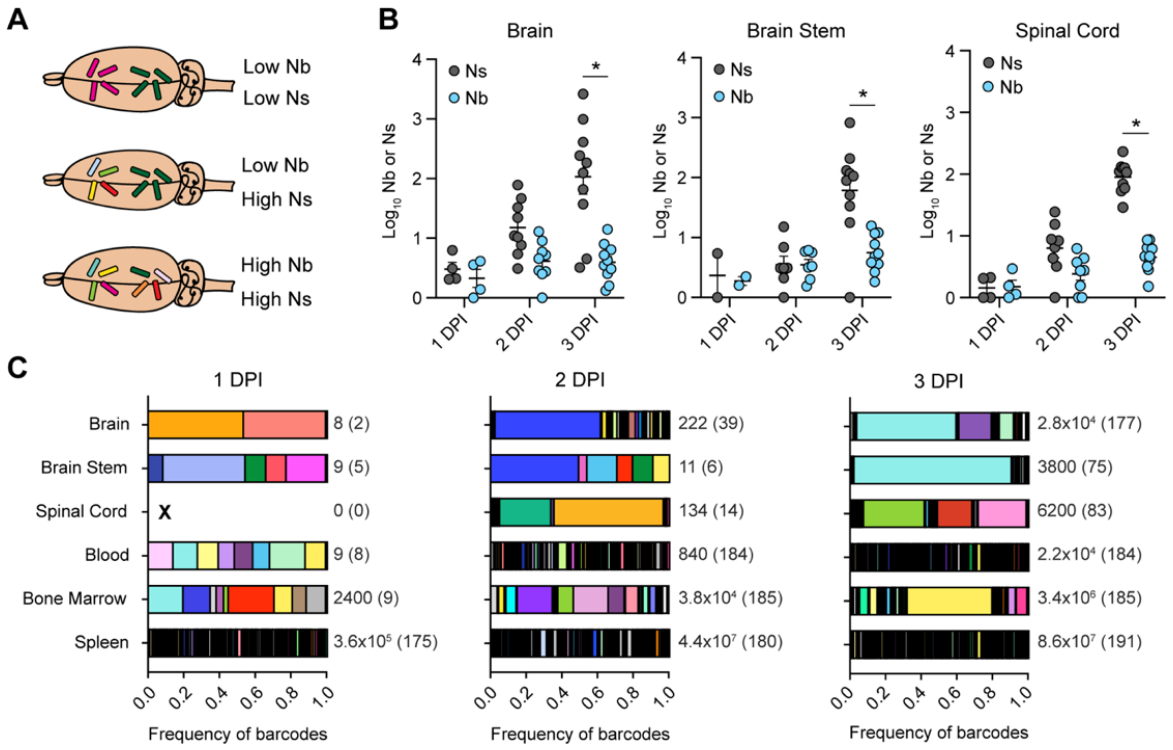


Figure 2.2: One Lm clone is dominant in the brain and highly abundant in the brain stem. (*A)* Graphical depiction of the two founding population (FP) metrics: Nb and Ns, in three hypothetical brain samples. Each unique barcode is represented by a color. *(B)* Bacterial FP of brain, brain stem, and spinal cord from the intravenously infected mice in Figure 1. Data are log-transformed values of Nb and Ns, with mean and SEM for each group. Only samples with CFU>0 were used: 1 DPI N=4, 2 DPI N=9, 3 DPI N=10. Results are from a minimum of two independent experiments. Statistical significance was calculated using multiple Mann-Whitney tests. *, p<0.01. *(C)* Frequency of barcodes per organ for mice in Fig. 1, where each graph is one mouse representative of its group (1 DPI, 2 DPI, 3 DPI). Each color represents one barcode and the same color scheme is applied to all graphs. "X" identifies a sample with no CFU, the number besides each sample is the bacterial load (CFU), and the number in parenthesis is the number of barcodes per sample.

2.3.4. All regions of the brain are susceptible to infection, but Lm clones display heterogenous patterns of regional segregation

We hypothesized that clonal dominance in the brain was spatially driven, where a permissive niche would enable a small number of clones to expand dramatically in one location in the brain. To evaluate this hypothesis, we assessed whether bacteria were concentrated in or limited to certain regions of the brain. Mice were infected IV with the barcoded Lm library, and at 3 DPI the brain and brain stem were collected, separated across the sagittal plane (left-right), and further dissected into a total of 14 compartments (Fig. S2A).

The total bacterial burden and founding populations were similar across all region (Fig. 3A). Thus, Lm infection was not restricted to a particular niche and all regions were capable of supporting Lm replication. Almost all compartments sampled also contained clones that were unique to that region (Fig. S2B), suggesting that all regions of the brain are susceptible to invasion. GD values were intermediate (Fig. 3C and S2C), and FRD values were consistently low (Fig. 3D and S2D) indicating that there was modest sharing of clones between compartments.

Of note, dissemination of clones between regions of the brain (moderate GD/low FRD, Fig. 3C and D) differed from the dissemination patterns between systemic organs and the brain (high GD/high FRD, Fig. 1D and 1E), suggesting that the processes that drive invasion of the brain are distinct from those that drive dissemination within the brain.

To obtain a deeper understanding of the distribution of Lm clones within the brain, we also quantified the number of regions in which each individual barcode was located. In every mouse, most barcodes were found in 1-7 of the 14 regions sampled, while a very small subset of clones were found throughout the entirety of the brain and brain stem (>10/14 regions, Fig. 3E). The spreading of dominant clones is especially apparent when examining individual mice, where 1-3 clones can be observed through all brain regions in each mouse (Fig. S2E). Computationally combining the barcode frequencies for all the brain regions into individual "whole brain" samples while taking into account the bacterial burden of each section further confirmed that the barcodes present in most brain subsections were indeed the most abundant ones overall (Fig. 3F). These analyses established that clones display heterogenous regional segregation at 3 DPI; some clones disseminated, while others were locally confined. The dominance of one clone in the brain observed in Fig. 2 is thus explained by a few Lm clones efficiently spreading throughout the brain, rather than by clones accessing a specific region of the tissue that would be more permissive to invasion or expansion.

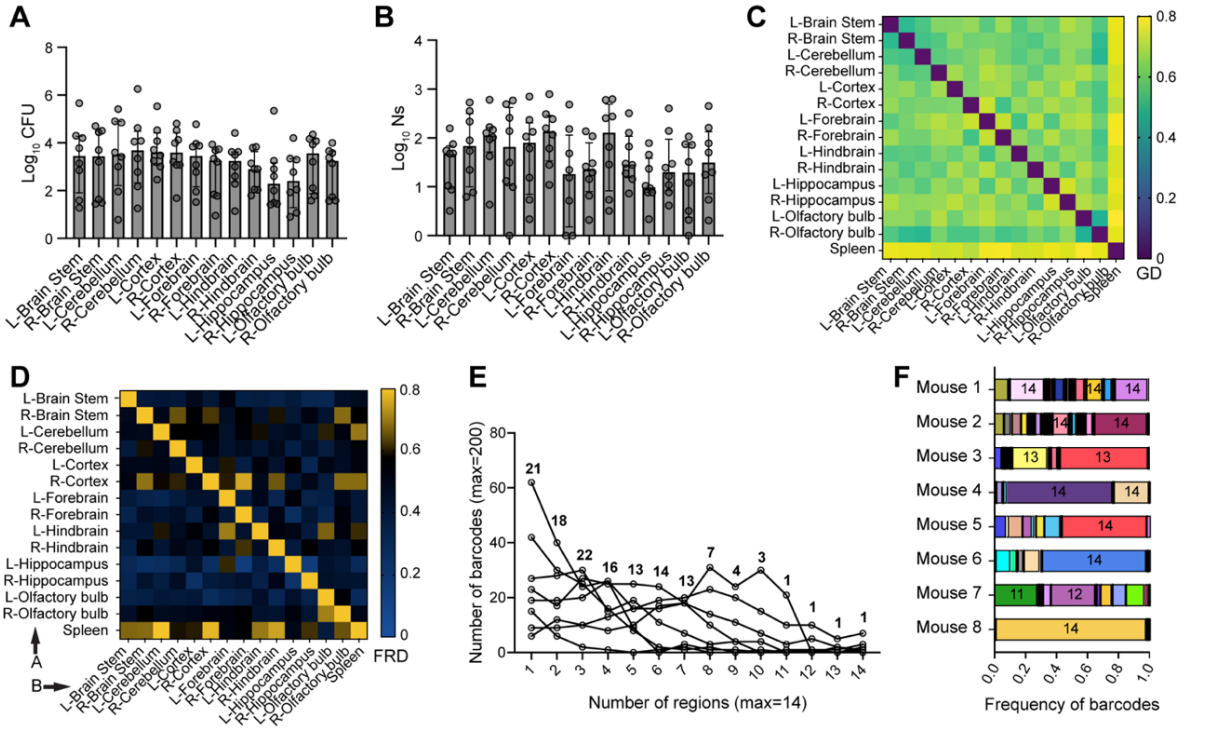


Figure 2.3: All regions of the brain are susceptible to infection, but *L. monocytogenes* clones display heterogenous patterns of regional segregation. *(A-F)* Intravenous infection of C57BL/6J mice with 1x10^4 CFU and collection of brain regions at 3DPI. *(A)* Bacterial burden (CFU) and *(B)* founding population (Ns) per sample. Data are expressed as log-transformed values with median and interquartile range. *(C)* Similarity between each sample as assessed by genetic distance (GD). Data are the average value of the pairwise comparison for all mice. *(D)* Prevalence of shared barcodes (FRD) between each sample. The letters "A" and "B" identify the directionality of the measure. Data are the average value of the pairwise comparison for all mice. *(E)* Distribution of barcodes throughout the brain, as measured by the number of barcodes that are present in each fraction of brain regions, i.e.

1/14= number of barcodes that are in only one region, 14/14= number of barcodes that are in every region for each mouse. The line connects the data for each mouse and the numbers indicate the median number of barcodes for each region. *(F)* Frequency of barcodes within the "whole brain" of each mouse, where each row represents one mouse. Data in each row represent the combined frequency of all 14 brain regions for one mouse, normalized by the bacterial burden of each brain region in that mouse. Each color represents one barcode, and the numbers represent the number of regions this barcode was identified in (out of 14 regions). For all panels N=8, and results are from two independent experiments.

2.3.5. Early invading Lm are the main drivers of clonal dominance in the brain

Since no region in the brain appeared to account for the dominance of Lm clones in the CNS, we hypothesized that clonality may be established by the timing of CNS invasion. In this model, the first clones that infect the brain would establish a niche, replicate, and spread within the tissue, while clones that invade subsequently would have a delay in colonization and thus seem more locally confined.

To assess whether the timing of CNS invasion is the main driver of clonal dominance in the brain, we experimentally imposed an order of invasion using a simplified system of tagged Lm. Mice were infected IV with 10^4 CFU of either wild-type (WT) or erythromycin-resistant (ErmR) bacteria. At 2 DPI, the animals were given a second IV dose with 10^6 CFU of the other Lm strain. A control group received a 1:1 dose of each strain in both infection rounds. The 10^6 CFU second dose corresponds to the bacterial burden in the liver at 2 DPI (Fig. S1E) which is where 90% of the inoculum is found 30 min post IV infection [84]. This dose was chosen to ensure it would neither be so low as to be immediately cleared by the already activated immune system, nor so high to cause the mice to immediately succumb to the infection. At 3 DPI the organs were collected, and the proportion of each strain was assessed per sample (Fig. 4A).

In the brain and brain stem, we observed a significant bias towards greater abundance of bacteria from the first inoculum. In the control group, where both strains were inoculated together, no bias was observed, confirming that the strains have equivalent fitness. In agreement with the barcoded Lm analyses, which revealed that the spinal cord populations were distinct from those of the brain and brain stem, the spinal cord samples were highly variable and less impacted by the timing of inoculation, suggesting that independent factors affect spinal cord and brain/brain stem population shifts. Similarly, neither strain was more abundant in the liver, blood, or spleen when compared to the control group, suggesting that infection of these organs is mostly unaffected by the timing of invasion. Notably, the bacterial population in the brain and brain stem samples were not entirely from the initial infection group, but rather a mix of bacteria from both waves of infection with a strong bias towards the first group (Fig. 4B). This suggests that the first invasion event does not prevent further infection by subsequent Lm waves. Together these observations suggested that timing provides an opportunity for "early arrivers" to become prevalent in the brain/brain stem.

To further probe the role of timing in the establishment of clonal dominance in the brain/brain stem, we bypassed all barriers to invasion and infected mice directly into the brain (Fig. 4C). Following inoculation of 500 CFUs, the brain burden exceeded those observed with IV inoculation, reaching 10^5 CFU by 12 HPI (Fig. 4D vs 1A). Ns was ~10^2 (Fig. 4D), which is similar to

the inoculum size, indicating a wide bottleneck to cerebral colonization and an ability to replicate *in situ*. Although bacterial burden dramatically increased during these first 12 hours, there was no difference between Ns and Nb in the brain (Fig. 4D) indicating that replication was relatively even across the population. Thus, during intracranial infection, when timing is removed as a variable, the Lm clones expand 1000-fold in the brain (CFU = 10^5, Ns = 10^2), but do so relatively evenly. Together these data further support timing as a critical factor that controls clonal dominance in the brain during cerebral listeriosis.

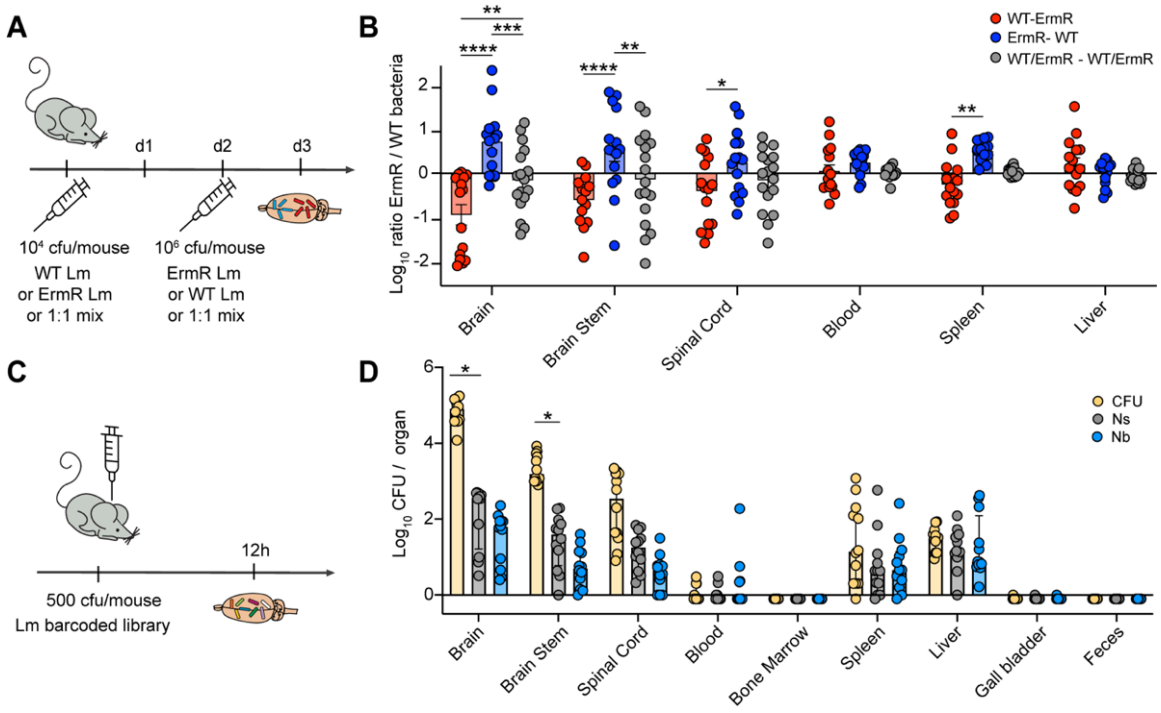


Figure 2.4: Early invading Lm are the main drivers of clonal dominance in the brain. (*A)* Graphical representation of the experimental design for sequential infections: C57BL/6J mice were inoculated intravenously with 1x10^4 CFU of either wild-type Lm (WT), or erythromycin-resistant Lm (ErmR), or a 1:1 mix of both populations. Two days later, mice were re-infected with 1x10^6 CFU of the converse strain. Mice were euthanized one day following the second infection and the ratio of WT to ErmR Lm was assessed. *(B)* Strain composition for each sample. Results are log transformed values of the ratio of ErmR to WT bacteria and bars represent means with SEM. Statistical significance was calculated using two-way ANOVA. ****, p<0.0001; ***, p<0.001; **, p<0.01; *, p<0.1. Results are from three independent experiments with red group N=15, blue group N=15, grey group N=17. *(C)* Graphical representation of the experimental design for intracranial (IC) injections: C57BL/6J mice were inoculated IC with 500 cfu of barcoded Lm. Samples were collected for sequencing 12 hours post injection. *(D)* Bacterial burden (CFU) and founding population metrics (Ns and Nb) following IC inoculation. Results are log-transformed values with median and interquartile range. Results are from three independent experiments for a total of N=12. Samples with no CFU are represented as -0.1. Statistical significance was calculated using multiple Mann-Whitney tests between CFU and Ns, and between Ns and Nb. *, p<0.01

2.3.6. Food-borne infection of immunocompromised mice reproducibly leads to cerebral listeriosis.

Most studies of cerebral listeriosis, including our work presented thus far, are based on non-natural routes of infection, including IV [36,38,39,76], intraperitoneal [37,38], intramuscular [77], intranasal [42], and intracranial [39], and intragastric[39,42]. These methods are valuable and allow us to probe specific aspects of the infection process, but bypass many of the host barriers that

ordinarily constrain Lm dissemination and restrict expansion during natural infections. We adapted foodborne infection models [5,85] with immunocompromised mice, in order to study the dynamics of severe CNS infection following a more natural inoculation. In this model, Rag1-deficient mice (Rag1 KO), which lack B and T cells, were treated with oral streptomycin for 2 days, fasted for ~20h, then inoculated by consumption of bread contaminated with 10^9 Lm CFU (Fig. 5A). Of note, STAMP barcodes are integrated at a fitness neutral site in the Lm chromosome and are expected to have little to no effect on bacterial physiology or pathogenesis [3,4], so oral infections were performed with either barcoded or non-barcoded Lm and all mice were pooled together for Fig. 5.

During the first 5 days post-ingestion of infected food, Rag1 KO mice lost up to 25% of their original weight followed by a phase of recovery, similar to their WT counterparts. Within a week most WT mice had recovered, and none succumbed to infection. In marked contrast, most Rag1 KO mice began losing weight again by 7 DPI and every animal reached an experimental endpoint criterium by 30 DPI, although the exact timing of disease progression varied between mice (Fig. 5B and 5C). The reason for euthanasia was variable, but ~70% of mice developed behavioral changes tied to cerebral infection such as circling, head tilt, or paralysis (Fig. 5D). Thus foodborne infection of Rag1 KO mice leads to disease outcomes similar to those exhibited by cerebral listeriosis-afflicted ruminants [86].

Changes in behavior are manifestations of brain damage [87] suggesting that Lm crosses the blood-brain barrier long before clinical signs become evident. To further characterize "early" stages of infection, mice were euthanized at 6 or 8 DPI and the Lm burden both within and outside the CNS was determined. Bacterial burdens in the CNS were highly variable (Fig. 5E), consistent with the variable rates of disease progression, and were generally lower than the burden found in other organs. At "late" times of infection, when mice reached the euthanasia criteria described in Fig. 5D, the median bacterial burden in the CNS remained variable, but was generally highest in the brain stem (median ~10^6 CFU) and lowest in the spinal cord (median ~10^4 CFU, Fig. 5F and S3C). Even though mice were euthanized at different DPI, the bacterial burden in the spleen and liver was less variable with a median of ~10^6 CFU and the blood and bone marrow were generally poorly infected at this late time point (Fig. 5F). Overall, these observations reveal that low bacterial burden at systemic sites, when compared to IV infection (Fig. 1A), still leads to consistent cerebral infection.

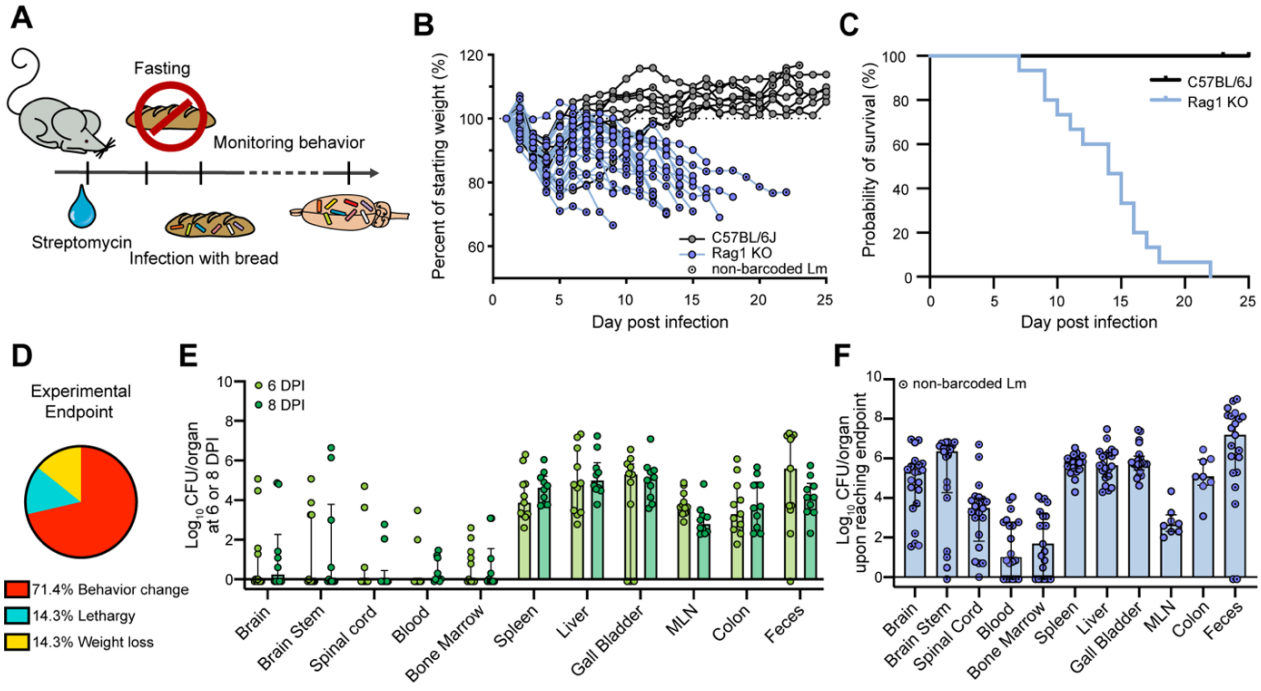


Figure 2.5: Food-borne infection of immunocompromised mice reproducibly leads to cerebral listeriosis. *(A)* Graphical representation of the experimental design for oral infections: mice were treated with streptomycin (20mg/mL) in the drinking water for 48h, fasted for 24h, then infected with $1x10^9$ CFU of either barcoded or non-barcoded Lm and monitored daily for behavioral changes and body weight loss. *(B)* Change in weight over time for Rag1 KO mice and C57BL/6J controls. Results are expressed as the percentage of body weight compared to one day post infection and each line represents one mouse. Mice that received non-barcoded Lm are marked with a black dot and the dashed line indicates 100%. *(C)* Survival rate for Rag1 KO and C57BL/6J mice. *(D)* Reason for euthanasia of Rag1 KO mice, where "behavior change" refers to circling behavior, head tilt, or mild to severe paralysis, "lethargy" refers to lack of activity, and "weight loss" refers to a loss of 30% of original weight. *(E)* Bacterial burden at "early" times of infection with barcoded Lm (6 DPI or 8 DPI) for Rag1 KO mice. Results are expressed as log-transformed values with median and interquartile range. *(F)* Bacterial burden at "late" times of infection (upon reaching experimental endpoint criteria) for Rag1 KO mice. Results are expressed as log-transformed values with median and interquartile range and mice that received non-barcoded Lm are marked with a black dot. Data for *(B-D* and *F)* are combined from three independent experiments with Rag1 KO N=21 (including barcoded Lm N=8) and C57BL/6J N=8. Data for (*E*) are combined from four independent experiments with 6 DPI N= 11 and 8 DPI N=10.

2.3.7. Dynamics of food-borne Lm invasion of the CNS differ from the IV model

We used STAMPR-based metrics to determine whether host bottlenecks and Lm dissemination patterns were similar in the foodborne and IV models of cerebral listeriosis. Mice were compared across multiple infections with barcoded Lm (with equivalent inoculums, Fig. S3D) where "early" samples were collected at 6- or 8 DPI from mice that have brain CFU>0 (subset of mice from Fig. 5E) and "late" samples were collected from mice upon reaching endpoint criteria (subset of mice from Fig. 5F). Since mice progress through infection at different rates (Fig. 5B and C), bacterial burden for "early" mice was variable, but overall we found that the Lm burden in the CNS increased by ~4logs from early to late times of infection (Fig. 6A) while founding population sizes remined low over time (Fig. 6B). Ns from orally infected mice was generally lower at all sites than during IV infections (Fig. 6B and 1B) suggesting that passage through the intestinal barrier in mice lacking Rag1 comprises a very stringent bottleneck. Notably, in the CNS, Ns was generally ~1 in both early and late time

points, suggesting a mostly monoclonal CNS (Fig. 6B, 6C, S3A and S3B). Thus, in marked contrast to the IV model where there is continued Lm invasion of the CNS over the 3-day infection period (Fig. 1B), increase in bacterial burden in the oral model is likely primarily driven by replication within rather than migration into the CNS. In addition, the total bacterial burden and founding population in spleen, liver, blood, and bone marrow remained lower in oral infections compared to IV infections (Fig. 6A, 6B, 1A, 1B and S1F), suggesting that systemic sites are overall more restrictive to Lm colonization in the oral model compared to IV.

At early times of infection, the Lm populations in the CNS were similar to each other (low GD and high FRD[organ-brain]), except the spinal cord which was often uninfected (Fig. 6D and 6E). At any time, the brain only ever harbored 1-3 clones and these barcodes were generally shared with the rest of the CNS (Fig. 6C, S3A and S3B). The clones in the brain were however consistently underrepresented in the colon (Fig. 6E) and the colon population was always highly dissimilar to the brain (GD, Fig. 6D), suggesting that Lm does not primarily depend on retrograde trafficking from peripheral neurons that innervate the gut to infect the brain. Taken together, our findings reveal that the dynamics of Lm CNS invasion in the oral and IV models differ; during oral infection in Rag KO mice, only a very small number of Lm clones invade the CNS and subsequently replicate locally.

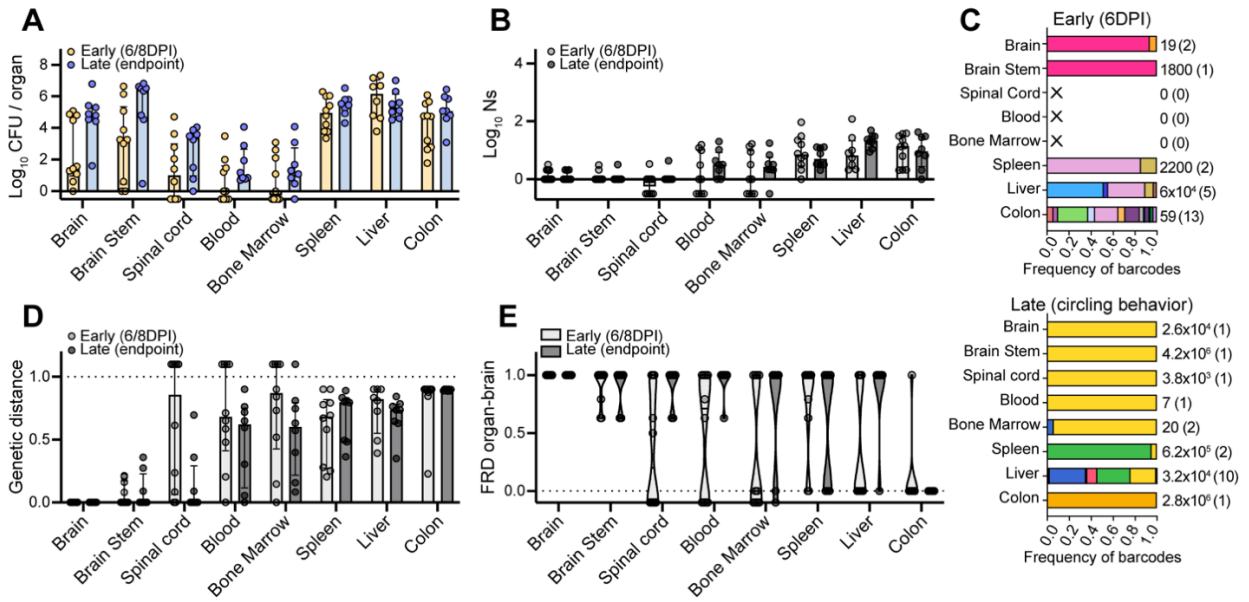


Figure 2.6: Dynamics of food-borne Lm invasion of the CNS differ from the IV model. *(A)* Bacterial burden (CFU) and *(B)* founding population (Ns) for the mice in Fig. 5*E* and *5F* that were infected with barcoded Lm. "Early" refers to samples collected at 6 or 8 DPI, but only from mice where brain CFU>0. "Late" refers to samples collected when mice reached experimental endpoint criteria as described in Fig. 5*D*. Results are log-transformed values with median and interquartile range. Organs with no CFU are represented as -0.5. *(C)* Frequency of barcodes for representative mice of the "early" and "late" groups. Each color represents one barcode and the same color scheme was applied to both graphs. "X" represents a sample with no CFU, the number besides each sample is the bacterial load, and the number in parenthesis is the number of barcodes per sample. *(D)* Genetic distance to brain (GD). Data are individual samples with median and interquartile range and samples with no CFU are represented as 1.1. *(E)* Prevalence of barcodes from the brain in other organs (FRD[organ-brain]). Data are individual samples with violin plots and median and samples with no CFU are represented as -0.1. Data for the "early" group are combined from four independent experiments (subset of mice from Fig. 5*E*) with N=8. Data for the "late" group are combined from two independent experiments (subset of mice from Fig. 5*F*, which received barcoded Lm) N=8.

2.4. Discussion

In this study, we used barcoded Lm and leveraged STAMPR analytics to uncover the patterns of pathogen trafficking, replication dynamics, and host bottlenecks in multiple models of CNS infection. Following IV inoculation, Lm infects the CNS in multiple waves, independently invading the brain, brain stem, and spinal cord (Fig. 1A-1E). All regions of the CNS shared most of their barcode diversity with the blood (Fig. 1F), establishing the blood as the most probable reservoir for continuous CNS invasion. Nevertheless, the brain and brain stem harbored a few highly expanded clones (Fig. 2). Clonal dominance was not due to a spatial advantage (Fig. 3), but the predominant clones instead had a temporal advantage in the brain, where the first Lm to invade became more prominent (Fig. 4). During foodborne infection in immunocompromised mice, we observed extremely tight bottlenecks, and the CNS was nearly monoclonal although robustly colonized (Fig. 5 and 6). Together, our findings quantify the contribution of several barriers that Lm must cross to infect the CNS and reveal the ability of a single clone to cause cerebral infection, highlighting the remarkable power of using barcoded bacteria to quantify pathogen dissemination during infection.

The use of barcoded Lm has previously been applied to models of systemic and foodborne infection, and our results build on these prior studies by mapping the dynamics of Lm invasion of the CNS. Zhang et. al. demonstrated that Lm can escape tissue containment and enter circulation from highly infected systemic organs, thus promoting pathogen exchange between the spleen and liver [4]. Our study reveals that pathogen exchange in systemic organs also facilitates continual invasion of the CNS. These results also mirror the findings of Wincott and colleagues [82], who used barcodes to study the neurotropic parasite *Toxoplasma gondii* and found that the BBB imparted limited restraint to CNS infection. Correspondingly, following Lm oral infection in Rag KO mice, the spleen and liver harbored fewer bacteria, the blood had a low burden, and the CNS remained monoclonal. These observations are consistent with the idea that a CFU threshold in systemic sites must be met to enable robust entry of Lm into circulation and allow continuous invasion of the brain. During oral infection, a failure to reach this threshold limits the ability of Lm to escape systemic organs, reducing bloodborne bacteria, and ultimately leading to a monoclonal CNS.

Multiple mechanisms have been proposed to explain how Lm first invades the CNS. The most accepted model proposes that Lm hijacks bone-marrow-derived monocytes to reach the BBB [36–39]. Although these cells are very efficient at promoting brain infection [36] and CCR2$^{-/-}$ mice show a decreased brain bacterial burden [39], the Lm populations in the brain and bone marrow did not converge over time during IV infection (Fig. 2C and S1D), suggesting that the dominant clones in the bone marrow do not continuously and robustly invade the CNS. However, in our study we only collected femurs, and it remains possible that other bone marrow sites harbor clones shared with the CNS, particularly the skull marrow [88]. Defining the heterogeneity of Lm across bone marrow sites could be facilitated by STAMPR in future studies. An alternative model proposed that Lm traffics within neurons via the peripheral nervous system [40–42,77–79]. This hypothesis is particularly attractive since the gastrointestinal tract is densely innervated [89] and harbors large numbers of Lm following oral infection [4,29]. However, we did not observe

similar bacterial populations between the colon and CNS (Fig. 6). It is possible that intraneural trafficking originates from other tissues, but our findings thus far argue against a direct gut-brain axis as the principal route for continuous pathogen trafficking into the CNS. Even though each of the proposed routes could be responsible for the first invasion event, our data support the blood as the most likely source of bacteria that invade in the brain over time.

We found that timing of CNS invasion drives clonal dominance in the brain, where clones that first invade the brain are more abundant than clones that arrive in subsequent waves. The dominance of the first organisms to arrive in a new niche is known as the "priority effect" and has been previously described in the study of complex microbial populations, including several models of intestinal colonization [90,91]. However, it is highly likely that the mechanisms that drive priority effects during intestinal colonization are distinct from those that drive priority effects during CNS invasion. Notably, direct antagonism between bacteria and competition for nutrients play major roles in priority effects in intestinal colonization by extracellular bacteria [92]. Since Lm is an intracellular pathogen and there is limited evidence for the presence of other abundant microbes in the brain, we hypothesize that neither play a major role in this context. We propose that the priority effect in the Lm-infected CNS is a consequence from the fact that the first clones to invade the brain have more time to replicate before the host succumbs to infection.

Our study further emphasizes the impact of the infection route in studies of pathogen dissemination, since the pathogen dynamics during foodborne infection were distinct from the dynamics during IV infection. To mimic a more natural CNS infection, we adapted a model of foodborne infection where mice were pre-treated with streptomycin [5]. Other models of oral cerebral listeriosis have previously been developed with no antibiotic treatment and/or the use of clinical isolates [39,85,93,94]. Antibiotic pretreatment promotes dysbiosis which limits colonization resistance in the gut and facilitates a more efficient infection [5,29]. Dysbiosis is also a common occurrence in immunocompromised individuals who are most at risk of cerebral listeriosis [95] and defining the role of the microbiota in Lm CNS invasion will be worthy of further study. The use of Rag1 KO mice enables infection in a context where pathogen clearance is not achieved. Indeed, $CD8^+$ T cells are required for clearance of Lm from a host [96,97], and SCID mice, which have limited B and T cells, become chronically infected with Lm [98]. Some bacterial factors are also known to facilitate CNS invasion [76] and many neurotropic clinical isolates have been identified [39,93]. Quantifying the specific contribution of host and bacterial factors on pathogen dissemination to the CNS will be facilitated by the use of barcoded Lm and provide substantially greater insight into the principles that underlie Lm CNS infection in nature. Overall, our work provides insights into the dissemination patterns of intracellular bacteria to the brain, laying the groundwork for barcode-based analysis of CNS invasion with other neurotropic pathogens.

2.5. Material and methods

Animal models

C57BL/6J mice were purchased from the Jackson Laboratory (stock #000664) and maintained under specific pathogen-free conditions at the University of California, Berkeley animal facility. Rag1 KO mice (B6.129S7-Rag1tm1Mom/J, Jackson Laboratories stock #003729) were obtained from the Barton lab at the University of California, Berkeley and maintained under specific pathogen-free conditions within the University of California, Berkeley animal facility. Only 8- to 12-week-old female mice were used for all experiments with sex- and age-matched controls according to institutional guidelines for animal care. This study was performed in strict accordance with the recommendations in the Guide for the Care and Use of Laboratory Animals of the National Research Council of the National Academy of Sciences [99] and with university regulations. All protocols were reviewed and approved by the Animal Care and Use Committee at the University of California, Berkeley (AUP-2016-05-8811).

Bacterial strains and growth conditions

All *L. monocytogenes* strains used in this study were derived from 10403S [100] which is streptomycin resistant and propagated in filter-sterilized brain heart infusion (BHI) medium (BD) at 37°C while shaking with streptomycin (200 µg/ml) overnight. Cell density was measured by optical density (OD600). Inoculums were prepared by washing log-phase bacteria twice in PBS and resuspending in the appropriate volume of PBS depending on the infection route. Frozen bacterial stocks were stored at -80°C in BHI plus 25% glycerol.

Intravenous infections

Mice were infected intravenously via the tail vein with 10^4 CFU of *L. monocytogenes* strains in 200µL of sterile PBS as previously described [101]. Briefly, 1-, 2-, or 3 days post-infection, mice were euthanized, and tissues were harvested as described below. For sequential infections, mice were infected intravenously via the tail vein with 10^4 CFUs of *L. monocytogenes* in 200µL of sterile PBS. 48 hours following the first injection, mice were injected again intravenously via the tail vein with 10^6 CFU of Lm in 200µL of sterile PBS. 24 h following the second infection, mice were euthanized, and tissues were harvested as described below.

Intracranial infections

Mice were infected intracranially with 500 CFU of *L. monocytogenes* strains with 5µL of sterile PBS as previously described [102]. Briefly, mice were anesthetized with 2% isoflurane, given pre-emptive analgesics (Buprenorphine 0.1mg/kg and Meloxicam 10mg/kg), and arranged on Angle-two stereotactic frame (Leica, Nussloch, Germany). The incision area was swabbed with three alternating wipes of 70% ethanol and betadine scrub with sterile applicators prior to performing minimally damaging craniotomies. The stereotaxic surgery coordinates used for targeting the striatum, relative to bregma, were 2mm anterioposterior, 1 mm mediolateral, 1.5 mm dorsoventral. Infusion of *L. monocytoge*nes (500 CFU) was performed with a syringe to deliver 0.5 µL per minute for a total volume of 5µL. Post-infusion, the syringes were left in position for 2 minutes before slow removal from the injection site, which was then cleaned, sutured, and surgically glued. Throughout the procedure, mice were kept at 37°C for warmth

and Puralube Vet Ointment (Dechra, NDC #17033-211-38, Northwich, England) was applied to the outside of the eyes. Mice were euthanized and tissues were harvested 12 hours post infection.

Foodborne infections

Prior to infection, 20 mg/ml of streptomycin sulfate was added to the drinking water. After 24 h, chow was removed to initiate an overnight fast and mice were transferred to fresh cages. 48 h after streptomycin was added to the water, mice were isolated, fed a 3-mm piece of bread with 3µL of butter and 10^9 CFU *L. monocytogenes* in 5uL PBS. Mice were then returned to cages containing standard drinking water and chow. The inoculum was plated for CFU to check the efficiency of each infection. Fecal pellets were collected at 1 DPI for each mouse and only animals with 1 DPI CFU/gram > $10^{6.5}$ were kept for further analysis. Mice were monitored daily for weight loss and behavioral changes including head tilt, circling, mild to severe paralysis, and lethargy. Upon reaching an endpoint criterium as described on our animal use protocol (any of the behaviors described in Fig. 5: behavior change, lethargy, or 30% weight loss), mice were euthanized, and tissues were harvested.

Tissue harvest

Blood (~500uL) was collected via cardiac puncture immediately after euthanasia in 100uL 50 mM EDTA as an anticoagulant (adapted from Senay et al.[93]). Immediately after blood collection, mice were perfused with 20mL PBS. Most samples were homogenized in 0.1% IGEPAL CA-630 (Sigma) and for bone marrow, the left femur and tibia were collected together then crushed with a mortar and pestle before homogenizing. Gallbladders and feces were homogenized in 1xPBS. Colons were cut longitudinally, washed with PBS, and incubated in RPMI (Gibco) containing 5% fetal calf serum, HEPES, L-glutamine, and 100 µg/ml gentamicin for 45 min at 37°C. This procedure kills all extracellular bacteria within the tissue. Colons were then washed 6 times to remove all gentamicin by placing the tissue into 10 ml of fresh PBS on a rotator at 4°C for 20 min before homogenizing in 1 ml 0.1% IGEPAL. Clean autoclavable probes were used and changed for the homogenization of each sample to avoid cross-contamination. Dilutions of homogenates were plated to enumerate CFU and full samples were plated for STAMPR analysis following incubation at 37°C overnight. In instances where growth of commensal bacteria was a concern, plates were supplemented with nalidixic acid, LiCl, and glycine, which does not affect Lm growth. Antibiotics and media supplements were used at the following concentrations: streptomycin at 200 µg/ml, nalidixic acid at 15 µg/ml, LiCl at 6 mg/ml, and glycine at 6 mg/ml.

STAMP

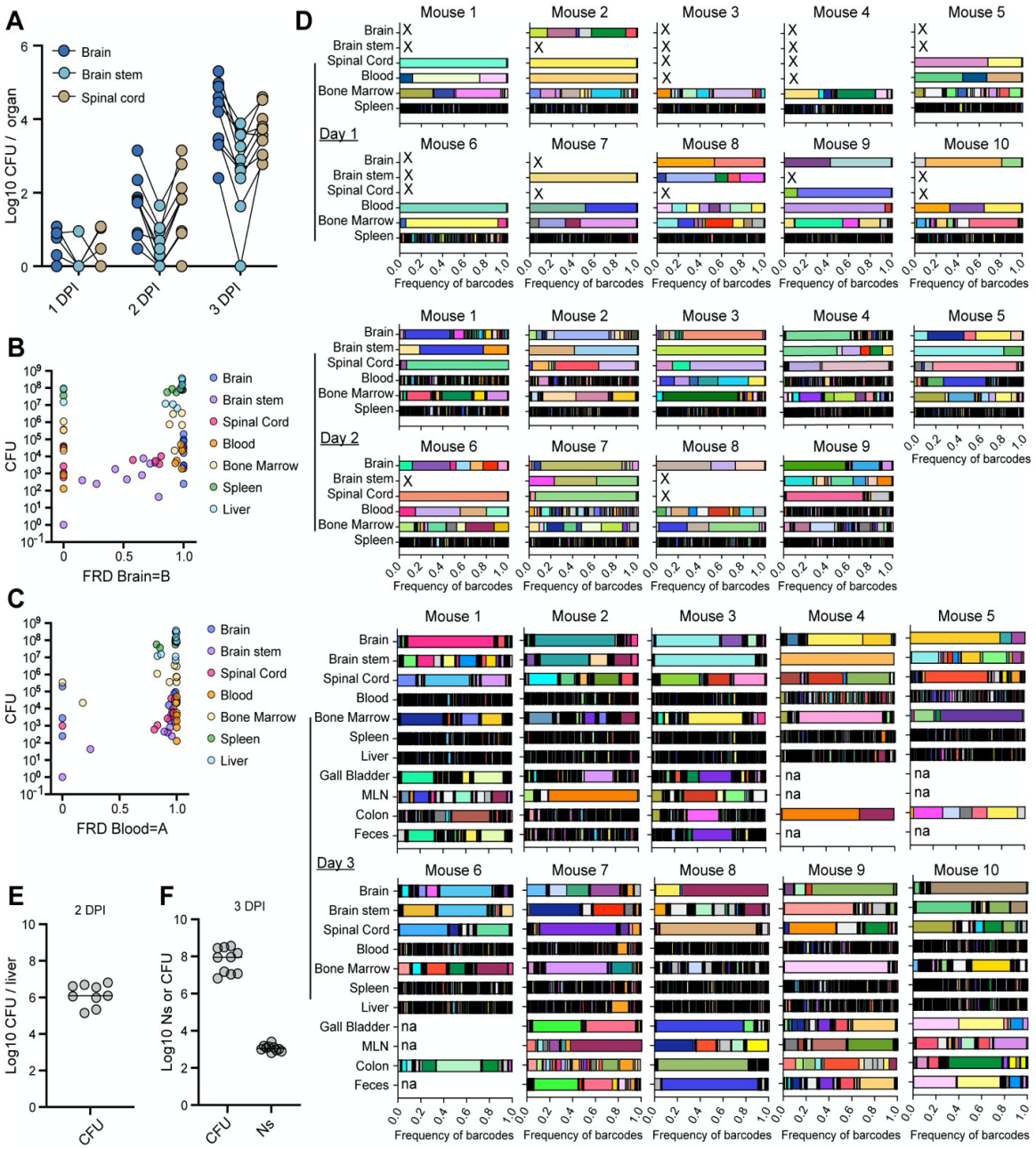
Sequence tag-based analysis of microbial populations (STAMP) was performed as previously described [3,20]. The library with ~200 barcodes, which was created by Dr. A. Louie in 2019 [29], was freshly inoculated into BHI broth from frozen stocks and grown to log-phase for each experiment. Inoculum samples were collected frequently to ensure that the population structure remained stable across all experiments. To process samples, Lm colonies were washed off plates, collected in PBS with 25% glycerol, diluted In water, and boiled for 1h at 80C. The barcode-containing region was amplified from the genome using custom forward and reverse primers (Supplementary Table S1) with OneTaq HS Quick-Load Master Mix (New

England Biolabs) on boiled samples. Samples were amplified using primers containing TruSeq indexes and adapters for Illumina sequencing. PCR products were pooled and purified using GeneJet PCR purification kit. Purified products were sequenced on either an Illumina MiSeq or Illumina NextSeq 1000. Reads were demultiplexed using a custom R script and trimmed and mapped to a list of ~200 barcodes using Qiagen CLC Genomics Workbench with default settings. Mapped reads were exported as a CSV table. Founding population estimates were determined using the STAMPR analysis toolset [20]. Genetic distance was estimated with Cavalli-Sforza chord distance [103] as previously described [3]. Founding population (Ns) sometimes were computed as <1 which is biologically aberrant so Nb<1 values were manually amended to Nb=1. Sequencing data and original script have been deposited on Github (https://github.com/hullahalli/stampr_rtisan) and are publicly available. Any additional information required to reanalyze the data reported in this paper is available from the lead contact upon request.

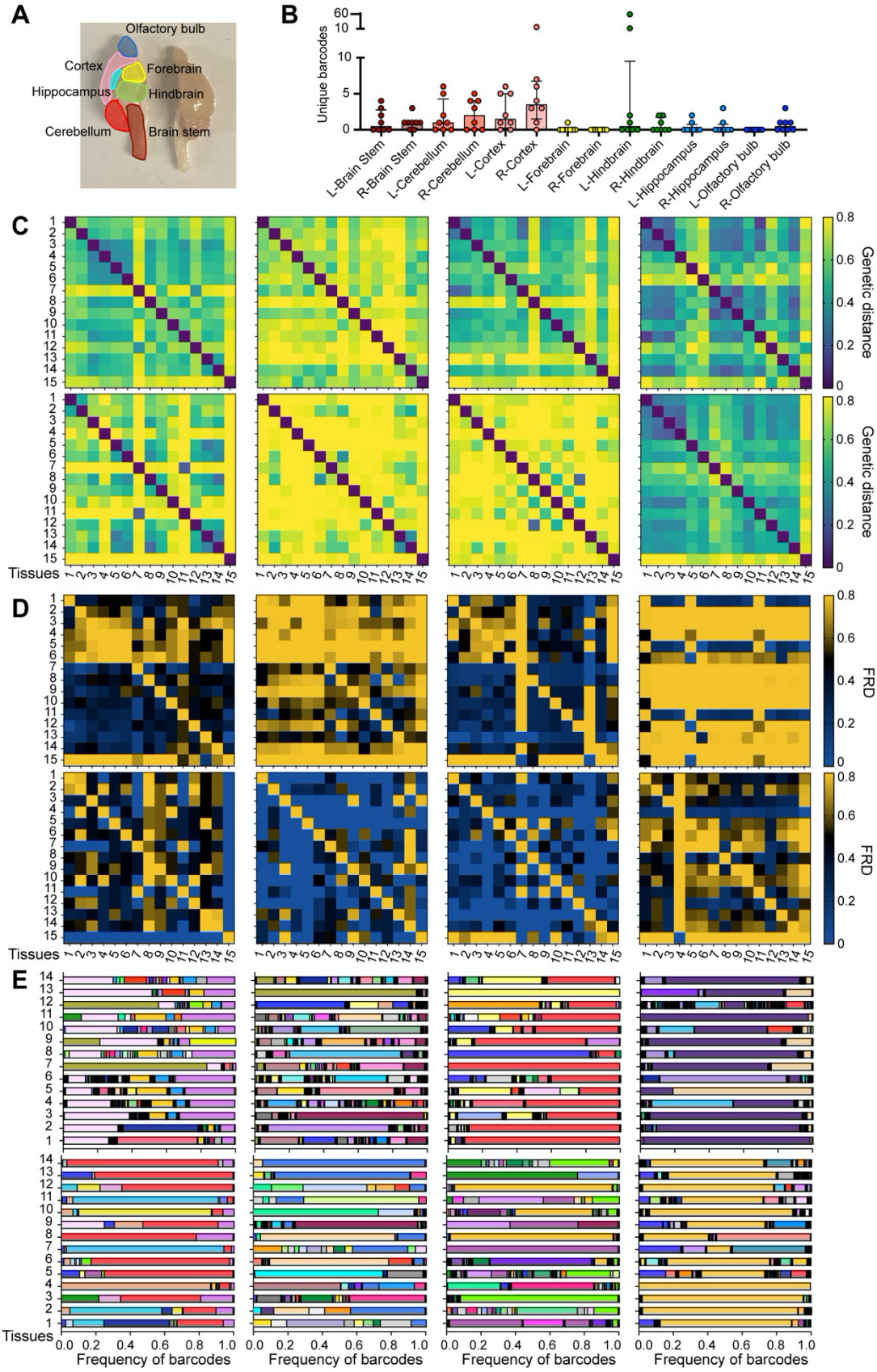
Statistical analysis

All statistical analyses were performed using GraphPad Prism version 10.0.1 for MacOS, GraphPad Software, San Diego, CA, USA. Details for all statistical analyses can be found in the figure legends.

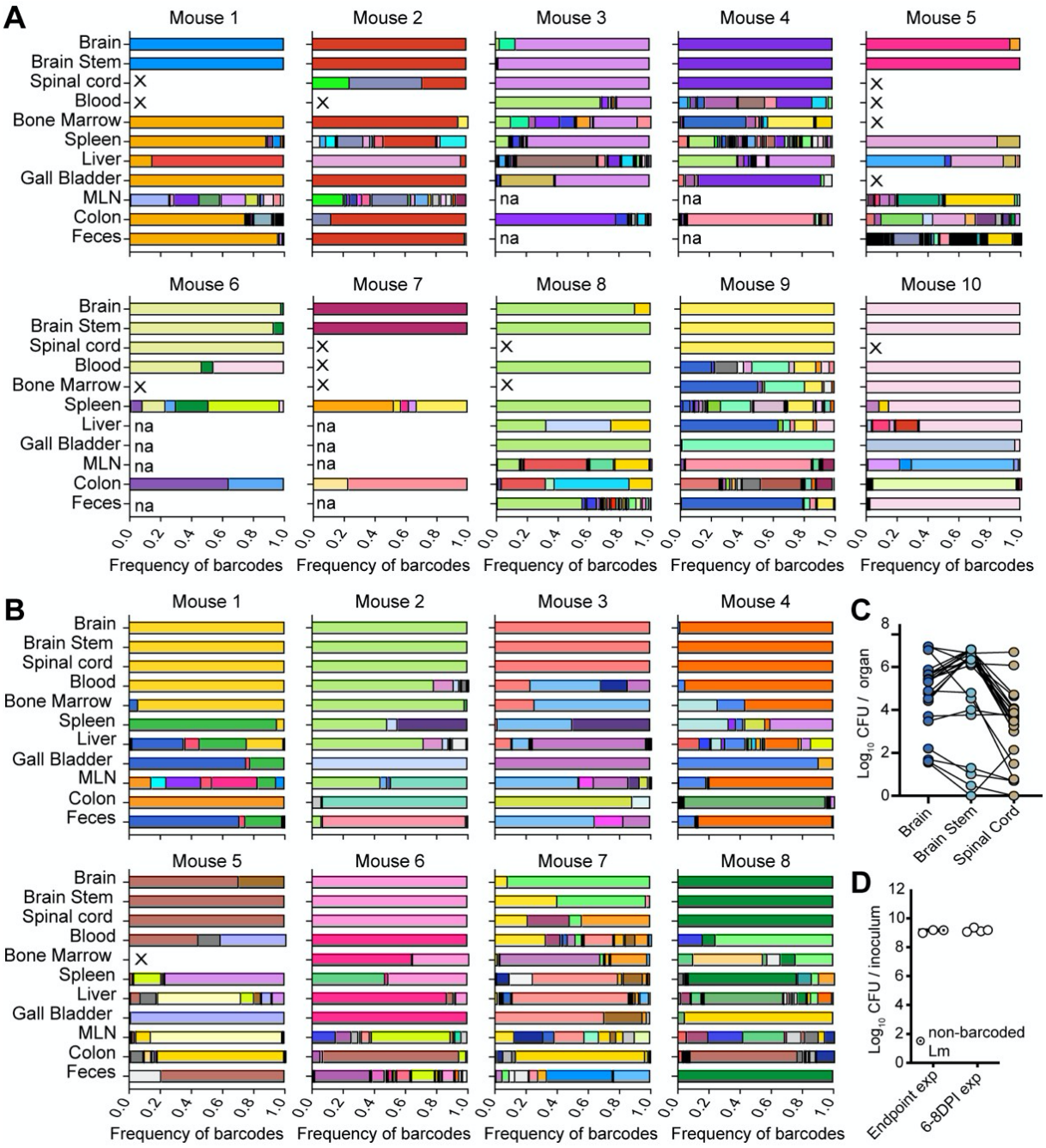
2.6. Supplementary Figures



Supplementary Figure S2.1: Intravenous infections of C57BL/6J mice intravenously infected with 1x10^4 CFU of *L. monocytogenes*. *(A)* Bacterial burden (CFU) in the central nervous system over 3 days post infection (DPI). Results are expressed as log-transformed CFU per organ and each line connects the samples from one mouse. *(B-C)* Comparison between bacteria burden and FRD[organ-brain] *(B)* or FRD[blood-organ] *(C)* for all mice at 3 DPI. Each dot represents one sample and is colored by the tissue type. *(D)* Frequency of barcodes per organ over 3 days post infection, where each graph represents one mouse, and each color represents one barcode (the same color scheme was applied to the entire panel). Data for *A-D* were collected from the same mice as Figure 1 and Figure 2. (E) Bacterial burden in the liver at 2 DPI. Results are expressed as log-transformed CFU with median. *(F)* Bacterial burden and founding population (Ns) in the liver at 3 DPI. Results are expressed as log-transformed values with median. Data for *E and F* are combined from at least two independent experiments each with 2 DPI n=9, 3 DPI n=10.


A
Olfactory bulb
Cortex
Forebrain
Hippocampus
Hindbrain
Cerebellum
Brain stem
B
Unique barcodes
L-Brain Stem
R-Brain Stem
L-Cerebellum
R-Cerebellum
L-Cortex
R-Cortex
L-Forebrain
R-Forebrain
L-Hindbrain
R-Hindbrain
L-Hippocampus
R-Hippocampus
L-Olfactory bulb
R-Olfactory bulb
C
Genetic distance
Tissues
D
FRD
Tissues
E
Tissues
Frequency of barcodes

Supplementary Figure S2.2: Dissection of brain regions 3 days post intravenous infection. *(A)* Depiction of the regions of the brains and brain stems collected 3 days post intravenous infection of C57BL/6J mice with $1x10^4$ CFU of *L. monocytogenes*. Brains were dissected into left and right hemispheres, then each further separated into the following 7 regions: olfactory bulbs, cortex, hippocampus, cerebellum, brain stem (medulla and pons only), and the remaining area was separated halfway along the coronal plane into two sections labeled "forebrain" and "hindbrain" (includes midbrain). *(B)* Sites of entry into the brain. Data represent the number of clones that are uniquely identified in only one brain region for each mouse, with median and interquartile range. *(C)* Genetic distance between samples at 3 days post IV infection. Each heatmap represents one mouse with a threshold for dissimilarity set at 0.8. *(D)* Fraction of shared barcodes (FRD) between samples at 3 days post IV infection. Each heatmap represents 1 mouse with a threshold for dissimilarity set at 0.8. *(E)* Frequency of tags at 3 days post IV infection. Each graph represents one mouse and each color represents one barcode (the same color scheme was applied to the entire panel). For *A*-*E* all data were collected from the same mice as Figure 3. For panels *C*-*E* the tissues are as follows: 1- left brain stem, 2- right brain stem, 3- left cerebellum, 4- right cerebellum, 5- left cortex, 6- right cortex, 7- left forebrain, 8-right forebrain, 9- left hindbrain, 10- right hindbrain, 11- left hippocampus, 12- right hippocampus, 13- left olfactory bulb, 14- right olfactory bulb, 15- spleen.



Supplementary Figure S2.3: Oral infection of mice with 1x10^9 CFU of *L. monocytogenes.* *(A-B)* Frequency of tags for Rag1 KO mice sacrificed at 6-8 DPI (*A*) or upon reaching endpoint criteria (*B*). Each graph represents one mouse, and each color represents one barcode (the same color scheme is applied to all graphs). "X" identifies a sample with no CFU and "na" means the sample was not collected. *(C)* Bacterial burden (CFU) in the central nervous system of Rag1 KO mice upon reaching endpoint criteria, where each line connects the samples of one mouse. (D) Inoculum for experiments where mice were collected upon reaching endpoint criteria (Fig. B-D,F and Fig. 6) or at 6-8 DPI (Fig. 5E and Fig. 6). Each dot represents the inoculum for one experiment. Results for (C-D) are expressed as log-transformed values.

Oligo Name	Sequence
Var13	AATGATACGGCGACCACCGAGATCTACACTCTTTCCCTACACGACGCTCTTCCG ATCTTACTTGTAAAACGACGGCCAGT
Var14	AATGATACGGCGACCACCGAGATCTACACTCTTTCCCTACACGACGCTCTTCCG ATCTGCTATTGTAAAACGACGGCCAGT
Var15	AATGATACGGCGACCACCGAGATCTACACTCTTTCCCTACACGACGCTCTTCCG ATCTCGACTGTTGTAAAACGACGGCCAGT
Var16	AATGATACGGCGACCACCGAGATCTACACTCTTTCCCTACACGACGCTCTTCCG ATCTTAGCGTATTGTAAAACGACGGCCAGT
Var17	AATGATACGGCGACCACCGAGATCTACACTCTTTCCCTACACGACGCTCTTCCG ATCTTGCTGAGTCTTGTAAAACGACGGCCAGT
Var18	AATGATACGGCGACCACCGAGATCTACACTCTTTCCCTACACGACGCTCTTCCG ATCTGCTGATAGTATTGTAAAACGACGGCCAGT
Var19	AATGATACGGCGACCACCGAGATCTACACTCTTTCCCTACACGACGCTCTTCCG ATCTCAACTGCGTAGCTTGTAAAACGACGGCCAGT
Var20	AATGATACGGCGACCACCGAGATCTACACTCTTTCCCTACACGACGCTCTTCCG ATCTATGACCGTCTCGATTGTAAAACGACGGCCAGT
AD002	CAAGCAGAAGACGGCATACGAGATACATCGGTGACTGGAGTTCAGACGTGTGC TCTTCCGATCTTGTCTCATGAGCGGATACA
AD004	CAAGCAGAAGACGGCATACGAGATTGGTCAGTGACTGGAGTTCAGACGTGTGC TCTTCCGATCTTGTCTCATGAGCGGATACA
AD005	CAAGCAGAAGACGGCATACGAGATCACTGTGTGACTGGAGTTCAGACGTGTGC TCTTCCGATCTTGTCTCATGAGCGGATACA
AD006	CAAGCAGAAGACGGCATACGAGATATTGGCGTGACTGGAGTTCAGACGTGTGC TCTTCCGATCTTGTCTCATGAGCGGATACA
AD007	CAAGCAGAAGACGGCATACGAGATGATCTGGTGACTGGAGTTCAGACGTGTGC TCTTCCGATCTTGTCTCATGAGCGGATACA
AD012	CAAGCAGAAGACGGCATACGAGATTACAAGGTGACTGGAGTTCAGACGTGTGC TCTTCCGATCTTGTCTCATGAGCGGATACA
AD013	CAAGCAGAAGACGGCATACGAGATTTGACTGTGACTGGAGTTCAGACGTGTGC TCTTCCGATCTTGTCTCATGAGCGGATACA
AD014	CAAGCAGAAGACGGCATACGAGATGGAACTGTGACTGGAGTTCAGACGTGTGC TCTTCCGATCTTGTCTCATGAGCGGATACA

Supplementary Table S2: Oligonucleotides for sequencing. Primers with names beginning with “var” are forward primers and primers with names beginning with “ad” are reverse primers.

2.7. Unpublished work

During our efforts to understand the spaciotemporal dynamics of cerebral infection, we performed a few additional/control experiments that did not make it into the final published manuscript but did provide additional information that we thought was worth including here.

2.7.1. Controlling for the effect of microbiota during oral infection with littermates

Many of the cerebral infections in this chapter were performed as foodborne infections. For the sake of continuity with the prior experiments using intravenous infections, C57BL6/J mice bought from the Jackson Laboratories (JAX) were used as control mice for all oral infections. However, as mentioned in the material and methods (Section 2.5), the Rag1 KO mice were a gift from the Barton lab at UC Berkeley (UCB) and were bred in house at the University of California, Berkeley animal facilities. Fecal bacterial burden was assessed one day post infection for all orally infected mice to ensure only animals that were efficiently infected (>10^6 CFU) were kept for further analysis. Nevertheless, these mice were bred in separate animal facilities which may affect their intestinal microbiota.

Indeed, the commensal communities of animals bred in separate facilities can be dramatically different.[104] This may seem innocuous, but it can heavily impact the response of mice to various infections, such as sepsis[104], malaria[105], or *Clostrioides difficile*[106]. These variabilities can be attributed to many downstream effects of commensal microbes, such as training the immune system during early life[107] and leading to different immunophenotypes,[104] or the ability of certain commensal species to directly impede intestinal colonization by competition for nutrients or direct antagonism[5].

We thus set out to probe whether the differences in the development of cerebral Listeriosis observed between C57BL6/J (JAX) and Rag1KO (UCB) mice (section 2.3.6) was microbiota dependent. C57BL6/J (JAX) and Rag1KO (UCB) mice were crossed in house (UCB) to obtain a cohort of littermates with all the genotypes of interest: $Rag1^{-/-}$, $Rag1^{+/-}$, and $Rag1^{+/+}$. Littermates are recognized as the best method for minimizing the impact of microbiota on genotype-phenotype studies because pups have a homogeneous microbiome from early life. Co-housing animals is an alternative option for normalizing microbiotas, but even though microbial communities may equilibrate over time the immune development from early life exposure will remain distinct in co-housed mice.[108]

Littermates of each genotype were thus orally infected with $1x10^9$ CFU of WT Lm following pre-treatment with streptomycin. C57BL6/J mice (JAX) were infected as well, as control. Weight loss and behavior were monitored daily, similarly to the experiments described earlier, and bacterial burden was assessed either at the time of reaching endpoint criteria (circling disease, mild to severe paralysis, lethargy, or >30% weight loss) or at 25-28 days post infection. $Rag1^{-/-}$ littermates were unable to recover from early weight loss and all reached endpoint criteria associated with high bacterial burden in the CNS in about 1-3 weeks post infection (Fig. 2.7), similarly to our previous findings (Section 2.3.6). On the other hand,

C57BL6/J (JAX) and Rag1$^{+/+}$ (UCB) all recovered from infection within a week and cleared Lm within a month, except for one mouse. The Rag1$^{+/-}$ mice were generally similar to Rag1$^{+/+}$ mice with ~90% mice recovering from infection and attaining bacterial clearance (Fig 2.7).

This work suggests that the differential response to cerebral listeriosis between C57BL6/J (JAX) and Rag1KO (UCB) mice identified in Sections 2.3.6 and 2.3.7 was indeed dependent on genetic differences rather than variations in intestinal communities, and brings additional validation to our earlier findings.

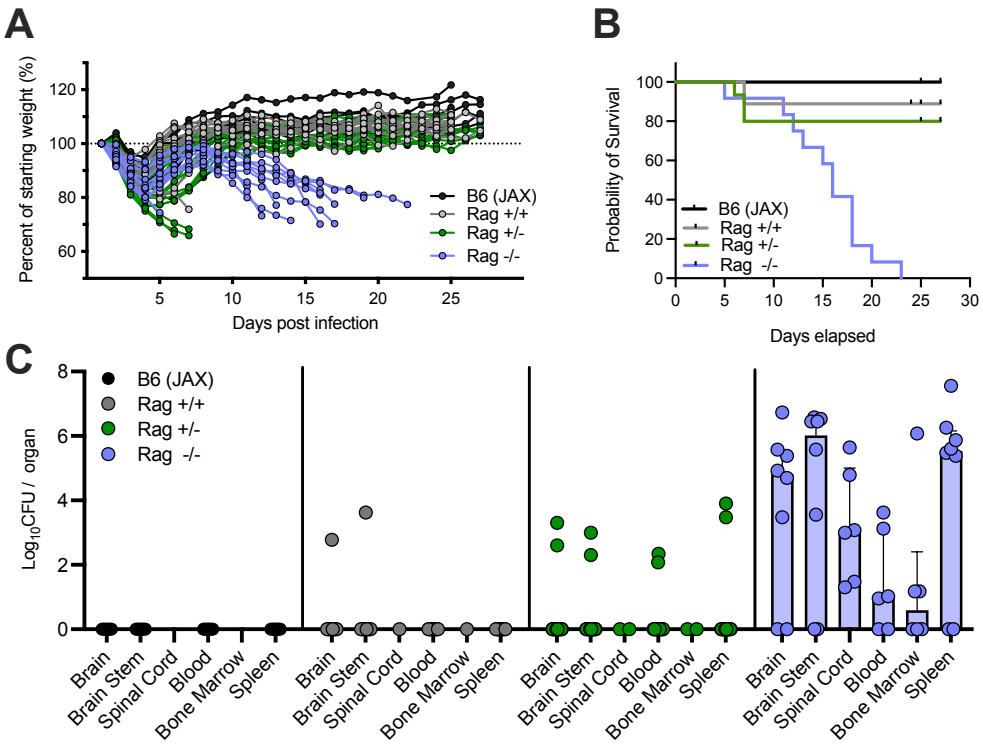


Figure 2.7: The microbiota does not drive the difference in development of cerebral listeriosis between store bought C57BL6/J mice and Rag1KO mice bred in house. C57BL6/J mice bought at the Jackson laboratories, and Rag1$^{+/+}$, Rag1$^{-/+}$, and Rag1$^{-/-}$ littermates bred in house at UC Berkeley were treated with streptomycin (20mg/mL) in the drinking water for 48h, fasted for 24h, then infected with 1x10^{9} CFU and monitored daily for behavioral changes and body weight loss. *(A)* Change in weight over time. Results are expressed as the percentage of body weight normalized to one day post infection and each line represents one mouse. The dashed line indicates 100%. *(B)* Survival rate where endpoint criteria were set as circling behavior, head tilt, mild to severe paralysis, lethargy, or weight loss >30% of original weight. *(C)* Bacterial burden upon reaching endpoint criterium or at the end of experiment (25-27 days post infection). Results are expressed as log-transformed values with median and interquartile range. Data are combined from two independent experiments with C57BL6/J (B6 JAX) n=10, Rag1$^{+/+}$ n=12, Rag1$^{-/+}$ n=19, and Rag1$^{-/-}$ n=8.

2.7.2. Assessing early brain damage with rotarod

As we continued our studies of orally-induced cerebral listeriosis, we sought to identify mice at early stages of brain infection. Indeed, circling behavior, lethargy, and paralysis ("endpoint criteria") are all dramatic phenotypes that are evidence of extensive neural damage[87] and suggest that cerebral infection has already been underway for some time. In our published work[109] we studied mice that were sacrificed at 6 to 8 days post infection, expecting

to identify animals with CFU>0 in the brain, yet little enough bacterial accumulation that mice would not be on the brink of developing "endpoint criteria" symptoms. This method allowed us to perform an analysis of "early" brain infection, but was not perfect at identifying mice with *some but few* CFUs in the brain. So, we attempted to identify other markers that would be evidence of early brain damage.

To this avail, we turned to a well-established model in the field of neurobiology, established in 1957: the rotarod[110]. A rotarod is an instrument where a horizontal rod will rotate along its long axis at increasing speed and mice are monitored for the duration they are able to walk forward and remain on the rod (latency to fall). An infrared sensor assesses the presence of the mouse on top of the rod and thus specifically and accurately marks the time to fall, providing detailed information about the mice's motor coordination, balance, and locomotion performance. Animals are trained for a few days prior to the start of the experiment so they learn to expect the bar to begin rotating and to remain on the bar as it moves. When motor deficits develop, mice have increased difficulty to remain on the rotating bar and fall earlier than healthy mice.[111] This tool has successfully been used to assess cerebral impairment following Zika infection[112] and *Toxoplasma gondii* infections[113,114] among others.

We trained Rag1KO and C57BL6/J female mice on the rotarod for 5 days prior to infection. A subset of the mice were then orally infected with $1x10^9$ CFU with streptomycin pre-treatment, as previously described, while the rest were left uninfected as control. Mice were monitored 3 times daily with 15 min between each testing session. Challenges lasted up to 5 min or until the mouse fell. Uninfected mice of either genotype as well as infected C57BL6/J (which we found in Fig 2.5 can recover from infection within a week) maintained a latency to fall around 200sec throughout the experiment. On the other hand, performance of infected Rag1KO mice varied dramatically after ~12 days of infection (Fig 2.8A). When we assessed the latency to fall for each infected Rag1KO mouse separately, we found that mice performed very poorly on the day they reached endpoint criteria, but performed well the day before developing symptoms of serious disease (Fig2.8B).

This suggested that the Rotarod system is not a helpful method to identify early Lm-induced cerebral damage. Other behavioral evaluations could be tested to identify early brain damage such as the elevated cross maze or the gait test, but our method of systematically sacrificing animals at 6-8 days post infection provided sufficient information to for our purposes.

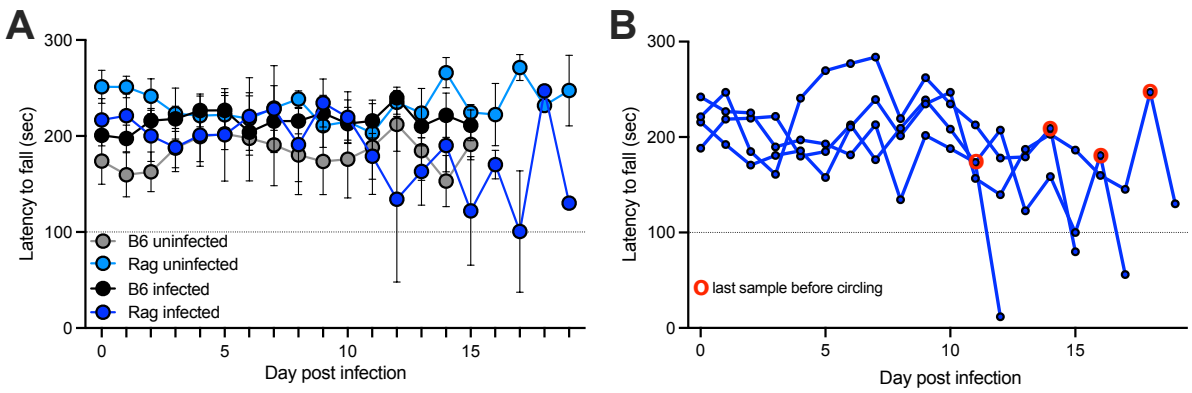


Figure 2.8 Rotarod did not allow for identification of early signs of cerebral listeriosis. C57BL6/J or Rag1KO 8-12 week old female mice were trained on the rotarod for 5 days prior to infection. A subset of mice were then infected orally with 1x10^9 CFU following streptomycin pre-treatment, and monitored 3 times daily for motor function. (A) Latency to fall in seconds for each group, where results are the mean with SEM. (B) Latency to fall in seconds for each individual Rag1KO mouse. The performance on the last day before developing "endpoint criteria" symptoms (i.e. circling disease, mild to severe paralysis, lethargy, or 30% weight loss) was highlighted in red. Data are combined from two independent experiments with B6 uninfected n=3, Rag uninfected n=5, B6 infected n=8 , and Rag infected n=4.

2.7.3. Clonal dominance in orally infected Rag1KO mouse brain regions

We previously identified that the brain of orally infected Rag1KO mice was almost entirely monoclonal upon reaching endpoint criteria (Fig 2.6 and S2.3B). However, brain CFU can reach ~10^6 CFU around that time (Fig 2.6 and S2.3B) so we wondered whether additional barcodes may be present at low levels in certain regions of the brain but could not be captured by looking at the brain as a whole tissue.

To address this concern, we infected Rag1KO mice orally with 1x10^9 CFU of barcoded Lm following streptomycin pre-treatment and CNS was harvested upon reaching endpoint criteria. The brain and brain stem were collected, then separated across the sagittal plane (left-right), and further dissected into a total of 14 compartments as previously described (Fig. 2.3 and S2.2A).

In orally infected mice, the bacterial burden was highest in the brain stem (as previously described in Fig. S2.3C), then tended to be highest in hind regions close to the brain stem such as the cerebellum, hindbrain, and cortex (Fig 2.9A). Upon assessing the frequency of barcodes in each region however, we found that one clone remained dominant throughout each region for each mouse (Fig. 2.9B).

This further validated our previous understanding that the CNS of orally infected mice is highly monoclonal upon reaching endpoint criteria.

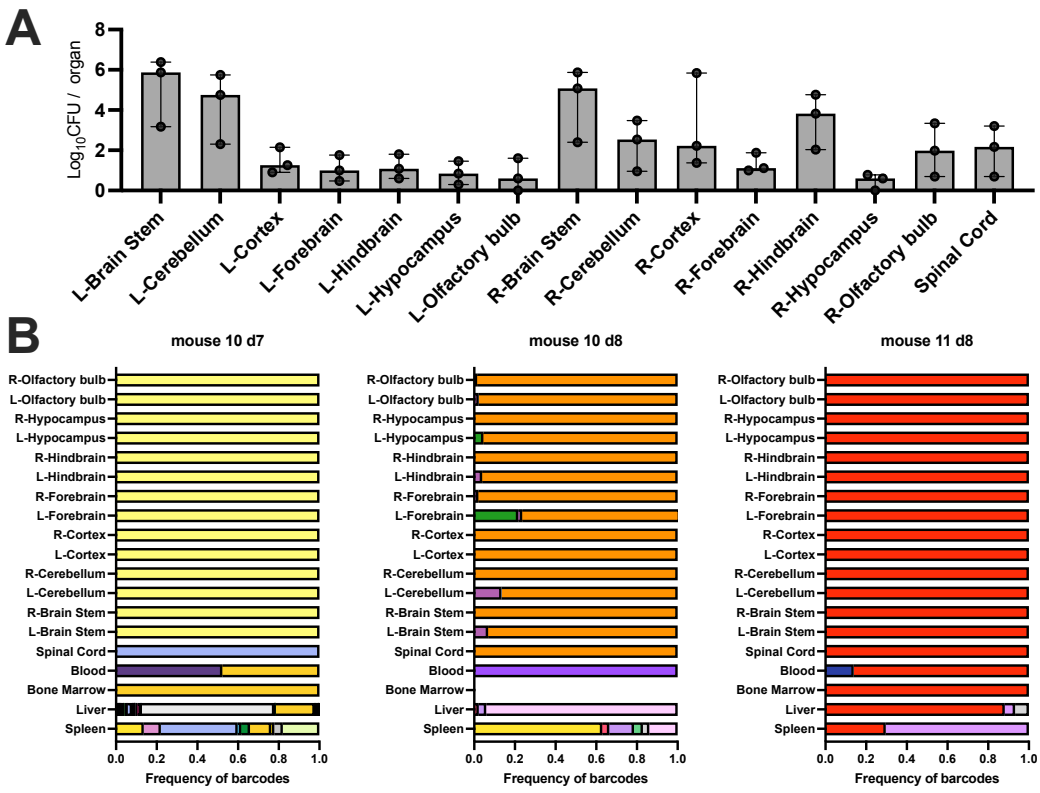


Figure 2.9: The CNS of orally infected Rag1KO mice at late stages of infection is monoclonal. 8-12 week old Rag1KO female mice were infected orally with $1x10^9$ CFU of barcoded Lm following streptomycin pre-treatment, and monitored daily for behavioral changes. Samples were collected when mice reached endpoint criteria (circling behavior, mild to severe paralysis, lethargy, weight loss >30%). *(A)* Bacterial burden (CFU) per sample. Results are expressed as log-transformed values with median and interquartile range. *(B)* Frequency of barcodes for each mouse. Each color represents one barcode and the same color scheme was applied to both graphs. "no bar" represents a sample with no CFU. Data are combined from two independent experiments with n=3.

2.7.4. Additional material and methods for unpublished work

Assessment of neuromotor functions:

Rotarod analysis was performed as previously described[111,115]. Briefly, mice were trained for 5 days prior to challenge. Before each training, the mice were placed in the procedure room for 5-20 min to let them get used to the environment. 3 trials were performed daily with 15min inter-training interval. The 1-4th trainings lasted 3 min with fixed speed, while the 5th included acceleration. If mice fell before the end of the 3min training period, they were put back onto the bar until the 3-min session was done.

Training schedule by day:

Day1: 4 rpm → 4 rpm → 6 rpm

Day2: 6 rpm → 8 rpm → 8 rpm

Day3: 8 rpm → 10 rpm → 10 rpm

Day4: 10 rpm → 12 rpm → 12 rpm

Day5: Acceleration 4-40 rpm x3

Following challenge (i.e. infection), mice were monitored 3 times daily during 5 min tests with 15min inter-testing interval. The speed of the acceleration of the rotarod during the testing period was 4-40rpm for each 5min (300sec) trial. Mice were allowed to acclimatize to the room for 20-30 minutes prior to testing. If a mouse fell within 10 second from the start, it was put back on, but if it failed three times to remain on the Rotarod within the first 10sec, the mouse was remove from the trial and the time was recorded as 0sec. If a mouse did a passive rotation (hanging on) it was repositioned once, but if the behavior was repeated it was considered as the time of fall. Data was plotted as latency to fall in seconds with means and SEM.

CHAPTER 3. INVESTIGATING THE ROLE OF THE INNATE IMMUNE RECEPTOR STING DURING LM DISSEMINATION TO THE BRAIN AND THE PLACENTA

3.1. Summary of Results

The stimulator of interferon genes (STING) has been shown to function as a cytosolic host pattern recognition receptor. Upon activation, STING promotes a variety of immune responses including expression of the chemoattractant MCP-1 which recruits monocytes to sites of infection. Leukocytes have been implicated in the dissemination of microbial pathogens such as *L. monocytogenes,* to various locations within their hosts including the brain and placenta. However, the role of STING in promoting or preventing bacterial dissemination to either of these tissues remains poorly understood. In this study, we used STING-deficient mice (*Goldenticket,* Gt) to assess the role of STING in cerebral and placental colonization. Following oral inoculation, bacterial burden peaked in the central nervous system (CNS, which encompasses brain, brain stem, and spinal cord) around 4 days post infection. This peak was associated with an increase in bacterial burden across the host. We showed that this increase in cerebral *L. monocytogenes* was independent of STING's ability to induce Type 1 interferon (IFN) but dependent on signaling via its C-terminal tail. Further studies in Rag1KO-*Gt* double mutant mice suggested that the role of STING in limiting cerebral infections was most relevant during early stages of infection, but these studies were still preliminary and will require further experimentation. Finally, this work addressed the role of STING during intravenous and oral infection of pregnant mice and found that STING-deficiency somewhat protected placentas following intravenous infection but could promote heightened placental colonization following oral infection. This work was again preliminary and will require further studies to confirm and expand upon our results. Collectively, we found that STING-deficiency most often led to a heightened rather than a diminished colonization of the brain and placenta in mice, suggesting that the loss of bacterial control from the absence of STING-induced monocytes is more impactful, than the loss of a monocyte "Trojan horses" for bacterial dissemination.

3.2. Introduction

Pattern recognition receptors (PRRs) are guardians that detect microbial pathogens. PRRs recognize specific patterns innately established as non-self and respond to various categories of ligands. This mostly non-specific method of response is particularly helpful because it provides protection against a broad range of pathogens.[116] STING, the stimulator of interferon genes, is one such pattern recognition receptor that is found in the cytosol of host cells, associated with the ER. STING is activated downstream of the DNA sensor cyclic GAMP-AMP synthase (cGAS) or can directly recognize pathogen derived- cyclic-di-nucleotides[60,117]. The main function of STING, as suggested by its name, is to induce Type 1 interferons (IFN) and IFN-stimulated genes[60], which are highly effective at protecting hosts from viral infections. However, some intracellular bacteria such as *Chlamydia trachomatis*[118], *Mycobacterium tuberculosis*[119], and *L. monocytogenes*[60] (Lm) induce STING and Type 1 IFN, which can be detrimental to the host.

Upon intravenous infection with the facultative intracellular, Gram-positive, foodborne bacterial pathogen Lm*,* mice reproducibly develop high bacterial burden in the spleen and liver. STING-dependent Type 1 IFN activation benefits Lm bacterial pathogenesis[120–122], yet bacterial

burden in the spleen and liver of infected *Goldenticket* (Gt, STING-deficient) mice is similar to C57BL6/J control mice.[61] This suggests that STING activity does not play a major role in the systemic phase of infection for Lm. Upon foodborne infection however, STING activation leads to a host-wide reduced bacterial burden[61], suggesting a timing/location sensitive aspect of STING-mediated protection. Of note, STING activation results in more than Type 1 IFN responses, such as NF-kB activation,[123] autophagy,[124] and STAT6 activation.[125] STAT6 can induce production of the chemokine MCP-1, also called CCL2[125], which is a ligand for the monocyte cell-surface receptor CCR2. CCR2 activation initiates migration of monocytes out of the bone marrow and into circulation.[126,127] During intestinal infection, Lm is predominantly associated with monocytes, yet these cells do not support bacterial intracellular growth.[128]

In humans, Lm infection is generally mild and leads to a self-limiting gastroenteritis. However, in the case of immunocompromised hosts, Lm infection can lead to cerebral infection, causing permanent brain damage or even death.[31] In the context of cerebral listeriosis, monocytes have been extensively studied as a possible conduit for bacterial dissemination. Indeed, Lm can infect inflammatory monocytes ($Ly6C^{hi}$, $CCR2^{+}$) and hijack these migratory immune cells to access the blood-brain barrier and invade the central nervous system (CNS), which together is referred to as the "Trojan horse" hypothesis.[36–39] Although we showed in Chapter 2 that the bone marrow is not a reservoir for continuous cerebral seeding, it is still possible that monocytes participate in bacterial dissemination and Lm is actually known to protect infected monocytes from CD8 T cell mediated killing.[39]

Similarly to cerebral listeriosis, infections in pregnant individuals can be a severe disease and lead to miscarriages. In the context of pregnancy, Lm has also been proposed to use a "Trojan horse" mechanism to disseminate. Indeed, Lm is able to access the cytosol of host cells, and take advantage of host actin polymerization machinery via the virulence factor ActA to spread from cell to cell without regaining the extracellular space.[32] Previous work suggested that ActA is required for bacterial dissemination across the placenta[51,129] and that extracellular bacteria in the blood are not a major contributor of placental colonization.[12] Together these findings suggest that Lm co-opts a host cell for transport across the placenta.

Knowing that orally infected STING-deficient mice have a defect in monocyte recruitment from the bone marrow to systemic sites[61], we hypothesized that this decreased availability of "Trojan horses" would lead to more limited opportunities for bacterial dissemination to the brain and placenta, and thus to a decreased Lm burden in these tissues. Our work however disproved this hypothesis, establishing that STING-deficiency instead leads to an increase in bacterial load in the brain and placenta that is associated with an increased systemic bacterial burden in orally infected mice.

3.3. Results

3.3.1. Dynamics of infection across organs in STING deficient mice

Previous work (Louie. A. data not shown) thoroughly characterized the daily dynamics of Lm expansion and clearance following oral infection in wild-type mice, and showed a peak of sickness on days 4-6 post infection (DPI)[29]. In addition, Louie et al. established that STING activation restricts intracellular Lm in intestinal tissues[61], so to assess the role of STING in bacterial dissemination to the brain, we first sought to characterize the overall dynamics of infection across foodborne-infected hosts.

We infected mice orally with $1x10^9$ CFU following pretreatment with streptomycin and monitored weight and bacterial load over the course of 8 days, collecting cohorts of mice every 24h. As previously reported[61], Gt mice lost about 20% of their starting weight by 5 DPI then mostly recovered by 8 DPI (Fig3.1A). Bacteria in the brain, brain stem and spinal cord all peaked at 4-6 days post infection, similar to bacteria within the rest of the host. However median CFU per organ rarely accumulated more than a few hundred bacteria in the CNS, which is ~1000-fold lower than in the spleen or liver (Fig. 3.1B-C), suggesting that bacterial colonization and/or expansion are more restricted in the CNS.

These data could imply that cerebral infections may indeed be promoted by STING activity and thus stalled in Gt mice. However, we needed to compare WT and Gt infections more directly, knowing that CNS infections peak at 4-6DPI.

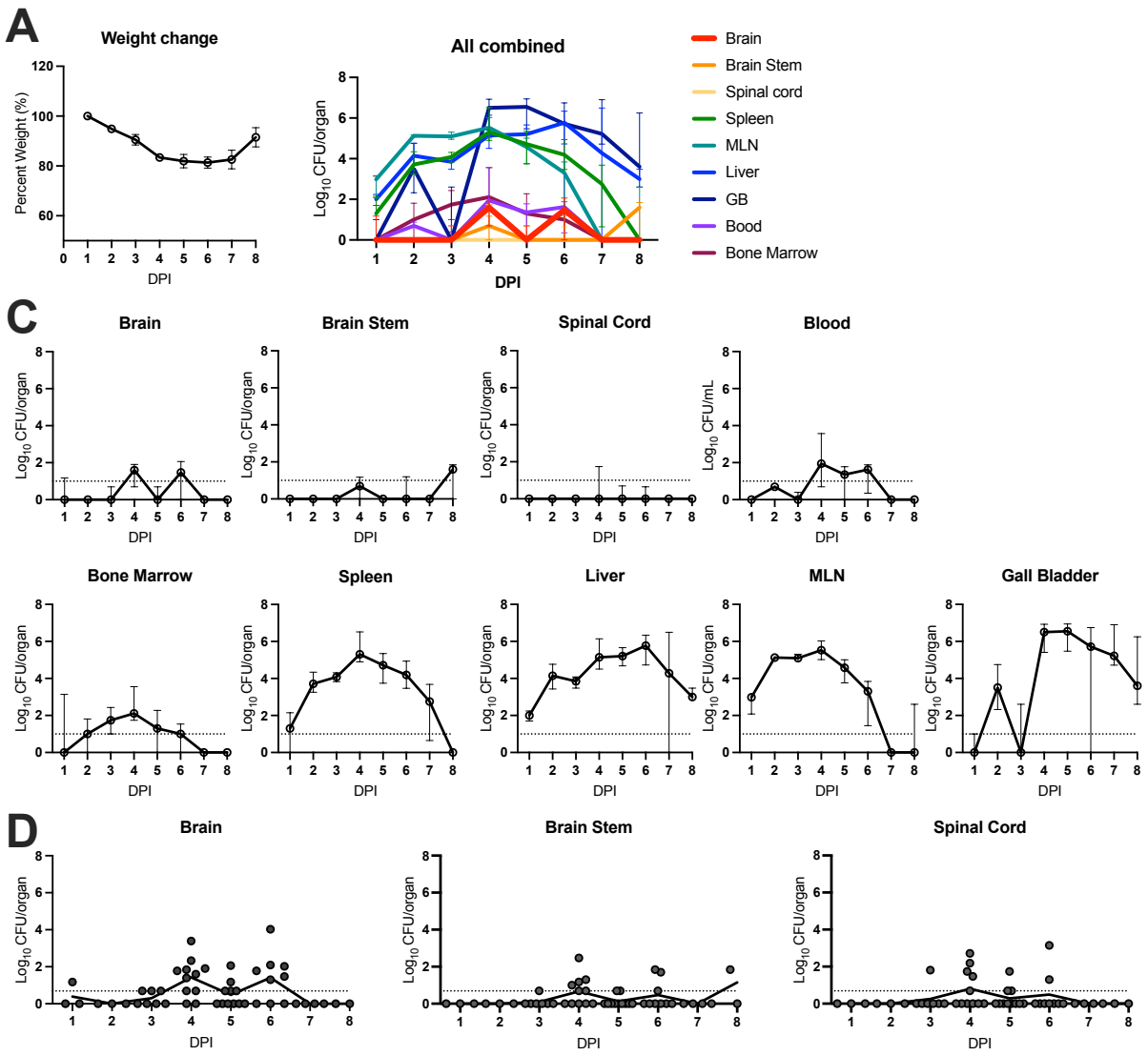


Figure 3.1. Tissue colonization dynamics in Sting-deficient mice. 8–12-week-old female goldenticket mice were infected orally with 1x10^9 CFU of WT Lm. All mice were monitored for weight change daily and cohorts of mice were sacrificed every day over the course of 8 days. (A) Percent weight change normalized to 1 day post infection. Results are expressed mean with SEM. (B) Bacterial burden determined by plating for CFU for all mice in all organs and (C) bacterial burden for all mice separated per organ: brain, brain stem, spinal cord, blood, bone marrow, spleen, liver, MLN, gall bladder. CFUs are expressed as log-transformed values with median and interquartile range, and dashed lines indicate limits of detection. (D) Same data as (C) but in CNS only, with CFUs plotted for each individual mouse. Line represents the median per day. Data are combined from 4 independent experiments and D1 n= 3, D2 n= 3, D3 n= 7, D4 n= 11, D5 n= 11, D6 n= 9, D7 n= 4, D8 n= 3.

3.3.2. Assessing which functions of STING are involved in bacterial control

The previous dataset focused on longitudinal data, i.e. the change in bacterial burden *over time*. However, the amplitude of the results was quite wide in the brain between 4-6 DPI (~4 logs, Fig 3.2D) so we sought to compare C57BL6/J (B6) and Gt mice in that specific time frame. We orally infected mice with 1x10^9 CFU following streptomycin pre-treatment and assessed bacterial burden and weight loss at 4-5DPI. STING-deficient mice became sicker than B6 mice, accumulating more bacteria at systemic sites (Fig 3.2A) and losing more weight (Fig

3.2B), as previously described[61]. In the CNS, we found an increase in accumulation of Lm in the brain, brain stem, and spinal cord of Gt mice compared to B6 mice. This suggested that STING activity may actually be involved in controlling CNS infection rather than promoting it, and differed from our original hypothesis. Indeed the STING-dependent decrease in monocyte recruitment to the intestines[61] would have two main effects: 1) fewer "Trojan horses" (infected monocytes) in circulation and fewer opportunities for bacteria to get to the brain, and 2) more dramatic loss of control of bacterial accumulation host-wide. Our results suggest that the second effect of monocyte decrease is more impactful in the context of CNS infection.

However, STING activity has more downstream effects than only STAT6-mediated monocyte recruitment. Indeed, upon STING activation, the kinase TBK1 is recruited and phosphorylates the transcription factor IRF3, which induces production of Type I IFN and subsequent induction of IFN stimulated genes[130]. However, mice lacking the Type1 IFN receptor do not have a Ly6C^{hi} monocytes migration defect to the liver during intravenous infections[131] and Type 1 IFN does not promote susceptibility in foodborne infections.[61,132] This suggests that STING-induced Type 1 IFN is not the main driver of resistance to Lm, but we still addressed this question specifically for CNS infection using mice with a serine 365-to-alanine (S365A) mutation in the C-terminal tail of STING, which specifically leads to a lack of STING-depended type I IFN response[133]. Upon oral infection, S365A mice tended to be different from Gt and somewhat phenocopy/ were more protected than B6 mice, both systemically and in the CNS (Fig 3.2). This confirmed that the Type 1 IFN-inducing function of STING is not the main driver of STING-depended control of cerebral listeriosis.

When STING is activated, TBK1 interaction with the C-terminal tail (CTT) leads to Type 1 IFN responses and STAT6-dependent MCP-1 production (monocyte recruitment), but is also involved in more evolutionarily conserved responses like NFkB activation and autophagy.[133–135] Orally infected ΔCTT mice, which entirely lack the STING C terminal tail, generally responded in a manner that was closer to Gt mice than to B6 or S365A mice, but not quite to the same level as Gt mice (Fig 3.2). This suggests that interferon-independent STING activity may be involved in controlling CNS infection and further establishes STING's early role in controlling systemic infection as its major impact on cerebral infection rather than modulation Trojan horse availability.

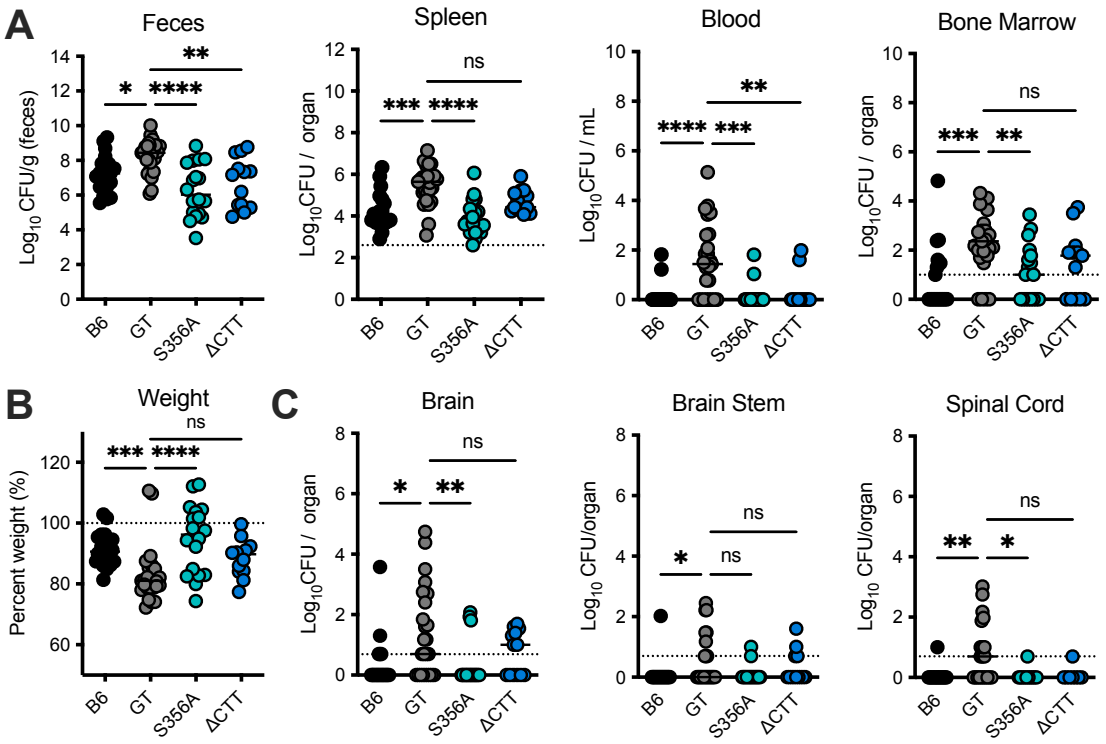


Figure 3.2. Assessing which functions of Sting are involved in cerebral infection. 8–12-week-old female mice were infected orally with 1x10^9 CFU of WT Lm. Mice were either C57BL6/J (B6), goldenticket (GT), S365A, or ΔCTT. Organs were collected 4-5 days post infection. (A) Bacterial burden in control tissues: feces, spleen, blood, bone marrow. (B) Percent weight change normalized to 1 day post infection. The bars represent mean value for each group and the dotted line is 100%. (C) bacterial burden in the central nervous system: brain, brain stem, spinal cord. Bacterial burden was determined by plating for CFU and expressed as log-transformed values with each dot representing one mouse. The lines are the median values and dashed lines indicate limits of detection. Data are combined from 5 independent experiments B6 n=19, GT n=25, S365A n=18, dCTT n=13. Statistical significance was calculated using one-way ANOVA against Gt: ****p<0.0001; ***, p<0.001; **, p<0.01; *, p<0.1.

3.3.3. Assessing the impact of STING deficiency in our newly developed model of food-borne induced cerebral listeriosis

Although we established that a limitation in monocyte "Trojan horses" did not lead to a less efficient brain infection at early stages of infection, we still wondered if STING could have a role in cerebral Lm accumulation over time. Indeed, our work in Chapter 2 suggested that Rag1KO mice take ~1-3 weeks to accumulate high levels of bacteria in the CNS. Thus, we bred Gt and Rag1KO mice together to establish a Rag1KO/Gt double mutant mouse colony that would allow us to test the role of STING in our efficient model of orally-induced cerebral listeriosis.

We orally infected Gt, Rag1KO, and Rag1KO/Gt double mutant mice with 1x10^9 CFU of WT Lm following streptomycin pre-treatment. At 4dpi, Rag1KO mice controlled the systemic infection better than Gt, possibly due to an increased production of IFN gamma by NK cells, while Rag1KO/Gt mice phenocopied Gt (Fig 3.3A). This suggested that effects of STING-deficiency were dominant over effects of Rag1-deficiency at early stages of infection. In the CNS, very few bacteria were recovered in any of the conditions, which could be expected with

this few mice, yet a small bacterial increase was noticeable in the brain of Rag1KO/Gt mice (Fig 3.3A).

When we monitored Rag1KO/Gt mice over longer periods of time, we found that these mice lost weight and reached endpoint criteria at a similar rate as Rag1KO mice: ~2weeks (chapter 2, Fig 3.3B). Two out of five mice were euthanized for developing behavioral changes, which was a lower rate than that of Rag1KO alone (chapter 2, Fig 3.3C), but this may again be due to the low number of mice in this experiment. When we assessed bacterial burden, we found that the bacterial burden in the CNS was slightly lower than previously observed in Rag1KO (~1log down) and the CFU in the blood was slightly higher (~1log up), although both datasets are highly variable (across 5 logs in chapter 2, across 3 logs in Fig 3.3D). The results from Rag1KO/Gt mice were slightly different from Rag1KO, but still fit within the bounds of our Rag1KO results and suggest that STING activity has little impact on development of cerebral infection over time.

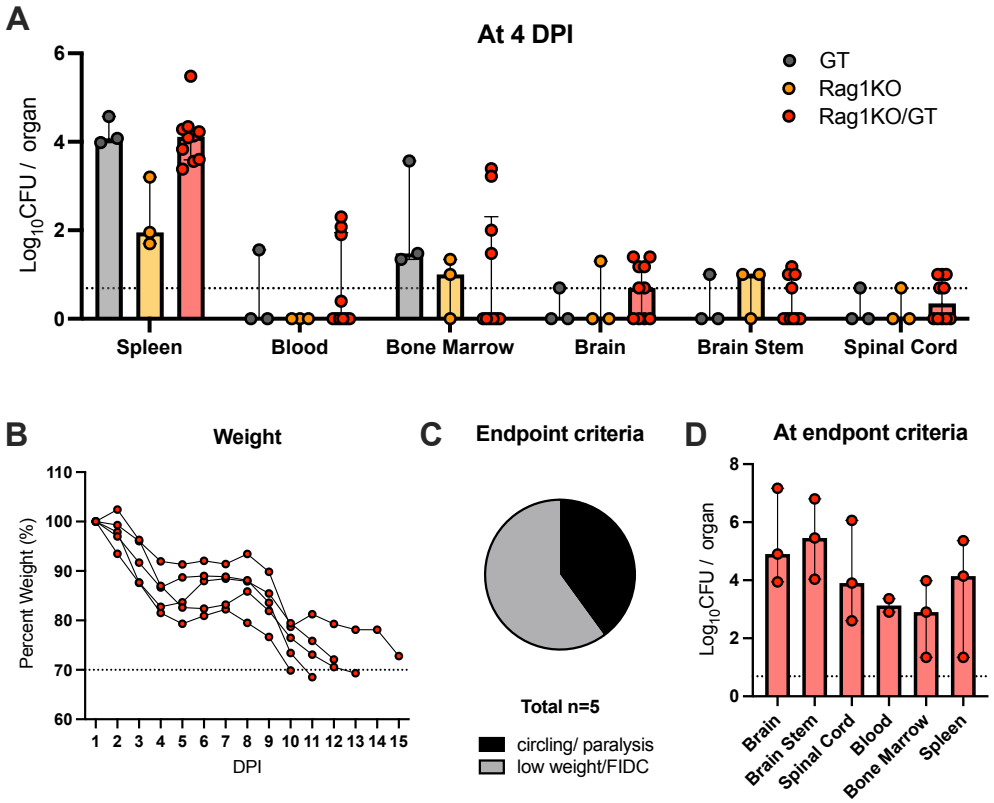


Figure 3.3. Cerebral infections at later stages of infection. 8–12-week-old female mice were infected orally with $1x10^9$ CFU of WT Lm. Mice were either goldenticket (GT), Rag1KO, or Rag1KO/Gt. (A) Bacterial burden at 4 days post infection (DPI). Data are combined from 2 independent experiments with GT n=3, Rag1KO n=3, Rag1KO/GT n=10. (B) Percent weight change normalized to 1 day post infection for Rag1KO/GT. Mice were monitored daily until they reached endpoint criteria. (C) Proportion of mice that reached each endpoint criteria: circling/paralysis (behavior change), or low weight (>30%)/FDIC(found dead in cage). (D) Bacterial burden of mice that reached endpoint criteria (excluded FDIC). Bacterial burden were determined by plating for CFU and expressed as log-transformed values with each dot representing one mouse and showing median values and interquartile range. Dashed lines indicate limits of detection for CFU (A and D) and 30% weight loss for weight (B). Data are from 1 experiment with Rag1KO/GT n=5.

3.3.4. Assessing the role of STING during pregnancy in mice

After establishing that STING did not to have a specific role in promoting cerebral infection and instead probably limited cerebral listeriosis by controlling host-wide bacterial accumulation, we wondered about the role of STING in another relevant context for listeriosis: Pregnant hosts.

To assess the role of STING during pregnancy, we first infected pregnant female mice on embryonic day 9-11 with 1-5x10^3 CFU intravenously. WT and Gt mothers had similar bacterial loads in the spleen at 2DPI (Fig 3.4A). This was expected since STING has been shown to only have a limited impact on disease development during the systemic phase of infection.[61] Previous work suggested that the bottleneck for colonization of the placenta is high, but that bacteria readily replicate within this tissue,[12] and that leukocytes may act as "Trojan horses" during bacterial dissemination.[46] Thus, similar to our hypothesis in the CNS, we questioned whether impaired STING-dependent monocyte recruitment would lead to decreased bacterial crossing of the placenta. In the placenta of IV infected mice, we found that the bacterial burden was not significantly different between B6 and Gt, yet the proportion of placentas that were colonized was 10% lower in STING-deficient mice (Fig 3.4B). This suggested a potential role for STING to indeed promote infection via monocytes in intravenously infected mice.

Since the effects of STING are different in intravenously and orally infected mice[61], we sought to assess the role of STING in orally infected pregnant mothers. Mice were again infected orally at embryonic days 9-11 with 1x10^9 CFU of WT Lm. Bacterial load in the spleen was similar across genotypes (Fig 3.4A), which slightly differed from naïve mice where STING-deficiency leads to higher bacterial burden (Fig 3.4A), but this may be affected by our animal numbers which were very limited in this experiment. With regards to placentas, STING-deficiency led to higher bacteria burden and higher probability of being infected (Fig 3.4B) suggesting an important role for STING to control infection – independent from the Trojan horse hypothesis, similar to our CNS results.

These experiments were preliminary and limited by overall difficulties to induce successful pregnancies (data not shown), but suggest that pursuing a better understanding of the role of STING during pregnancy might be revealing.

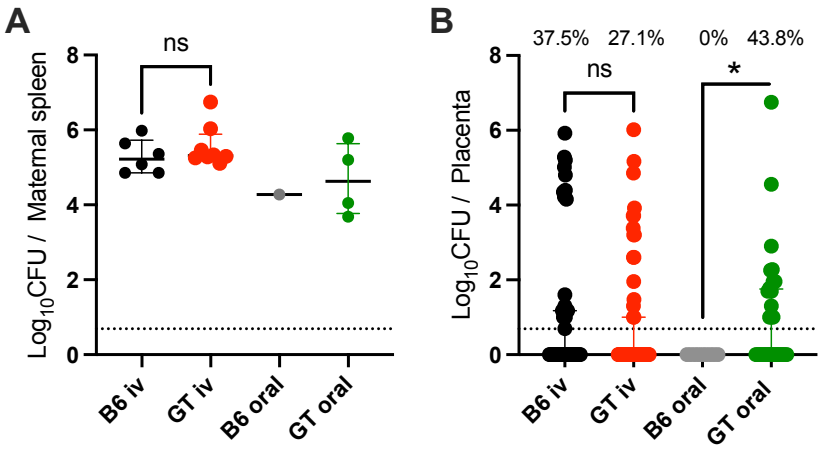


Figure 3.4. Placentas of Sting deficient mice are not protected from infection. 8–12-week-old C57BL6/J (B6) and goldenticket (GT) female mice were infected intravenously (iv) with 1-5x10^3 CFU or orally with 1x10^9 CFU (following streptomycin pre-treatment) of WT Lm on embryonic day 9-11. At 2 days post infection, bacterial burden was assessed by plating for CFU in (A) spleens and (B) individual placentas. Results show individual organs expressed as log-transformed values with median and interquartile range, and the dashed line indicates the limit of detection. In (B) the percentages represent the number of individual placenta with CFU>0. Statistical significance was established by Mann-Whitney test with significance threshold set at $p<0.05$. IV data are combined from 4 independent experiments with B6 n=6/placenta n=48 and GT n=8/placenta n=59. Oral data are combined from 2 independent experiments with B6 n=1/placenta n=9, GT n=4/placenta n=32.

3.4. Discussion

In this study, we sought to understand the role of the innate immune receptor STING on dissemination of Lm during cerebral and placental infection in mice. Based on the literature, we hypothesized that monocytes recruited upon STING activation may be hijacked by Lm to promote its dissemination to immunopriviledged tissues. In this context, we expected the CNS and placentas of STING-deficient mice to be protected from Lm infection. We first performed an in-depth characterization of bacterial change over time in STING-deficient (Gt) mice following oral infection and found that bacterial counts in the CNS were multiple logs lower than the bacterial load in the spleen or liver (Fig 3.1). These data may have suggested that STING activity indeed limited bacterial infection of the brain. However, upon comparison of STING-deficient mice with wild-type mice at peak CNS infection (Fig 3.1), the bacterial burden in the CNS of B6 mice was lower still than in Gt mice, contradicting our hypothesis and suggesting that STING-activity instead limits cerebral infection (Fig 3.2). We leveraged multiple previously established mouse models to specifically assess the impact of the different functions of STING during infection (Gt, S365A, and ΔCTT) and confirmed that the Type1 IFN-induction function of STING is not responsible for control of cerebral infection (Fig 3.2). We previously established that cerebral infection is often low during early days of infection, but that Rag1KO mice could develop much more severe cerebral listeriosis over time (Chapter 2). We thus developed a Rag1KO/Gt mouse model to assess the role of STING over the course of a more prolonged infection but found that STING does not play a major role at late stages of infection (Fig 3.3). Finally, we assessed the role of STING following intravenous (IV) infection and oral infection of pregnant mice. Placentas from IV infected STING-deficient mice were similar to those from wild-type mice, yet they tended to have fewer instances of infected placentas. Following oral infection, the reverse was true with STING-deficient mice generally harboring a higher bacterial

load (Fig3.4). Together, our findings suggest that STING-induced monocytes are not a main driver of bacterial dissemination via "Trojan horses", but rather confirms and expands upon previous work suggesting that STING activity impacts bacterial control at the intestinal barrier in a type 1 IFN-independent manner. Of note, some of our work in this chapter was quite preliminary so conclusions are made knowing that further experimentation will be required to validate our claims.

The spread of Lm to the CNS was extensively studied in Chapter 2 and these results shed additional light upon our results in this chapter. Indeed, Chapter 2 established that infections of the brain upon food-borne infection are very rare, but that bacterial replication after the initial invasion event is highly efficient, as evidenced by highly infected yet monoclonal brains following infection with barcoded Lm[136]. Thus, it makes sense that a defect in bacterial dissemination, such as a limitation in STING-mediated recruitment of monocytes, would not dramatically affect bacterial burden in the CNS so long as bacteria have a different way of accessing the CNS. Indeed, Lm is able to spread to the CNS efficiently from extracellular bacteria in the blood and inefficiently from intraneural transport from the intestines or another organ. Interestingly, orally infected STING-deficient mice have a higher systemic bacterial burden, which may provide increased opportunities for Lm to invade nerve endings in the periphery and use intraneural trafficking to disseminate to the brain. It is tempting to propose that Lm will travel directly from the highly infected intestines[61] to the CNS but our previous work established that this is unlikely since barcoded bacterial populations in the intestines diverge from the brain population overtime[136]. Yet it is still possible that Lm would efficiently disseminate from another tissue via the intraneural route and this would be very interesting to pursue with the use of barcoded bacteria and the STAMPR toolkit[3,20].

With regards to placenta infection, our results are still very preliminary because of technical difficulties with breeding (data not shown). We postulated that transfer of pregnant mice between facilities may be a source of our difficulties, but matings were mostly unsuccessful within the BSL-2 facility even when mice were not infected. We believe this may be due to the high traffic of individuals within the small room in the shared BSL2 facility and recommend that further explorations with pregnant mice, be done by ordering pregnant mice directly from vendors. In addition, we chose to use mice as our model system, in order to have comparable data across our studies. However, mouse placentas are physiologically very distinct from humans,[46] and future studies could focus on more relevant models such as guinea pigs[12,14,49,52] or non-human primates[137,138].

Despite the small number of animals, our findings in pregnant mice are very intriguing as they suggest that STING-deficiency leads to opposite responses depending on the route of infection. In order to further assess the role of STING in bacterial spread to the placenta, heterozygous male and female mice could be mated, leading to an array of embryos with different genotypes within the same uterus. This system would provide a controlled environment to assess of the role of fetal STING-activity during infection. Infection of pregnant Gt mothers mated with WT males, or WT mothers mated with Gt males could also provide insights into the role of maternal STING in a context where pups are all heterozygous. In

addition, prenatal infections have been linked with an increased risk of neonatal neurodevelopment disorders(ref). With Lm, a low-grade infection of pregnant female mice, leads the surviving pups to develop neurodevelopmental disorders in adulthood.[10] Assessing the role of STING in neural development following in utero infection would be an additional interesting axis of research.

Overall, our work provides insights into the impact of STING on the dissemination patterns of Lm to the brain and placenta, laying the groundwork for future analyses on the effect of innate immunity on bacterial spread.

3.5. Materials and Methods

Animal models

C57BL/6J mice were purchased from the Jackson Laboratory (stock #000664) and maintained under specific pathogen-free conditions at the University of California, Berkeley animal facility. *Goldenticket* mice (Gt, C57BL/6J-*Sting1*^{gt}/J, Jackson Laboratories stock #017537), STING S365A mice (C57BL/6J-*Sting1*^{em1Vnce}/J, Jackson Laboratories stock #035660), and STING ΔCTT mice (C57BL/6J-*Sting1*^{em2Vnce}/J, Jackson Laboratories stock #035661) were obtained from the Vance lab at the University of California, Berkeley. Rag1KO mice (B6.129S7-Rag1tm1Mom/J, Jackson Laboratories stock #003729) were obtained from the Barton lab at the University of California, Berkeley. Rag1KO/Gt mice were generated in house by crossing founders from Rag1KO and Gt lines. Homozygous lines were generated by interbreeding and final genotypes were assessed using the genotyping services from Transnetyx and the probes suggested by the Jackson laboratories (see stock numbers above). All mice were maintained under specific pathogen-free conditions within the University of California, Berkeley animal facility. Only 8- to 12-week-old female mice were used for all experiments with sex- and age-matched controls according to institutional guidelines for animal care. This study was performed in strict accordance with the recommendations in the Guide for the Care and Use of Laboratory Animals of the National Research Council of the National Academy of Sciences [99] and with university regulations. All protocols were reviewed and approved by the Animal Care and Use Committee at the University of California, Berkeley (AUP-2016-05-8811).

Bacterial strains and growth conditions

All *L. monocytogenes* strains used in this study were derived from 10403S[100] which is streptomycin resistant and propagated in filter-sterilized brain heart infusion (BHI) medium (BD) at 37°C while shaking with streptomycin (200 μg/ml) overnight. Cell density was measured by optical density (OD600). Inoculums were prepared by washing log-phase bacteria twice in PBS and resuspending in the appropriate volume of PBS depending on the infection route. Frozen bacterial stocks were stored at -80°C in BHI plus 25% glycerol.

Foodborne infections

Prior to infection, 20 mg/ml of streptomycin sulfate was added to the drinking water. After 24 h, chow was removed to initiate an overnight fast and mice were transferred to fresh cages. 48

h after streptomycin was added to the water, mice were isolated, fed a 3-mm piece of bread with 3µL of butter and $1x10^9$ CFU *L. monocytogenes* in 5uL PBS. Mice were then returned to cages containing standard drinking water and chow. The inoculum was plated for CFU to check the efficiency of each infection
Mice were either euthanized on designated days as specified in the text and figure legends, and tissues were harvested as described below, or mice were monitored daily for weight loss and behavioral changes until development of "endpoint criteria" (i.e. head tilt, circling, mild to severe paralysis, >30% weight loss, and lethargy, as described in our protocol). Upon reaching an endpoint criterium, mice were euthanized, and tissues were harvested.

Intravenous infections
Mice were infected intravenously via the tail vein with $1\text{-}5x10^3$ CFU of wild-type *L. monocytogenes* in 200µL of sterile PBS as previously described[101]. 48 hours post-infection, mice were euthanized, and tissues were harvested as described below.

Infection of pregnant mice
Timed pregnancies were set up in the evening either in the BSL2 or BSL1 facilities at UC Berkeley and embryonic day 0.5 was set upon observation of a mating plus as described by the UC Berkeley Office of Laboratory Animal Care – Rodent colony management handbook. Pregnant female mice were then left undisturbed until time of infection which proceeded as described above. Mice were euthanized 48 hours post-infection, and maternal spleens and individual placentas were harvested as described below.

Tissue harvest
Blood (~500uL) was collected via cardiac puncture immediately after euthanasia in 100uL 50 mM EDTA as an anticoagulant (adapted from Senay et al.[93]). Immediately after blood collection, mice were perfused with 20mL PBS. Most samples were homogenized in 0.1% IGEPAL CA-630 (Sigma) and for bone marrow, the left femur and tibia were collected together then crushed with a mortar and pestle before homogenizing. Gallbladders and feces were homogenized in 1xPBS. Dilutions of homogenates were plated to enumerate CFU and full samples were plated for STAMPR analysis following incubation at 37°C overnight. In instances where growth of commensal bacteria was a concern, plates were supplemented with nalidixic acid, LiCl, and glycine, which does not affect Lm growth. Antibiotics and media supplements were used at the following concentrations: streptomycin at 200 µg/ml, nalidixic acid at 15 µg/ml, LiCl at 6 mg/ml, and glycine at 6 mg/ml.

Statistical analysis
All statistical analyses were performed using GraphPad Prism version 10.0.1 for MacOS, GraphPad Software, San Diego, CA, USA. Details for all statistical analyses can be found in the figure legends.

CHAPTER 4. DYNAMICS OF L. MONOCYTOGENES DISSEMINATION IN TUMOR-BEARING MICE

4.1. Summary of results

Listeria monocytogenes (Lm) is a facultative intracellular bacterial pathogen that induces potent cell-mediated immunity. This ability can be leveraged in the context of cancer immunotherapy by using Lm as a live vector that promotes immunological responses in the tumor microenvironment (TME). Previous work established a model of intravenous (IV) and intratumoral (IT) combination therapy with attenuated Lm that led to control of tumor growth, but these results were not recapitulated with IV or IT injections alone. In addition, Lm was found to persist in the TME regardless of inoculation route. Here, we follow-up on this work with a preliminary investigation of the impact of the route of inoculation on bacterial spread in tumor-bearing mice using barcoded Lm. Following IV injection, Lm colonized tumors within 4 hours, but only to a limited degree. Bacteria then dramatically expended locally with little to no further migration of bacteria from systemic sites into the tumor. Following IT inoculation, Lm was able to spread beyond the tumor quite efficiently, seeding systemic organs with diverse populations, but again migration between tissues was limited by 3 days post injection. In the context of IV and IT combination therapy, where only IT injected bacteria were barcoded, Lm again migrated into systemic tissues from the tumor during the first 4 hours post inoculation, but this was followed by a massive clearance event where most of the Lm biomass and clonal diversity were lost by 3-16 days post injection. If bacteria still remained in the TME, then the bacterial burden was generally high with a mostly clonal population, suggesting that some host pressure cleared most of the early colonizing bacteria, but a few clones found a niche that allowed them to evade clearance and persist efficiently. Overall, our work provides a more detailed picture of the pressures faced by Lm in the context of tumor-bearing mice, which may provide insights into the mechanisms of tumor clearance in IV+IT combination immunotherapy.

4.2. Introduction

In the late 1800s, Dr. William Coley, a sarcoma surgeon, injected live bacteria into patients with inoperable tumors, hypothesizing that the infection may have the side-effect of reversing tumor progression[139]. Around this time the field of immunology was emerging as an academic study with discoveries such as Louis Pasteur's germ theory of infection, Robert Koch's exploration of the roots of infectious diseases, and Élie Metchnikoff's discovery of phagocytosis.[140] Coley's first experiment was successful and led to a long exploration of the impact of allosteric activation of the immune system on tumor regression using bacteria and bacterial compounds that became known as "Coley's toxin".[139] Nowadays, injection of cultured bacteria remains a method used to treat certain bladder cancers[141] and an active area of study for cancer immunotherapies.

Listeria monocytogenes (Lm) is a facultative intracellular pathogen that induces potent innate and adaptive immune responses[58] and has been a source of interest for such bacteria-based cancer immunotherapies. Lm can infect antigen-presenting cells, then grow and secrete antigens into their cytosol, without rapidly inducing host cell death, thus promoting highly effective cell-mediated immune responses.[142] Lm can also be attenuated by deletion of specific virulence factors, such as ActA which mediates cell-to-cell spread,[32] making it a subject of

interest for bacteria-based human therapies.[63,143–147] In addition, Lm can easily be manipulated to express tumor-associated antigens and provide optimal tumor-targeted immune responses. All of these characteristics have made genetically engineered Lm the subject of multiple bacteria-based immunotherapy clinical trials for cancer,[147] but results have been variable.[70,72,73,148,149] Recent work is now turning back towards Coley's work and investigating the use of live-attenuated but otherwise unmodified Lm as a treatment for cancer.

Garcia-Castillo et al.[74] investigated the possibility of harnessing Lm-specific immune responses to stimulate anti-tumoral responses within the highly immunosuppressive tumor microenvironment (TME).[150,151] They injected attenuated Lm (ΔactA) either intravenously (IV), intratumorally (IT) or a combination of both (IV+IT) into tumor-bearing mice. Neither of the first two conditions led to control of tumor growth, but combination therapy was successful at restricting tumor progression. Further assessment of bacterial burden in various organs established that Lm was cleared from systemic organs ~1week post injection, regardless of inoculation route, yet Lm persisted within the hard-tumor tissue for up to 15 days in IV or IT infected mice. Following combination therapy, Lm also persisted in most tumors for up to 10 days post IT inoculation but was eventually controlled to below the limit of detection. This work established that Lm is disseminating and experiencing host pressures differentially depending on inoculation routes, which may have an impact on treatment efficacy.

The study of bacterial colonization, spread, replication, and clearance after invading a host can be efficiently conducted using barcoded bacteria[3]. Populations of non-clonal yet physiologically equivalent microbes have been extensively used to investigate bacterial dissemination patterns and quantify bottlenecks in various model systems. This includes intestinal colonization,[4,4,29] systemic spread,[4,17] cerebral infections,[82,136] and many others, but has yet to be done in tumor-bearing mice. The previously described STAMPR pipeline[20] provides multiple metrics that are helpful for these investigations. In particular STAMPR provides an assessment of the number of bacteria from the inoculum that establish the population within a particular tissue at a particular time, and we refer to this metric as the founding population (Ns). In addition, the genetic distance (GD) establishes how broadly similar two bacterial populations are, while FRD provides insights into the prevalence of shared barcodes (for more information about each of these metrics, please refer to Chapter 2). Overall, understanding pathogen dynamics would provide insights into the tissues that efficiently exchange bacteria with the tumor and establish whether specific organs behave as reservoir for bacterial shedding into the tumor.

Here, we generated a library of ~200 barcoded Lm in a ΔactA- attenuated background to quantify the bottlenecks involved in Lm spread into and persistence within tumors. We found that bacterial dissemination into the tumor was mostly limited following IV injection, but quite efficient out of the tumor following IT injection. Regardless of inoculation route, little to no further bacteria exchange was observed between tissues. After 3 days, bacterial population structure in tumors of IT injected mice were quite variable suggesting host responses to infection that were variable as well. In mice that received combination therapy, Lm somewhat spread to systemic sites but we observed a massive clearance event by 3-16 days post infection

(DPI), and any tumors that remained infected were generally quite monoclonal. These results are still quite preliminary, but showcase the promise of barcoded bacteria as an efficient method for understanding Lm spread to the tumor and more broadly how to improve bacteria-based cancer treatments.

4.3. Results

4.3.1. Library generation and quality control

In order to investigate the dissemination patterns of Lm in tumor-bearing mice, we first generated a library of barcoded Lm in the ΔactA background strain. Once the plasmids were stably inserted into the Lm chromosome using an integration vector and the library was completed, we assessed the quality of the library along a calibration curve. Overnights started from frozen stock where diluted into fresh media and grown to mid-log before plating dilutions ranging from 1-10^6 CFU. The calibration curve consisted of a comparison between the number of bacteria experimentally identified in the sample (CFU), and the computationally acquired value of "founding population" (Ns)[3]. Since Ns is a measure of the number of bacteria from the inoculum that were at the origin of the population in a sample[3] and there were no host bottlenecks that restricted the population in the calibration curve, we expected a 1:1 ratio between CFU:Ns, until reaching the computational upper limit of detection. Assessment of the population size was highly accurate until ~10^4 CFU, at which point the size of the library itself (~200 barcodes) became too stringent of a bottleneck and the founding population began to plateau (Fig4.1A).This limitation was expected from our library size and it mirrored results from the calibration curve for the WT barcoded library (Fig 4.1B), which we and many other have successfully used.[4,29,136] This library size is sufficient for our purposes as it still allows us to identify changes between bacterial population structures efficiently.

We further analyzed the quality of the ΔactA library by checking the frequency of each barcode in the qualibration curve samples. Our results confirmed that all barcodes were represented mostly evenly (Fig 4.1C), so we prepared samples for *in vivo* inoculation. Inoculum preparation involves growing bacteria from the frozen stock over night, then diluting back into fresh media until bacteria reach exponential phase of growth. Bacteria are then diluted to the desired dose in sterile PBS. In this context, we noticed that 3 barcodes (Lm12(green), Lm65(red), Lm111(brown)) were over-abundant in our starting dose (Fig 4.1D). For all further analyses, we made sure to specifically monitor the proportion of these three barcodes during *in vivo* experiments, but in almost all mice, these 3 barcodes did not become overly dominant (Fig 4.S1-3), suggesting that their slightly overabundance in the inoculum did not translate into an advantage *in vivo* and validating our use of the library.

However, three different barcodes (Lm5 (purple), Lm23 (blue), Lm 70(orange)) did consistently become overly abundant in systemic organs at 3 DPI (Fig S4.1-S4.2) across IV and IT inoculated mice. We first expected that this was a sign of contamination during sample preparation, but this dominance phenotype manifested specifically at 3DPI rather than 4 hours post injection (HPI) and was consistent across mice in independent experiments. This suggested

that our library included bacteria with barcodes that were neither overly represented in the stock library (Fig 4.1C), nor had an advantage during inoculum preparation and growth in broth (Fig 4.1D), but did gain a competitive advantage during *in vivo* infection. Interestingly, these barcodes were most abundant in the spleen and liver of mice, but less so in tumors (Fig S4.1-S4.2), suggesting that any mutation these bacteria acquired during preparation of the library, did not provide them with an advantage that was specific to growth within tumors. We thus proceed with our analysis of bacterial dissemination using the newly generated library.

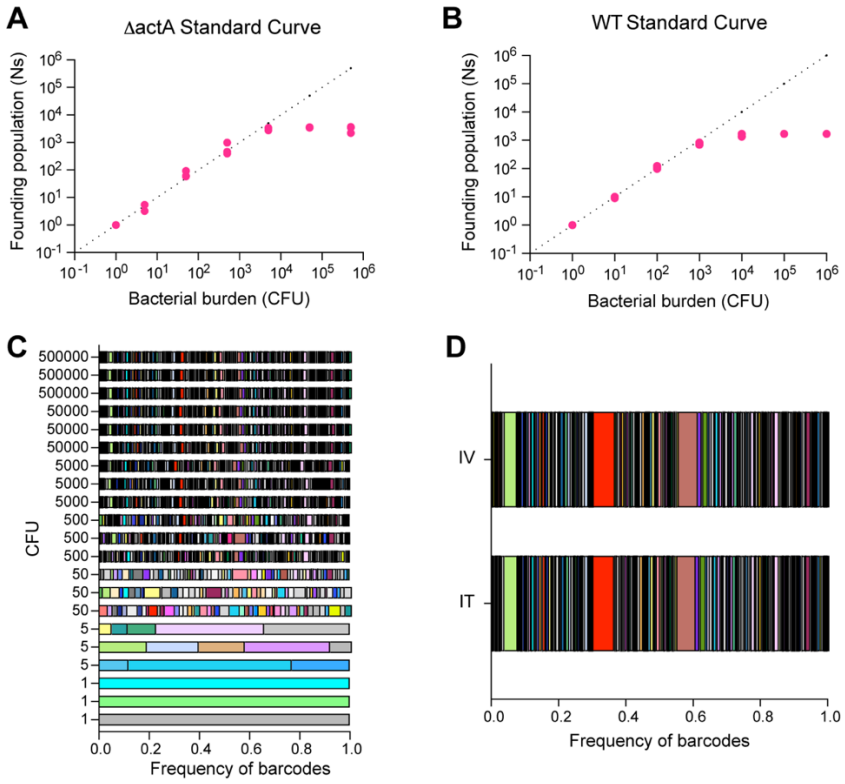


Figure 4.1: Quality control of the newly generated barcoded library in ΔactA Lm. The library was generated by insertion of a pooled plasmid library containing 200 unique barcodes and stably integrated into the Lm chromosome. (A and B) standard curve for the newly generated ΔactA Lm library (A) and the standard wild-type Lm library (B). The dots represent each sample with the experimentally assessed bacteria burden (CFU) and the computationally assessed founding population. Each dose was included at least two replicates and the dotted line represents a 1:1 ratio. (C and D) Frequency of barcodes for each sample in the ΔactA Lm standard curve (C) and the inoculums for one experiments where mice were infected either intravenously (IV) or intratumorally (IT). Each row represents one sample, and each color represents one barcode (the same color scheme was applied to all graphs).

4.3.2. IV inoculation leads to low colonization of the tumor, high replication within the tumor, and little to no migration from systemic sites into the tumor

In studies of Lm pathogenesis bacteria are most often delivered via intravenous injection.[143] In their investigation of ΔactA Lm as a therapy to help control tumor progression, Garcia-Castillo et al. found that IV injection of $1x10^6$ CFU did not provide tumor control.

However, they did find that Lm was cleared from systemic organs within a week (Limit of detection >10^2 CFU) but was maintained at ~10^5 CFU in the tumor for up to 15 days.[74] Here we similarly injected tumor-bearing mice IV with 1x10^6 CFU of barcoded ΔactA Lm and assessed bacterial population shift between 4HPI and 3DPI. Of note, this experiment was done once so it will need to be repeated to garner more statistical significance.

At 4HPI, livers and spleens were the most highly infected tissues and remained highly infected by 3DPI (Fig 4.2A). Early on, these tissues were highly diverse with a founding population close to our upper limit of detection (~10^4 Ns, Fig 4.2B, 4.1A), suggesting that most of the inoculum was recapitulated in the systemic organs. Tumors on the other hand had low bacterial burden at 4HPI (~10^2 CFU, Fig 4.2A) and the founding population was low as well (~10^1 Ns, Fig 4.2B), suggesting a stringent bottleneck to invade the tumor from IV inoculation.

By 3DPI, bacterial burden dramatically increased in the tumor to ~10^6 CFU (Fig 4.2A), yet this increase was not associated with an increase in founding population (Fig 4.2B), suggesting little migration into the tumor from an outside source and rather a massive local expansion event. Of note, the barcodes that were most dominant in the tumor were neither the ones that were slightly more abundant in the inoculum, nor the ones that took over the systemic organs (Fig S4.1), confirming little migration from systemic sites to the tumor past the first colonization event.

In addition, assessment of the genetic distance (GD) between bacterial populations in various tissues and the tumor established that the tumor was highly different from all other organs (GD>0.8, Fig 4.2C) and generally shared none of its barcodes with other tissues (Fig 4.2D). This was particular striking with regards to the tumor draining lymph nodes, the bone marrow, and the blood, which we expected to be somewhat similar to the tumor as possible dissemination conduits for Lm, yet all three were highly dissimilar at all times (Fig 4.2C-D). Collectively our results suggest that following the first colonization even, little to no bacteria are transported from systemic tissues to the tumor in IV infected tumor-bearing mice.

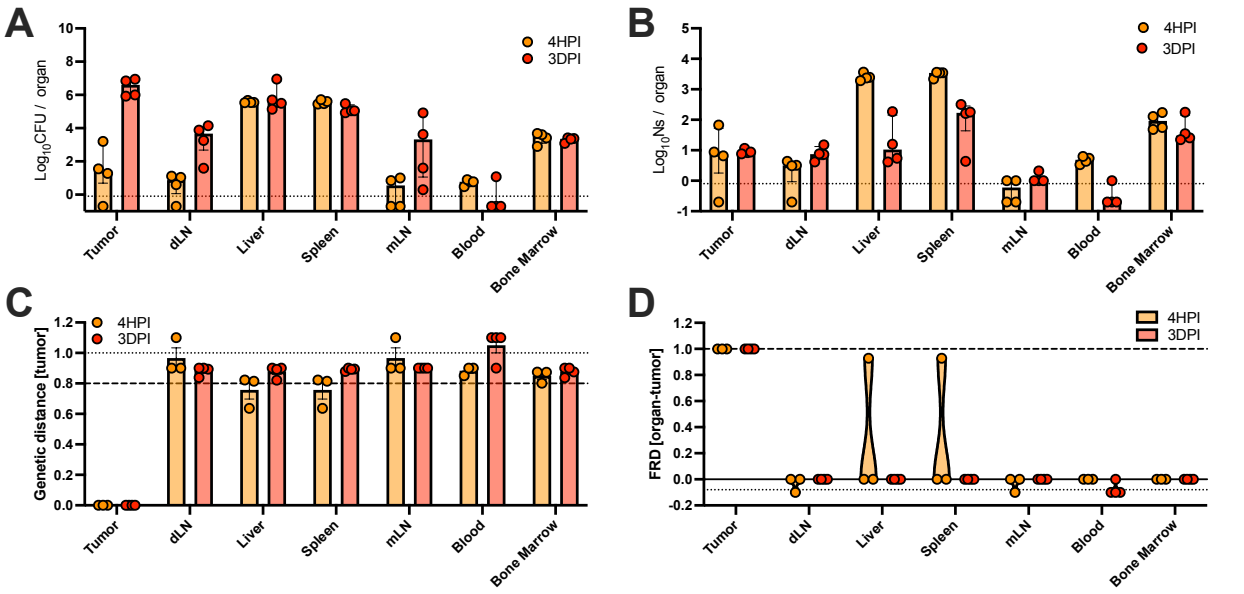


Figure 4.2: Intravenous inoculation with barcoded ΔactA Lm. Intravenous injection of C57BL/6J mice with 1x10^6 CFU and collection of organs at 4 hours post injection (4HPI) or 3 days post infection (3DPI). Bacterial burden (CFU, *A)* and founding population (Ns, *B*) per organ. Data are individual samples expressed as log-transformed values with median and interquartile range. *(C)* GD between all organs and the tumor at 4HPI or 3DPI. Data are individual samples with mean and SEM. The dashed line at 0.8 marks a "high" GD i.e. samples that are dissimilar. *(D)* Prevalence of barcodes from the tumor in other organs (FRD[organ-tumor]). Data are individual samples with violin plots and median, and the dashed line marks 100% barcode sharing with the tumor. For all panels, limit of detection is noted by a dotted line and samples with zero CFU are found past this dotted line. Samples with no CFU are not included in *C* and *D*. Data are from one experiment with 4HPI N=4 and 3DPI N=4.

4.3.3. IT inoculation leads to efficient migration from the tumor to systemic site, then limited further bacterial exchange between tissues

Garcia-Castillo et al. further established that IT injections with attenuated Lm led to bacterial persistence in the tumor and some level of clearance in systemic organ within a week, similar to IV injections, yet it also led to a surprising loss of tumor control. This established that Lm could induce either a beneficial or a detrimental response for tumor control depending on the route of inoculation. We thus assessed the bacterial dissemination pattern in IT injected tumor-bearing mice using barcoded ΔactA Lm.

Upon IT injection, tumors were generally highly infected with ~10^8 CFU at 4HPI, as expected, then bacteria burden was somewhat controlled by 3DPI (Fig 4.3A). Founding population was high as well and remained stable over time (Fig 4.3B), suggesting that the diversity of the inoculum was recapitulated immediately in the tumor and that increase in bacterial control that limited CFU did not affect the amount of diversity within the tissue.

In the systemic organs, bacterial burden remained stable over time but was overall lower than following IV infections (10^4 Fig 4.3A and 10^6 Fig 4.2A). In the same period, the founding population drastically decreased (~100-fold in spleen and ~1000 fold in liver, Fig 4.3B), suggesting some pressure that constricted the population diversity. This was due the expansion

of the mutated clones in the stock library that were discussed earlier as having an advantage *in vivo* (Fig S4.2). These barcodes rarely became dominant in tumors however, suggesting that even bacteria with an advantage at systemic sites were not more prone to migrating into the tumor. Other organs such as the blood and bone marrow were often uninfected at 4HPI and remained so by 3DPI (Fig 4.3A), suggesting limited bacterial spread across the rest of the host as well.

These observations were further supported by assessing the genetic distance with the tumor which started quite low in the spleen, liver, draining lymph nodes and sometimes mesenteric lymph nodes, suggesting similarities between the population structures, but increase over time (Fig 4.3D), which means that the tumor became more distinct as time passed after the first colonization event. Similarly, the proportion of barcodes shared with the tumor started high then (clones shared represented a large part of the population), then drastically decreased by 3DPI (Fig 4.3E). Collectively these results suggested that Lm migrated from the inoculation site in the tumor during early infection, then there was limited further bacterial exchange and additional pressures that affected each populations separately, similar to our results upon IV injection.

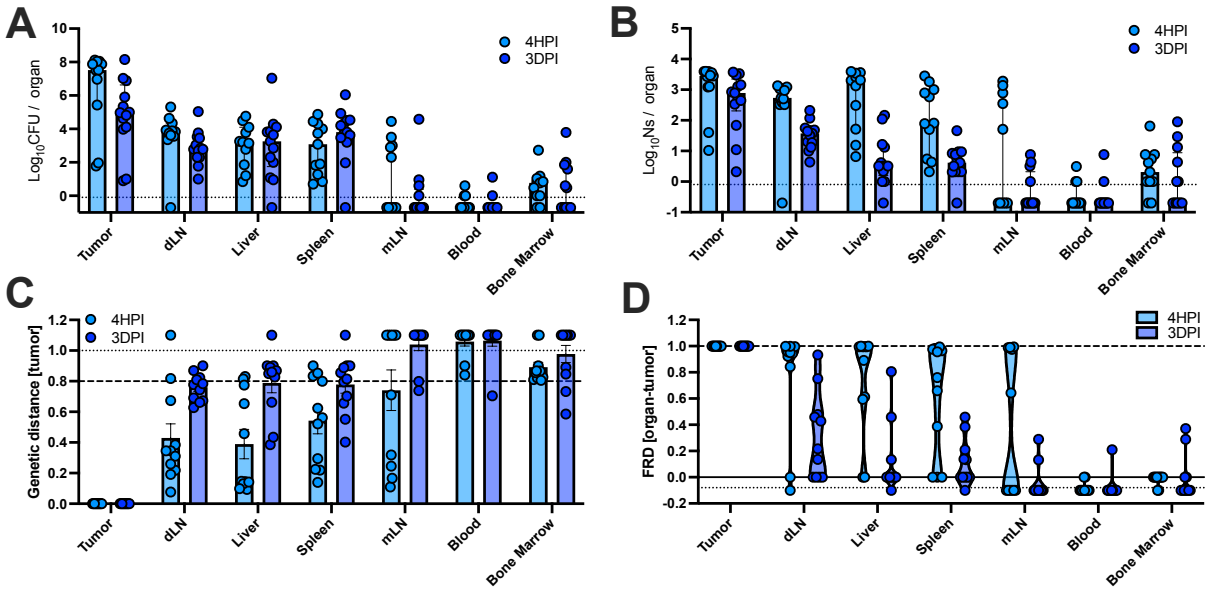


Figure 4.3: Intratumoral inoculation with barcoded ΔactA Lm. Intratumoral injection of C57BL/6J mice with 5x10^7 CFU and collection of organs at 4 hours post injection (4HPI) or 3 days post infection (3DPI). Bacterial burden (CFU, *A)* and founding population (Ns, *B*) per organ. Data are individual samples expressed as log-transformed values with median and interquartile range. *(C)* Genetic distance between all organs and the tumor at 4HPI or 3DPI. Data are individual samples with mean and SEM. The dashed line at 0.8 marks a "high" Genetic distance i.e. samples that are dissimilar. *(D)* Prevalence of barcodes from the tumor in other organs (FRD[organ-tumor]). Data are individual samples with violin plots and median and the dashed line marks 100% barcode sharing with the tumor. For all panels, limit of detection is marked by a dotted line and samples with zero CFU are found past this dotted line. Data are combined from three independent experiments with 4HPI N=11 and 3DPI N=13.

4.3.4. IV and IT combination therapy led to early Lm spread out of the tumor, then massive clearance events host-wide, but bacteria that persisted in tumors became mostly monoclonal

Neither IV nor IT injections promote tumor control, but a priming injection of attenuated Lm IV, which boosts Lm-specific responses, followed by an IT recall injection does provide tumor control.[74] To assess bacterial dissemination in this context, we first injected tumor-bearing mice IV with non-barcoded Lm, then one week later gave the mice an IT booster with the barcoded ΔactA Lm library. Garcia-Castillo et al. previously found that Lm persisted in some tumors by 10 days post IT injection, but was cleared by 15-20 days. Of note, we plated the entirety of our samples here, rather than a representative portion, which allowed us to lower the limit of detection and assess bacterial population structure in poorly infected samples that previously seemed "cleared". In addition, this experiment was only done once, which limited the reach of our conclusions.

Our results following IV+IT combination therapy mirrored our observations IT only inoculations in that at 4HPI tumors had high bacterial burden, variable amounts but generally few bacteria were found in the liver and spleen, and little to no Lm was found in the bone marrow, blood, and MLN (Fig 4.4A). This first dissemination of bacteria was associated with mixed but generally low founding population in the systemic organs (Fig 4.4B), suggesting a more stringent bottleneck for spread than in the context of only IT inoculation. As time passed most mice cleared the infection, but in mice that remained infected, tumor bacterial load was often very high around 10^6 CFU (Fig 4.4A). This maintenance of bacterial load however was not due to bacteria simply persisting within the TME, because founding population dramatically diminished over time with Ns<10 in most organs by 3DPI (Fig 4.4B). Instead, host pressures probably cleared most bacteria from the inoculum, leading to less diversity, but a few clones were able to escape this pressure and thrive.

Of note, the barcodes that became dominant in the tumor at either 3 or 16DPI were not any of the confounding barcodes that were mentioned earlier and were actually absent from livers and spleens as well (Fig S4.3). The samples that still harbored bacteria past 3 DPI generally had low genetic distance (similar to tumors, Fig 4.4.C) and higher proportion of shared barcodes with the tumor (high FRD, Fig 4.4D). Bacterial burden at systemic sites was lower than in the tumors (Fig 4.4A) suggesting that bacteria may disseminate away from the tumor at a low level over time.

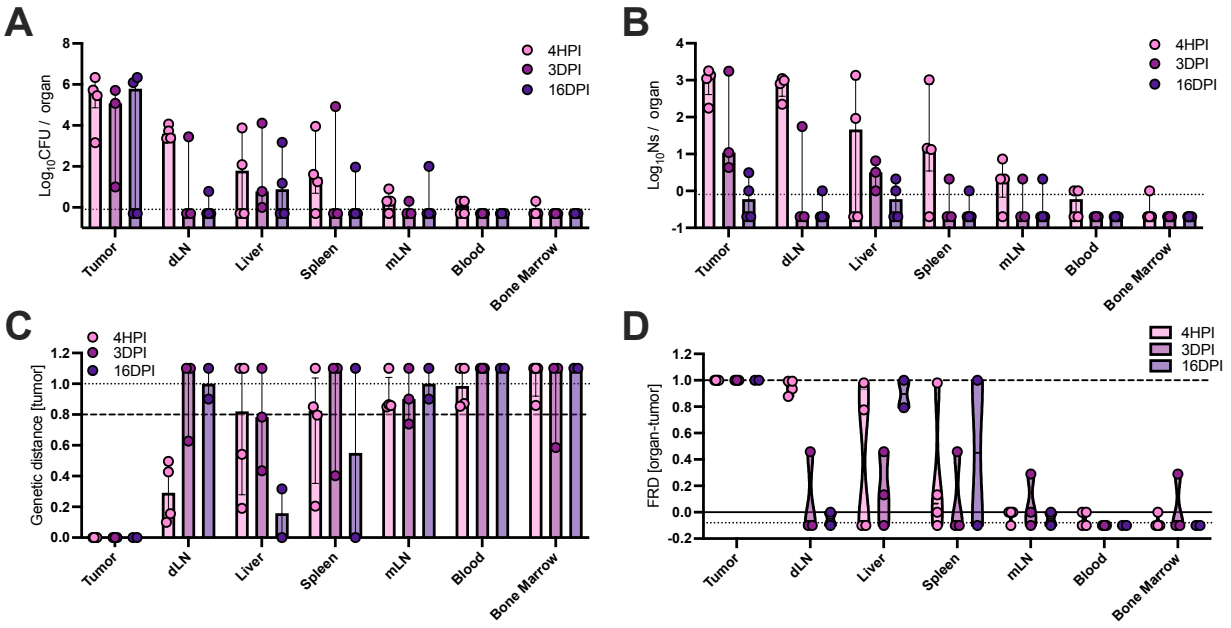


Figure 4.4: Combination therapy with intravenous and intratumoral inoculation of barcoded ΔactA Lm. Intravenous injection of tumor-bearing C57BL/6J mice with $1x10^6$ CFU of non-barcoded ΔactA Lm, followed one week later by intratumoral injection with $5x10^7$ CFU of barcoded ΔactA Lm. Organs were collected 4 hours post injection (4HPI), 3 days post injection (3DPI), or 16 days post injection (16DPI). Bacterial burden (CFU, *A)* and founding population (Ns, *B*) per organ. Data are individual samples expressed as log-transformed values with median and interquartile range. *(C)* Genetic distance between all organs and the tumor at 4HPI, 3DPI, or 16DPI. Data are individual samples with mean and SEM. The dashed line at 0.8 marks a "high" Genetic distance i.e. samples that are dissimilar. *(D)* Prevalence of barcodes from the tumor in other organs (FRD[organ-tumor]). Data are individual samples with violin plots and median and the dashed line marks 100% barcode sharing with the tumor. For all panels, limit of detection is marked by a dotted line and samples with zero CFU are found past this dotted line. Data are from one experiment with 4HPI N=4, 3DPI N=3, 16DPI N=4. Two mice cleared the infection entirely and are not in *D* or *E*.

4.4. Discussion

Infections with attenuated bacteria can be harnessed to convert the tumor microenvironment from a state of immunosuppression to one of tumor control. The efficacy of such treatments with Lm is dependent on the route of inoculation, and is associated with varying bacterial persistence across the tumor-bearing host[74]. Here, we set out to quantify the bottlenecks faced by ΔactA Lm as the bacteria disseminate through tumor-bearing hosts. We found that following either IV or IT only injection, Lm immediately colonized the tissues that came in contact with the inoculum, but the tumor was subsequently mostly isolated. Indeed, little to no bacterial exchange happened between the tumor and other organs after the first few hours of infection, and barcodes that were able to take over the spleen and liver did not necessarily permeate into the tumors. In IV infected mice, the founding population was quite low at 4HPI, but it was very high following IT inoculation, suggesting that colonization from the IV route is not as efficient. Although bacterial burden increased over time following IV injection and decreased following IT injection, the founding population remained stable in either case between 4HPI and 3DPI and suggesting little migration into the tissue and no massive clearance events. During preliminary work with IV+IT combination therapy we observed Lm clearance in most mice by 3DPI as expected[74], but mice that sustained systemic Lm at 3-16DPI often had

similar population structure in all organs including the tumor. This implied a possible low level bacterial spread between the tumor and systemic sites, which was not observed in IV only and IT only mice. Collectively our findings provided a deeper understanding of bacterial dynamics in the tumor-microenvironment and raised new questions about the bottlenecks faced by Lm in this very specific context.

We established that tumors were quite isolated from other organs in IV and IT only inoculated mice and that ΔactA Lm rarely ever spread between tissues past 4HPI. Paradoxically, the tumor was colonized in every single mouse at 4HPI, implying that bacteria must have been able to enter the tumor at some point in time. We hypothesize that the inoculum itself is at the origin of tumor colonization. Upon IV injection of tumor-bearing mice with 10^7 CFU of barcoded ΔactA Lm, we found that tumors were highly diverse at 4HPI and remained so by 3DPI (data not shown), suggesting that dose, in addition to inoculation route, may impact colonization and responses in the TME. Further assessment of the timing of colonization by sampling earlier than 4HPI, such as 20min post inoculation, would provide evidence on the origin of the first colonization event; if our hypothesis were correct, the dynamics we observed at 4HPI would already have happened by then.

However, our IV+IT observations suggested that bacteria may actually be able to disseminate between tissues, albeit at a low level, which may have been masked by the high CFU and mostly high diversity of samples in the IV only and IT only models. Seeing as the blood was very poorly infected in all IV+IT mice, the draining lymph nodes were mostly uninfected by 3DPI, and our model bacterium cannot spread from cell to cell, how could bacteria migrate between tissues? The generally non-existent bacteria in the draining lymph nodes suggested that the lymphatics were not a major migration route, but we could not entirely rule out the vasculature as primary trafficking pathway for Lm. Indeed, such a low level of bacterial presence within circulation may not be captured by plating for CFU. Our blood collection protocol assumes that we harvested about half of the total blood, but we only sampled at one instant, and blood is recirculated through a host multiple times per minute,[152] so the high turnover would make it virtually impossible to identify traces amounts of bacteria. Hence, even though the blood is poorly infected in our model, we still expect that any bacterial exchange between tissues would happen via the circulation.

Garcia-Castillo et al, showed that Lm inoculated IT in tumor-bearing mice mediates recruitment of polymorphonuclear cells (PMN) that become immunosuppressive and permissive for bacterial survival within the TME. Yet, upon depletion of these cells, tumor control was somewhat restored but bacterial persistence remained.[74] This led us to question whether most bacteria in the TME were intracellular or extracellular. This could normally be assessed via treatment with the antibiotic gentamycin which kills extracellular bacteria[12] but this the TME is intricately vascularized[153] and may not allow for efficient delivery of gentamycin throughout the tumor tissue. Instead, a microscopy-based approach may be more successful at discerning the location of the bacteria and providing a deeper understanding of bacterial interactions with host cells within the TME.

If Lm was mostly intracellular, it would be very interesting to sort single cell suspensions from tumors, then assess the diversity of barcodes recovered in each cell. This method is particularly attractive since many tumors, across all models, become somewhat dominated by very few clones over time. Since our experimental layout relies on ΔactA Lm, bacteria are unable to spread from cell to cell, so it is possible that each cell will host a different bacterial subpopulation. For this to be the main mechanism for bacterial population shifting, we hypothesize that the first bacteria that infect permissive host cells would have a growth advantage. Although ΔactA Lm cannot spread intracellularly, the host cell should eventually burst from replicating bacteria within its cytosol, releasing clonal Lm that replicated within the cell and leading to a higher probability for this particular clone to becomes phagocytosed/invade a new host cell and increase its overall abundance within the tissue. One limitation with this hypothesis is that we also proposed that the first colonization event (from the inoculum) is highly polyclonal so many bacteria should have the possibility to be the first to invade host cells and start this cycle. More work will need to be conducted to gain a better understanding of the bacterial dynamics within tumor-bearing mice. Collectively our findings advance the work of Garcia-Castillo et al. by providing a more detailed understanding of the bacterial experience with the TME. Our results indicate that tumors are colonized upon inoculation, but mostly isolated from other tissues thereafter, regardless of inoculation route, and that IV+IT combination therapy leads to highly infected yet mostly monoclonal tumors at late stages of infection. Understanding how this dominance phenotype is established would provide a clearer picture for bacterial persistence in tumor-bearing mice and help develop better anti-cancer therapies with antigen-free, attenuated Lm.

4.5. Material and Methods

Animal models

8- to 12-week-old female C57BL/6J mice were purchased from the Jackson Laboratory (stock #000664). Mice maintained under specific pathogen-free conditions amd fed with standard chow at the University of California, Berkeley animal facility. This study was performed in strict accordance with the recommendations in the Guide for the Care and Use of Laboratory Animals of the National Research Council of the National Academy of Sciences [99] and with university regulations. All protocols were reviewed and approved by the Animal Care and Use Committee at the University of California, Berkeley (AUP-2016-05-8811 and AUP-2016-06-8878).

Cell lines

For tumor studies, mice were inoculated subcutaneously in the right hind limb with $5x10^5$ MC38 cells in PBS. These injections were performed by our collaborators in the DuPage laboratory who also kindly provided, maintained and grew the cell lines.
MC38 cell lines were maintained in DMEM (GIBCO) supplemented with 10% FBS, sodium pyruvate (GIBCO), 10mM HEPES (GIBCO), and penicillin-streptomycin (GIBCO). Tumor cell were then grown at 37C with 5% CO2.

Bacterial strains generation and growth conditions

The Lm strain used in this study was derived from 10403S [100] which is streptomycin resistant. For vector construction, plasmids were introduced into Lm by conjugation as previously described[154], using a donor E. coli SM10 (Stratagene) and a compatible ΔactA Lm strain[154,155] (DP-L4029, phage-cured). Barcoded Lm libraries were constructed as previously described using pTZ200.mix,[4] which is a pooled plasmid library containing 200 unique barcodes assembled onto a pPL2 backbone that stably integrates into the Lm chromosome[154]. Pooled ΔactA Lm libraries were propagated in filter-sterilized brain heart infusion (BHI) medium (BD) at 37°C while shaking with streptomycin (200 μg/ml) overnight. Cell density was measured by optical density (OD600). Frozen stocks were stored at -80°C in BHI with 25% glycerol. Inoculums were prepared by freshly inoculating into BHI broth from frozen stocks and growing to log-phase for each experiment. The log-phase bacteria were washed twice in PBS and resuspended in the appropriate volume of PBS depending on the infection route.

Quality control for the newly generated ΔactA Lm library

Calibration curves were performed by washing log-phase bacteria twice in PBS then diluted to the appropriate CFU and plated on BHI media. Colonies were then washed off the plates with PBS, and frozen down with 25% glycerol until further processing. Samples were then diluted in water, boiled for 1h at 80C and the barcode-containing region was amplified from genome DNA using custom forward and reverse primers (see Chapter 2 - Supplementary Table S1) to assess the founding population (Ns).

Tumor-bearing mice injections

Intravenous (IV) injections were performed via the tail vein with $1x10^6$ CFU of ΔactA Lm barcoded library in 200μL of sterile PBS as previously described.[101] Intratumoral (IT) injections were performed as subcutanerous inoculations above the established tumor mass with $5x10^7$ CFU of ΔactA Lm barcoded library in 100μL of sterile PBS as previously described.[74] For IV and IT only challenge mice were inoculated 11 days post MC38 tumor cell implantation. For IV and IT combination therapy, mice were vaccinated IV with $1x10^6$ CFU non-barcoded ΔactA Lm (DP-L4029) 4 days post implantation of MC38 cells, then challenged IT with $5x10^7$ CFU barcoded ΔactA Lm 7 days later (11 days following MC38 tumor cells implantation)[74]. Mice were euthanized 4 hours, 3 days, or 16 days following challenge and tissues were collected as described below.

Tissue harvest and processing

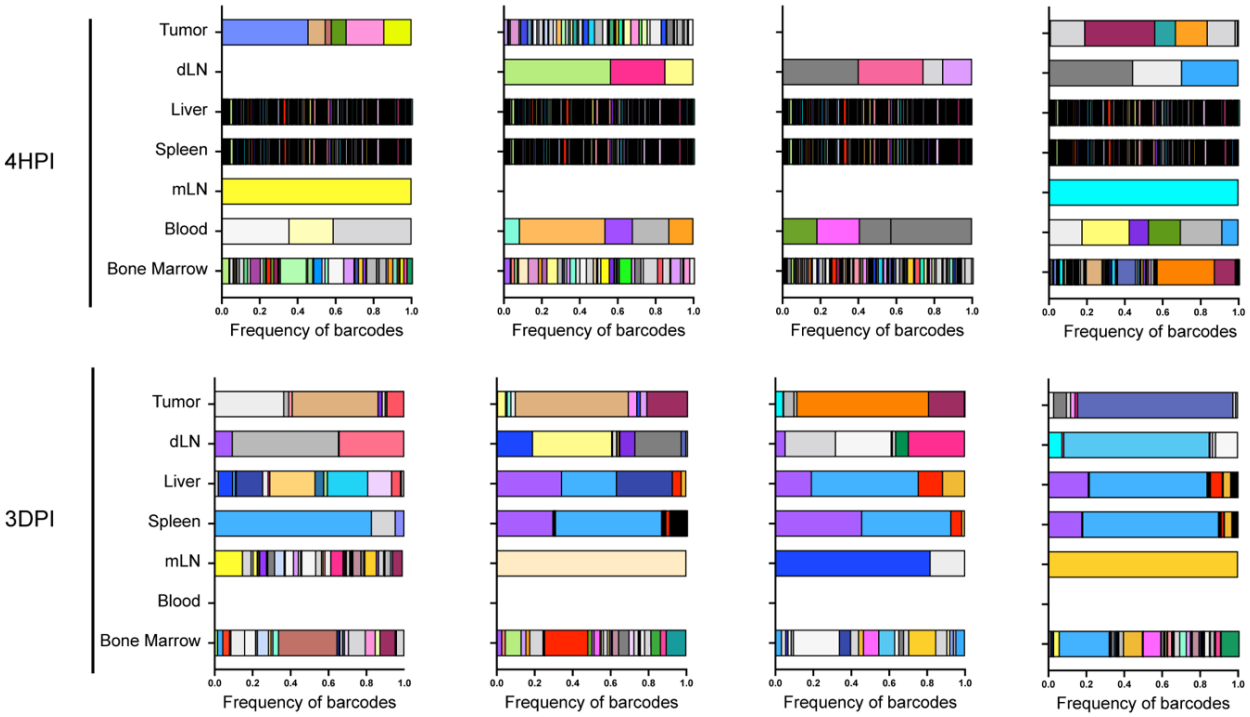
All samples were collected and homogenized in 1mL 0.1% IGEPAL CA-630 (Sigma), except for blood (~500uL), which was collected via cardiac puncture immediately after euthanasia in 100uL 50 mM EDTA as an anticoagulant (adapted from Senay et al.[93]). Livers were collected in 3mL to account for larger volume of these organs, and so were tumors but only on day 16 post challenge, when tumors were very large. Bone marrow was collected from the left femur and tibia bones which were crushed with a mortar and pestle before homogenizing. Sterile autoclavable probes were used to homogenize each sample to avoid cross-contamination. Dilutions of homogenates were plated to enumerate CFU and the entirety of the sample volume was then plated on BHI plates with streptomycin at 200 μg/ml (broadly selects for Lm)

for STAMPR analysis following incubation at 37°C overnight. Colonies were then washed off the plates with PBS, and frozen down in 25% glycerol until further processing.
For samples from mice that received combination IV+IT therapy, the plating on streptomycin only allowed for growth of both barcoded Lm from the IT injection and any remaining non-barcoded Lm from the IV injection. We took advantage of the fact that the Lm library is resistant to chloramphenicol 7.5µg/mL, which non-barcoded Lm is sensitive to, and patched ~50 colonies per tissue. CFU/sample were calculated as the proportion of bacteria that were chloramphenicol resistant (almost always 100%).

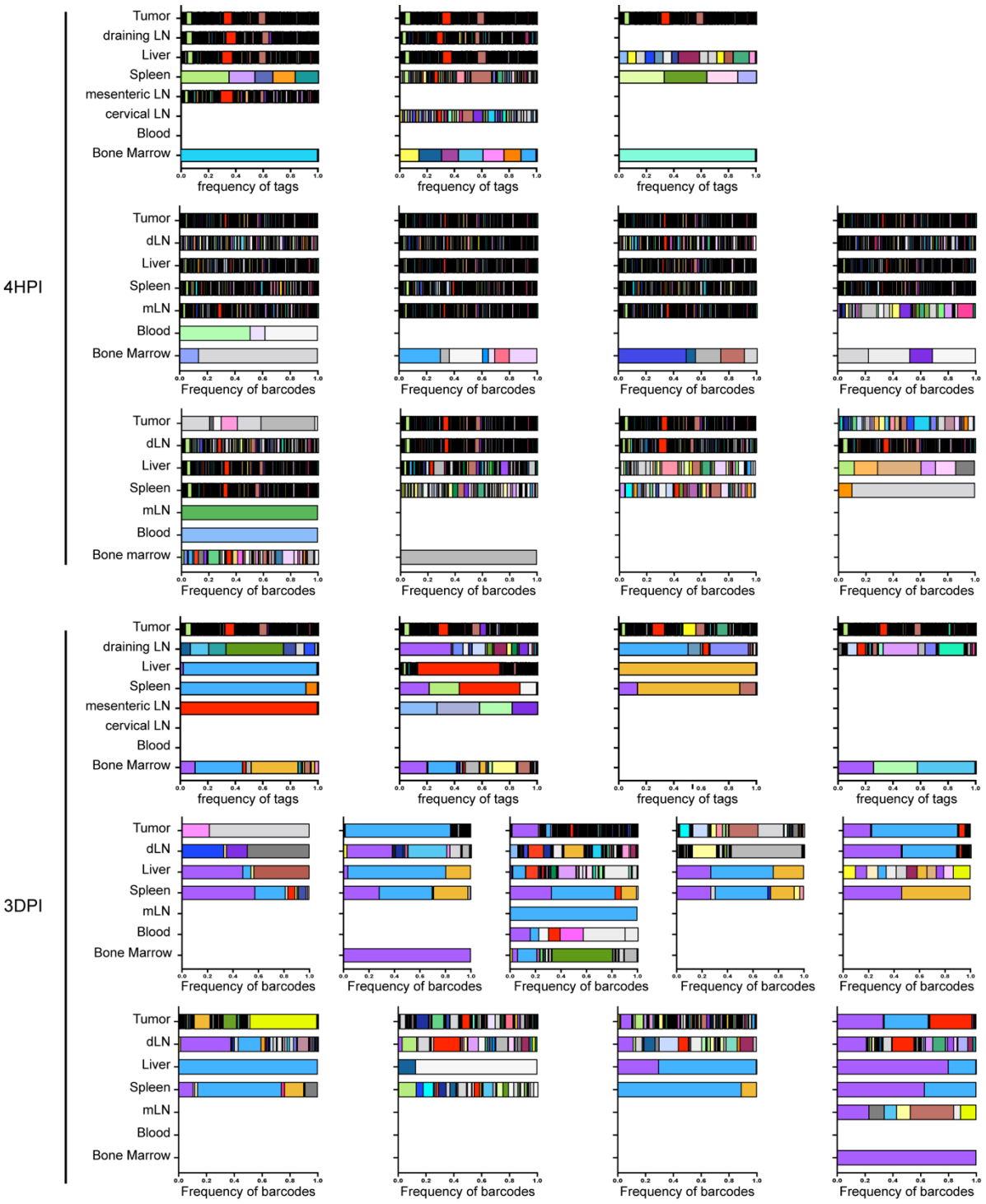
STAMP

Sequence tag-based analysis of microbial populations (STAMP) was performed as previously described[3,20] using the library generated in this study, as described earlier. Inoculum samples were collected frequently to ensure that the population structure remained stable across all experiments. Briefly, frozen samples were diluted in water and boiled for 1h at 80C. The barcode-containing region was amplified from the genome using custom forward and reverse primers (see Chapter 2, Supplementary Table S1) with OneTaq HS Quick-Load Master Mix (New England Biolabs). Samples were amplified using primers containing TruSeq indexes and adapters for Illumina sequencing, then pooled and purified using GeneJet PCR purification kit. Purified PCR products were sequenced on either an Illumina MiSeq or Illumina NextSeq 1000. Reads were demultiplexed using a custom R script then trimmed and mapped to a list of ~200 barcodes using Qiagen CLC Genomics Workbench with default settings. Founding population estimates were determined using the STAMPR analysis toolset [20] and genetic distance was estimated with Cavalli-Sforza chord distance [103] as previously described.[3] Original script and sequencing data were deposited on Github (https://github.com/hullahalli/stampr_rtisan) and are publicly available. Any additional information about the data reported in this paper is available upon request.

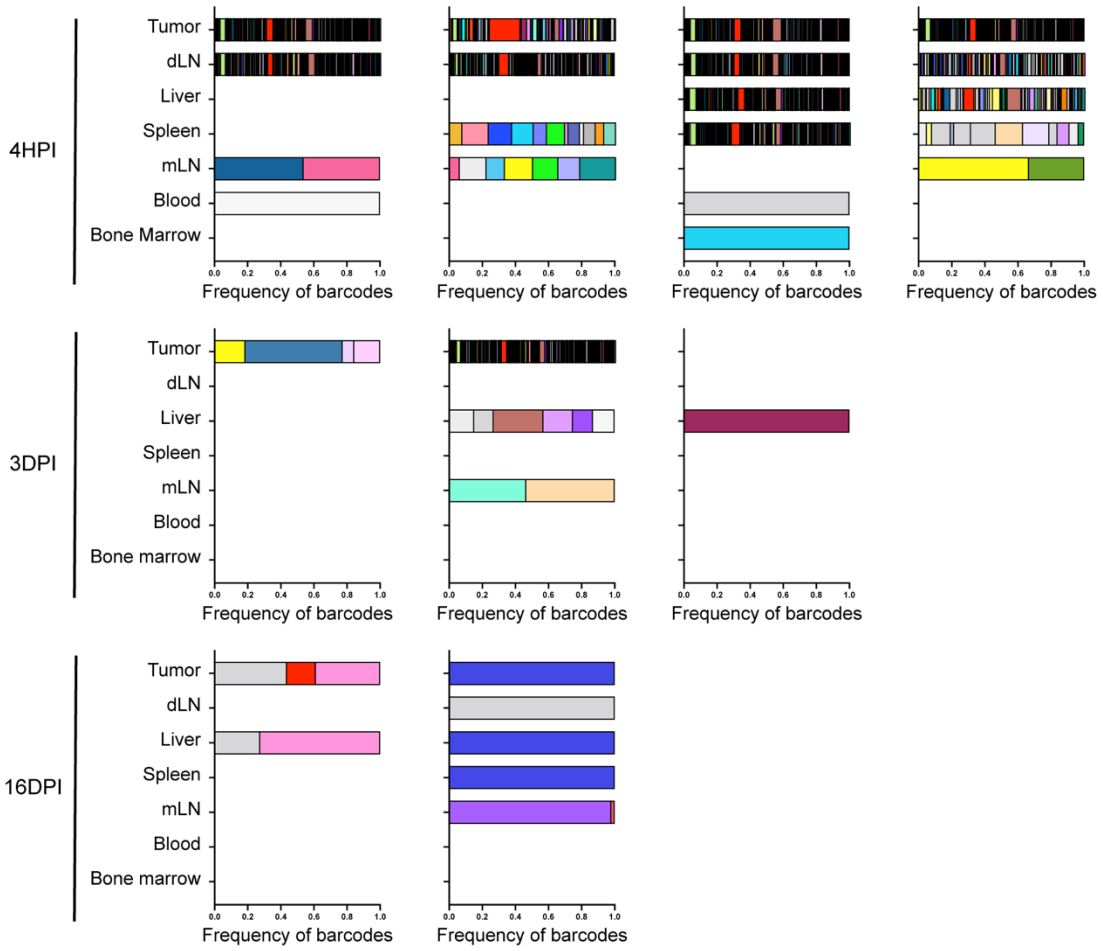
4.6. Supplementary figures



Supplemental Figure S4.1: Frequency of barcodes in mice from the IV only group. Frequency of barcodes for intravenously infected tumor-bearing C57BL6/J mice sacrificed at 4 hours post injection (4HPI) or 3 days post injection (3DPI). Each graph represents one mouse, and each color represents one barcode (the same color scheme was applied to all graphs). Samples with no CFU were left blank. Data are from one experiment with 4HPI N=4 and 3DPI N=4.



Supplemental Figure S4.2: Frequency of barcodes in mice from the IT only group. Frequency of barcodes for intratumorally inoculated tumor-bearing C57BL6/J mice sacrificed at 4 hours post injection (4HPI) or 3 days post injection (3DPI). Each graph represents one mouse, and each color represents one barcode (the same color scheme was applied to all graphs). Samples with no CFU were left blank. Data are combined from three independent experiments with 4HPI N=11 and 3DPI N=13.



Supplemental Figure S4.3: Frequency of barcodes in mice from the IV + IT combination therapy group.
Frequency of barcodes for tumor-bearing C57BL6/J mice that received combination therapy. Mice were sacrificed at 4 hours post injection (4HPI), 3 days post injection (3DPI), or 16 days post injection (16DPI). Each graph represents one mouse, and each color represents one barcode (the same color scheme was applied to all graphs). Samples with no CFU were left blank. Data are from one experiment with 4HPI N=4, 3DPI N=3, 16DPI N=2.

CHAPTER 5. CONCLUDING REMARKS AND FUTURE DIRECTIONS

5.1. Conclusions and summary of results

The interaction between pathogens and hosts is a very dynamic process both in space and in time. Upon invasion, pathogens must evade host pressures and access niches that allow them to sustain their population over time. The study of these *population dynamics* is an ecological principle that was described in the 1990s and can be investigated across two broad components. The first is a quantitative description of the changes in population structure with regards to growth and decline. The second is an investigation of the forces that shape these structural changes, generally referred to as *bottlenecks*.[156] In this work, we attempted to address both components using cerebral listeriosis as our main model system, then venturing into the study of pregnant-or tumor-bearing hosts. Chapter 2 provided an in-depth characterization and quantification of population changes during cerebral listeriosis across time, using multiple methods of pathogen delivery. Chapter 3 investigated some of the host factors that may shape population structure and provided insights into Lm dissemination to the placenta. Chapter 4 established a preliminary assessment of attenuated-Lm trafficking pathways upon infection of tumor-bearing hosts across multiple inoculation routes.

In the first part of our study, we used a library of 200 barcoded Lm to quantify the bottlenecks and bacterial population shifts that occur during cerebral listeriosis. Our analysis revealed that following intravenous infection multiple and independent infection events seed different parts of the central nervous system (CNS; brain, brain stem and spinal cord), but a single clone establishes dominance in the brain. Dissection of infected brains established that all regions of the CNS are susceptible to infection and hold diverse populations, but a small subset of clones are present throughout the brain. Sequential infections and intracranial infections with tagged-Lm provided evidence that timing of brain colonization drives this clonal dominance phenotype. Intravenous infections however are not the natural route of infection for Lm and leads to high bacterial load and barcode diversity in the blood, which is absent in models of oral infection. In a new model of foodborne-induced cerebral infection using streptomycin-pre-treated Rag1KO mice, we were able to recapitulate the neurological symptoms seen in ruminants with cerebral listeriosis. The CNS of orally infected Rag1KO mice was highly infected and consistently dominated by a single barcode, suggesting a limited ability of Lm to colonize the brain, but little restriction on bacterial replication locally after invasion. In this model, barcodes were generally shared between the blood and CNS, supporting a model in which blood-borne invasion is an efficient route of infection. Both the bone marrow and the intestines had been suggested as reservoirs for bacterial dissemination towards the CNS. Instead, we found that the bacterial populations in the bone marrow following intravenous infections, and in the colons following oral infection both diverged from the brain bacterial population over time. This does not mean that Lm cannot disseminate from these tissues towards the CNS, but establishes that they are not efficient reservoirs for continuous shedding of bacteria over time. Collectively our work clarified our understanding of bacterial trafficking pathways, quantified population shifts both temporally and spatially, and established a framework for studying the dynamics of other cerebral infections.

In the second part of our study, we investigated whether the innate immune receptor STING is a restrictive bottleneck that limits Lm spread to the brain and placenta, or if STING activity facilitates bacterial dissemination. Following oral inoculation, STING-deficient mice (*Goldenticket*, Gt) accumulated higher bacterial burden in the CNS than wild-type mice (C57BL6/J, WT) with a peak of infection at 4-6 days post infection. This established that STING activity does not promote bacterial dissemination to the brain but rather participates in controlling system-wide infection. The increased susceptibility of Gt mice to cerebral listeriosis was independent of STING-derived Type 1 interferon, but dependent on signaling via the STING C-terminal tail. Preliminary work with Rag1KO-*Gt* double mutant mice suggested that STING had little impact on restriction of bacterial accumulation in the CNS over time. Finally, further preliminary work assessed the role of STING during infection of pregnant mice, which is one of the main aspects of disease presentation in humans. We found that Gt placentas were somewhat protected following intravenous infection, but instead showed increased sensitivity following oral infection. Collectively, we propose that the impact of STING-deficiency is most relevant in leading to a loss of bacterial control, rather than from the loss of a monocyte "Trojan horse" for bacterial dissemination.

The third part of our study required that we first generate a library of barcoded Lm in an attenuated background. We then used this library of ~200 barcoded attenuated-Lm to quantify the bottlenecks and bacterial population shifts that occur upon invasion of tumor-bearing hosts. Our results suggested that Lm colonized tumors directly from the inoculum but was subsequently mostly isolated from population changes within the rest of the host. Between 4HPI and 3DPI the founding population remained stable following either IV only or IT only inoculation, suggesting little to no migration into the tissue and no dramatic clearance events. During IV+IT combination therapy however, we observed dramatic Lm clearance in most mice along with a loss of population diversity. Few hosts still harbored bacteria past 4HPI, but when they did tumors were generally highly infected and mostly monoclonal. This suggested an early clearance event that limited bacterial diversity but did not always lead to a sterile TME, which provided an opportunity for remaining Lm to re-expand. Collectively our findings provided a deeper understanding of bacterial dynamics in the TME and raised new questions about the bottlenecks faced by Lm in this unique context.

5.2. Remaining questions and avenues for future work

A few questions remain unanswered so we would like to propose some experimental ideas to expand upon our work.

Our opposing results in placenta infections depending on the route of inoculation in STING-deficient mice is puzzling since mothers seem to be similarly infected. Yet, previous work and our results in Chapter 2 clearly establish that the route of inoculation affects pathogen dynamics and bacterial spread, so this question might be interesting to dissect with a thorough barcoding analysis. Pregnant mouse uteruses contain multiple placenta-fetus pairs so possible interesting results might include:

-polyclonal placentas, but monoclonal fetuses, suggesting a tight bottleneck that limits dissemination specifically at the placenta-fetus interface.
-monoclonal placenta-fetus pairs, but different clones taking over each pair, suggesting a tight bottleneck to invade to the placenta but efficient dissemination to and replication within the fetus.
-one clone taking over all the placentas and all the embryos within one mouse, suggesting an incredibly stringent dissemination to the uterus but efficient dissemination between placentas and fetuses and no exchange with the rest of the maternal organs
- highly polyclonal placentas and fetuses throughout the uterus, suggesting a very wide bottleneck for dissemination thought the placentas/fetuses.
Of note, Bakardjiev et al already established, using only 2 tagged strains of Lm, that there is a somewhat tight bottleneck that limits invasion of the placenta, but that overtime bacteria begin to spread and exchange between the maternal organs and the fetus.[12] We thus anticipate that the STAMP analysis would be most fruitful if conducted as a time course. In addition, to further analyze the bottlenecks that affect Lm spread to the placenta in a STING-dependent manner, infection of S365A mice or ΔCTT mice with barcoded bacteria would disentangle which functions of STING are involved in bacterial dissemination. Conversely, we could generate a barcoded library in Lm mutants that secrete more or less cyclic-di-AMP[61] and thus fine tune the impact of variable STING activation in bacterial dissemination to the placenta.

With regards to cerebral infections, our work established that the blood is a main source of bacteria that invade the CNS and that the bone marrow is not a continuous reservoir for infection, yet we do not currently know if Lm is intracellular or intracellular in the blood or in the CNS. This would have implications in better understanding the mechanism for bacterial spread into the brain and replication/protection from the immune system within the brain. In particular, cranial intra-cranial injections with free-living bacteria led to a fulgurant expansion in only 12h suggesting that extracellular bacteria may be particularly suited to grow extracellularly in brains. Possible methods to answer this question include a microscopy assay with constitutively fluorescently labeled Lm and staining with a secondary antibody for Lm before permeabilization of cell membranes, as previously done i*n vitro.*[40] This would allow for direct visualization of intra/extracellular bacteria. If most bacteria are intracellular further staining would be beneficial to assess the celltypes Lm is associated with (neural, peri-neural, or immune).
In addition, infection of mice with Lm that express RFP under the ActA promoter which will only be fluorescently labeled upon reaching the cytosol of host cells[157]. This approach can be combined with microscopy or flowcytometry analysis to again distinguish whether Lm is primarily found inside or outside of cell and which cell types it associates with.

In addition, our work established that the bone marrow and the intestines were not the main reservoirs for bacterial shedding to the CNS. However, we did not identify the first invasion event, which could still originate from a source that does not efficiently shed Lm. Possible avenues of study include using an osmotic pump that dispenses gentamycin in the bloodstream and kills extracellular bacteria,[12] and assessing how limitation of circulating free-living Lm affects the CNS bacterial population structure. Alternatively, a specific antibody-

mediated depletion of monocytes with a Ly6C-antibody or a broad clodronate-mediated depletion of phagocytes would help assessing how limitation of monocyte "Trojan horses" might change the barcodes found in the CNS. However, monocytes are highly involved in bacterial systemic control, which may confound our results, as suggested by our data in Chapter 3. Finally, a surgical vagotomy, which severs the vagus nerve that connects the CNS with most abdominal tissues[158], would help assess how limitations in intraneural trafficking impact bacterial population structure in the CNS, as previously done with intramuscular injections[77].

Finally, with regards to bacterial dissemination in tumor-bearing mice, our work supported Garcia-Castillo and coworkers' findings that IV+IT combination therapy generally led to bacterial clearance in about a week, but that a few hosts were unable to clear the infection entirely. Our work additionally established that remaining bacterial populations were generally quite monoclonal, so while efficient Lm-specific cell-mediated immunity[74] probably provided the first clearance event, some clones were able to escape. As mentioned earlier, our understanding of bacterial presence in the extracellular space is incomplete so if bacteria were able to grow extracellularly in tumors, they could possibly evade the cell-mediated killing and become dominant. However, we expect that bacteria in the extracellular space would be polyclonal so it would be surprising for very few clones to take over. Another possibility is that This hypothesis still needs much work to be addressed properly, but one interesting experiment would be again to sort cells from tumors of mice that received barcoded IV+IT combination therapy, across multiple days post challenge, and assess which cellular compartment (or extracellular) becomes clonal.

Our findings also suggested that the library we generated had 2-3 mutant bacteria that gained an advantage *in vivo*. These clones were not dominant in the stock library, had no advantage during growth in broth, but did become prominent in the liver and spleen of most mice by 3 DPI following IV or IT only inoculation. The mutants did not generally permeate into tumors, but there were a few cases where this did happen. It would be interesting to see if these mutated clones would become dominant in the tumor when given enough time. If these clones were able to become reproducibly dominant in tumors, they would be very interesting to pursue as possibly carrying mutations that eventually give them an advantage in the TME. We would then be interested in isolating these clones from one of our frozen samples (where they are the dominant clone rather than the library where they would be hard to identify), confirm the barcode by PCR, then whole genome sequence the DNA to identify the mutations of interest and take this project in a whole new direction.

Overall, a few axis of research still remain unexplored and if followed would provide a more comprehensive understanding of Lm pathogenesis and of broader pathogen dissemination patterns to the CNS, the placenta, and the tumor.

CHAPTER 6. REFERENCES

1. Global health achievements 2023 https://www.who.int/news-room/spotlight/global-health-achievements-2023.

2. Antimicrobial resistance https://www.who.int/news-room/fact-sheets/detail/antimicrobial-resistance.

3. Abel, S., zur Wiesch, P.A., Chang, H.-H., Davis, B.M., Lipsitch, M., and Waldor, M.K. (2015). STAMP: Sequence tag-based analysis of microbial population dynamics. Nat. Methods *12*, 223–226. 10.1038/nmeth.3253.

4. Zhang, T., Abel, S., Abel Zur Wiesch, P., Sasabe, J., Davis, B.M., Higgins, D.E., and Waldor, M.K. (2017). Deciphering the landscape of host barriers to Listeria monocytogenes infection. Proc. Natl. Acad. Sci. U. S. A. *114*, 6334–6339. 10.1073/pnas.1702077114.

5. Becattini, S., Littmann, E.R., Carter, R.A., Kim, S.G., Morjaria, S.M., Ling, L., Gyaltshen, Y., Fontana, E., Taur, Y., Leiner, I.M., et al. (2017). Commensal microbes provide first line defense against Listeria monocytogenes infection. J. Exp. Med. *214*, 1973–1989. 10.1084/jem.20170495.

6. Buffie, C.G., and Pamer, E.G. (2013). Microbiota-mediated colonization resistance against intestinal pathogens. Nat. Rev. Immunol. *13*, 790–801. 10.1038/nri3535.

7. Contag, C.H., Contag, P.R., Mullins, J.I., Spilman, S.D., Stevenson, D.K., and Benaron, D.A. (1995). Photonic detection of bacterial pathogens in living hosts. Mol. Microbiol. *18*, 593–603. 10.1111/j.1365-2958.1995.mmi_18040593.x.

8. Hardy, J., Chu, P., and Contag, C.H. (2009). Foci of Listeria monocytogenes persist in the bone marrow. Dis. Model. Mech. *2*, 39–46. 10.1242/dmm.000836.

9. Hardy, J., Francis, K.P., DeBoer, M., Chu, P., Gibbs, K., and Contag, C.H. (2004). Extracellular Replication of Listeria monocytogenes in the Murine Gall Bladder. Science *303*, 851–853. 10.1126/science.1092712.

10. Lee, K.H., Kiupel, M., Woods, T., Pingle, P., and Hardy, J. (2023). Infection of the murine placenta by Listeria monocytogenes induces sex-specific responses in the fetal brain. Pediatr. Res. *93*, 1566–1573. 10.1038/s41390-022-02307-1.

11. Auerbuch, V., Lenz, L.L., and Portnoy, D.A. (2001). Development of a Competitive Index Assay To Evaluate the Virulence of Listeria monocytogenes actA Mutants during Primary and Secondary Infection of Mice. Infect. Immun. *69*, 5953–5957. 10.1128/IAI.69.9.5953-5957.2001.

12. Bakardjiev, A.I., Theriot, J.A., and Portnoy, D.A. (2006). Listeria monocytogenes Traffics from Maternal Organs to the Placenta and Back. PLOS Pathog. *2*, e66. 10.1371/journal.ppat.0020066.

13. Grant, A.J., Restif, O., McKinley, T.J., Sheppard, M., Maskell, D.J., and Mastroeni, P. (2008). Modelling within-host spatiotemporal dynamics of invasive bacterial disease. PLoS Biol. *6*, e74. 10.1371/journal.pbio.0060074.

14. Melton-Witt, J.A., Rafelski, S.M., Portnoy, D.A., and Bakardjiev, A.I. (2012). Oral infection with signature-tagged Listeria monocytogenes reveals organ-specific growth and dissemination routes in guinea pigs. Infect. Immun. *80*, 720–732. 10.1128/IAI.05958-11.

15. Kaiser, P., Slack, E., Grant, A.J., Hardt, W.-D., and Regoes, R.R. (2013). Lymph node colonization dynamics after oral Salmonella Typhimurium infection in mice. PLoS Pathog. *9*, e1003532. 10.1371/journal.ppat.1003532.

16. Lim, C.H., Voedisch, S., Wahl, B., Rouf, S.F., Geffers, R., Rhen, M., and Pabst, O. (2014). Independent bottlenecks characterize colonization of systemic compartments and gut lymphoid tissue by salmonella. PLoS Pathog. *10*, e1004270. 10.1371/journal.ppat.1004270.

17. Hullahalli, K., and Waldor, M.K. (2021). Pathogen clonal expansion underlies multiorgan dissemination and organ-specific outcomes during murine systemic infection. eLife *10*, e70910. 10.7554/eLife.70910.

18. Fakoya, B., Hullahalli, K., Rubin, D.H.F., Leitner, D.R., Chilengi, R., Sack, D.A., and Waldor, M.K. (2022). Nontoxigenic Vibrio cholerae Challenge Strains for Evaluating Vaccine Efficacy and Inferring Mechanisms of Protection. mBio *13*, e0053922. 10.1128/mbio.00539-22.

19. Campbell, I.W., Hullahalli, K., Turner, J.R., and Waldor, M.K. (2023). Quantitative dose-response analysis untangles host bottlenecks to enteric infection. Nat. Commun. *14*, 456. 10.1038/s41467-023-36162-3.

20. Hullahalli, K., Pritchard, J.R., and Waldor, M.K. (2021). Refined Quantification of Infection Bottlenecks and Pathogen Dissemination with STAMPR. mSystems *6*, e00887-21. 10.1128/mSystems.00887-21.

21. Mahmutovic, A., Gillman, A.N., Lauksund, S., Robson Moe, N.-A., Manzi, A., Storflor, M., Abel Zur Wiesch, P., and Abel, S. (2021). RESTAMP - Rate estimates by sequence-tag analysis of microbial populations. Comput. Struct. Biotechnol. J. *19*, 1035–1051. 10.1016/j.csbj.2021.01.017.

22. Hullahalli, K., Dailey, K.G., Hasegawa, Y., Torres, E., Suzuki, M., Zhang, H., Threadgill, D.W., Navarro, V.M., and Waldor, M.K. (2023). Genetic and immune determinants of E. coli liver abscess formation. Proc. Natl. Acad. Sci. *120*, e2310053120. 10.1073/pnas.2310053120.

23. Hullahalli, K., Dailey, K.G., and Waldor, M.K. (2023). Innate immune responses yield tissue-specific bottlenecks that scale with pathogen dose. Proc. Natl. Acad. Sci. *120*, e2309151120. 10.1073/pnas.2309151120.

24. Bachta, K.E.R., Allen, J.P., Cheung, B.H., Chiu, C.-H., and Hauser, A.R. (2020). Systemic infection facilitates transmission of Pseudomonas aeruginosa in mice. Nat. Commun. *11*, 543. 10.1038/s41467-020-14363-4.

25. Gillman, A.N., Mahmutovic, A., Abel Zur Wiesch, P., and Abel, S. (2021). The Infectious Dose Shapes Vibrio cholerae Within-Host Dynamics. mSystems *6*, e0065921. 10.1128/mSystems.00659-21.

26. Liu, X., Kimmey, J.M., Matarazzo, L., de Bakker, V., Van Maele, L., Sirard, J.-C., Nizet, V., and Veening, J.-W. (2021). Exploration of Bacterial Bottlenecks and Streptococcus pneumoniae Pathogenesis by CRISPRi-Seq. Cell Host Microbe *29*, 107-120.e6. 10.1016/j.chom.2020.10.001.

27. Hullahalli, K., Dailey, K.G., Hasegawa, Y., Suzuki, M., Zhang, H., Threadgill, D.W., and Waldor, M.K. (2023). Genetic and immune determinants of E. coli liver abscess formation. BioRxiv Prepr. Serv. Biol., 2023.06.11.543319. 10.1101/2023.06.11.543319.

28. Woodward, S.E., Vogt, S.L., Peña-Díaz, J., Melnyk, R.A., Cirstea, M., Serapio-Palacios, A., Neufeld, L.M.P., Huus, K.E., Wang, M.A., Haney, C.H., et al. (2023). Gastric acid and escape to systemic circulation represent major bottlenecks to host infection by Citrobacter rodentium. ISME J. *17*, 36–46. 10.1038/s41396-022-01321-9.

29. Louie, A., Zhang, T., Becattini, S., Waldor, M.K., and Portnoy, D.A. (2019). A Multiorgan Trafficking Circuit Provides Purifying Selection of Listeria monocytogenes Virulence Genes. mBio *10*, e02948-19. 10.1128/mBio.02948-19.

30. CDC (2023). Frequently Asked Questions about Listeria. Cent. Dis. Control Prev. https://www.cdc.gov/listeria/faq.html.

31. Medicine, C. for V. (2023). Get the Facts about Listeria. FDA.

32. Tilney, L.G., and Portnoy, D.A. (1989). Actin filaments and the growth, movement, and spread of the intracellular bacterial parasite, Listeria monocytogenes. J. Cell Biol. *109*, 1597–1608. 10.1083/jcb.109.4.1597.

33. Welch, M.D., Iwamatsu, A., and Mitchison, T.J. (1997). Actin polymerization is induced by Arp2/3 protein complex at the surface of Listeria monocytogenes. Nature *385*, 265–269. 10.1038/385265a0.

34. Meningitis https://www.who.int/news-room/fact-sheets/detail/meningitis.

35. Cain, M.D., Salimi, H., Diamond, M.S., and Klein, R.S. (2019). Mechanisms of Pathogen Invasion into the Central Nervous System. Neuron *103*, 771–783. 10.1016/j.neuron.2019.07.015.

36. Join-Lambert, O.F., Ezine, S., Le Monnier, A., Jaubert, F., Okabe, M., Berche, P., and Kayal, S. (2005). Listeria monocytogenes-infected bone marrow myeloid cells promote bacterial invasion of the central nervous system. Cell. Microbiol. *7*, 167–180. 10.1111/j.1462-5822.2004.00444.x.

37. Drevets, D.A., Jelinek, T.A., and Freitag, N.E. (2001). Listeria monocytogenes-Infected Phagocytes Can Initiate Central Nervous System Infection in Mice. Infect. Immun. *69*, 1344–1350. 10.1128/IAI.69.3.1344-1350.2001.

38. Drevets, D.A., Dillon, M.J., Schawang, J.S., van Rooijen, N., Ehrchen, J., Sunderkötter, C., and Leenen, P.J.M. (2004). The Ly-6Chigh Monocyte Subpopulation Transports Listeria monocytogenes into the Brain during Systemic Infection of Mice1. J. Immunol. *172*, 4418–4424. 10.4049/jimmunol.172.7.4418.

39. Maudet, C., Kheloufi, M., Levallois, S., Gaillard, J., Huang, L., Gaultier, C., Tsai, Y.-H., Disson, O., and Lecuit, M. (2022). Bacterial inhibition of Fas-mediated killing promotes neuroinvasion and persistence. Nature *603*, 900–906. 10.1038/s41586-022-04505-7.

40. Dramsi, S., Lévi, S., Triller, A., and Cossart, P. (1998). Entry of Listeria monocytogenes into neurons occurs by cell-to-cell spread: an in vitro study. Infect. Immun. *66*, 4461–4468. 10.1128/IAI.66.9.4461-4468.1998.

41. Henke, D., Rupp, S., Gaschen, V., Stoffel, M.H., Frey, J., Vandevelde, M., and Oevermann, A. (2015). Listeria monocytogenes Spreads within the Brain by Actin-Based Intra-Axonal Migration. Infect. Immun. *83*, 2409–2419. 10.1128/IAI.00316-15.

42. Pägelow, D., Chhatbar, C., Beineke, A., Liu, X., Nerlich, A., van Vorst, K., Rohde, M., Kalinke, U., Förster, R., Halle, S., et al. (2018). The olfactory epithelium as a port of entry in neonatal neurolisteriosis. Nat. Commun. *9*, 4269. 10.1038/s41467-018-06668-2.

43. CDC (2022). Prevent Listeria Infections. Cent. Dis. Control Prev. https://www.cdc.gov/listeria/risk-groups/pregnant-women.html.

44. Listeriosis https://www.who.int/news-room/fact-sheets/detail/listeriosis.

45. Vigliani, M.B., and Bakardjiev, A.I. (2013). First Trimester Typhoid Fever with Vertical Transmission of Salmonella Typhi, an Intracellular Organism. Case Rep. Med. *2013*, 973297. 10.1155/2013/973297.

46. Vázquez-Boland, J.A., Krypotou, E., and Scortti, M. (2017). Listeria Placental Infection. mBio *8*, e00949-17. 10.1128/mBio.00949-17.

47. Lamond, N.M., and Freitag, N.E. (2018). Vertical Transmission of Listeria monocytogenes: Probing the Balance between Protection from Pathogens and Fetal Tolerance. Pathog. Basel Switz. *7*, 52. 10.3390/pathogens7020052.

48. Lecuit, M., Nelson, D.M., Smith, S.D., Khun, H., Huerre, M., Vacher-Lavenu, M.-C., Gordon, J.I., and Cossart, P. (2004). Targeting and crossing of the human maternofetal barrier by Listeria monocytogenes: role of internalin interaction with trophoblast E-cadherin. Proc. Natl. Acad. Sci. U. S. A. *101*, 6152–6157. 10.1073/pnas.0401434101.

49. Bakardjiev, A.I., Stacy, B.A., Fisher, S.J., and Portnoy, D.A. (2004). Listeriosis in the pregnant guinea pig: a model of vertical transmission. Infect. Immun. *72*, 489–497. 10.1128/IAI.72.1.489-497.2004.

50. Faralla, C., Rizzuto, G.A., Lowe, D.E., Kim, B., Cooke, C., Shiow, L.R., and Bakardjiev, A.I. (2016). InlP, a New Virulence Factor with Strong Placental Tropism. Infect. Immun. *84*, 3584–3596. 10.1128/IAI.00625-16.

51. Le Monnier, A., Autret, N., Join-Lambert, O.F., Jaubert, F., Charbit, A., Berche, P., and Kayal, S. (2007). ActA is required for crossing of the fetoplacental barrier by Listeria monocytogenes. Infect. Immun. *75*, 950–957. 10.1128/IAI.01570-06.

52. Bakardjiev, A.I., Stacy, B.A., and Portnoy, D.A. (2005). Growth of Listeria monocytogenes in the guinea pig placenta and role of cell-to-cell spread in fetal infection. J. Infect. Dis. *191*, 1889–1897. 10.1086/430090.

53. Rowe, J.H., Ertelt, J.M., Xin, L., and Way, S.S. (2012). Listeria monocytogenes cytoplasmic entry induces fetal wastage by disrupting maternal Foxp3+ regulatory T cell-sustained fetal tolerance. PLoS Pathog. *8*, e1002873. 10.1371/journal.ppat.1002873.

54. Erlebacher, A. (2013). Immunology of the maternal-fetal interface. Annu. Rev. Immunol. *31*, 387–411. 10.1146/annurev-immunol-032712-100003.

55. Mor, G., and Cardenas, I. (2010). The immune system in pregnancy: a unique complexity. Am. J. Reprod. Immunol. N. Y. N 1989 *63*, 425–433. 10.1111/j.1600-0897.2010.00836.x.

56. Rowe, J.H., Ertelt, J.M., Aguilera, M.N., Farrar, M.A., and Way, S.S. (2011). Foxp3(+) regulatory T cell expansion required for sustaining pregnancy compromises host defense against prenatal bacterial pathogens. Cell Host Microbe *10*, 54–64. 10.1016/j.chom.2011.06.005.

57. Zenewicz, L.A., and Shen, H. (2007). Innate and adaptive immune responses to Listeria monocytogenes: a short overview. Microbes Infect. *9*, 1208–1215. 10.1016/j.micinf.2007.05.008.

58. D'Orazio, S.E.F. (2019). Innate and Adaptive Immune Responses during Listeria monocytogenes Infection. Microbiol. Spectr. *7*, 10.1128/microbiolspec.gpp3-0065–2019. 10.1128/microbiolspec.gpp3-0065-2019.

59. Pamer, E.G. (2004). Immune responses to Listeria monocytogenes. Nat. Rev. Immunol. *4*, 812–823. 10.1038/nri1461.

60. Sauer, J.-D., Sotelo-Troha, K., von Moltke, J., Monroe, K.M., Rae, C.S., Brubaker, S.W., Hyodo, M., Hayakawa, Y., Woodward, J.J., Portnoy, D.A., et al. (2011). The N-ethyl-N-nitrosourea-induced Goldenticket mouse mutant reveals an essential function of Sting in the in vivo interferon response to Listeria monocytogenes and cyclic dinucleotides. Infect. Immun. *79*, 688–694. 10.1128/IAI.00999-10.

61. Louie, A., Bhandula, V., and Portnoy, D.A. (2020). Secretion of c-di-AMP by Listeria monocytogenes Leads to a STING-Dependent Antibacterial Response during Enterocolitis. Infect. Immun. *88*, e00407-20. 10.1128/IAI.00407-20.

62. Patel, S., and Jin, L. (2019). TMEM173 variants and potential importance to human biology and disease. Genes Immun. *20*, 82–89. 10.1038/s41435-018-0029-9.

63. Ding, Y.-D., Shu, L.-Z., He, R.-S., Chen, K.-Y., Deng, Y.-J., Zhou, Z.-B., Xiong, Y., and Deng, H. (2023). Listeria monocytogenes: a promising vector for tumor immunotherapy. Front. Immunol. *14*, 1278011. 10.3389/fimmu.2023.1278011.

64. Fu, A., Yao, B., Dong, T., Chen, Y., Yao, J., Liu, Y., Li, H., Bai, H., Liu, X., Zhang, Y., et al. (2022). Tumor-resident intracellular microbiota promotes metastatic colonization in breast cancer. Cell *185*, 1356-1372.e26. 10.1016/j.cell.2022.02.027.

65. Riquelme, E., Zhang, Y., Zhang, L., Montiel, M., Zoltan, M., Dong, W., Quesada, P., Sahin, I., Chandra, V., San Lucas, A., et al. (2019). Tumor Microbiome Diversity and Composition Influence Pancreatic Cancer Outcomes. Cell *178*, 795-806.e12. 10.1016/j.cell.2019.07.008.

66. Pushalkar, S., Hundeyin, M., Daley, D., Zambirinis, C.P., Kurz, E., Mishra, A., Mohan, N., Aykut, B., Usyk, M., Torres, L.E., et al. (2018). The Pancreatic Cancer Microbiome Promotes Oncogenesis by Induction of Innate and Adaptive Immune Suppression. Cancer Discov. *8*, 403–416. 10.1158/2159-8290.CD-17-1134.

67. Poore, G.D., Kopylova, E., Zhu, Q., Carpenter, C., Fraraccio, S., Wandro, S., Kosciolek, T., Janssen, S., Metcalf, J., Song, S.J., et al. (2020). Microbiome analyses of blood and tissues suggest cancer diagnostic approach. Nature *579*, 567–574. 10.1038/s41586-020-2095-1.

68. Dang, L.H., Bettegowda, C., Huso, D.L., Kinzler, K.W., and Vogelstein, B. (2001). Combination bacteriolytic therapy for the treatment of experimental tumors. Proc. Natl. Acad. Sci. U. S. A. *98*, 15155–15160. 10.1073/pnas.251543698.

69. Zhou, M., Tang, Y., Xu, W., Hao, X., Li, Y., Huang, S., Xiang, D., and Wu, J. (2023). Bacteria-based immunotherapy for cancer: a systematic review of preclinical studies. Front. Immunol. *14*, 1140463. 10.3389/fimmu.2023.1140463.

70. Hassan, R., Alley, E., Kindler, H., Antonia, S., Jahan, T., Honarmand, S., Nair, N., Whiting, C.C., Enstrom, A., Lemmens, E., et al. (2019). Clinical Response of Live-Attenuated, Listeria monocytogenes Expressing Mesothelin (CRS-207) with Chemotherapy in Patients with

Malignant Pleural Mesothelioma. Clin. Cancer Res. Off. J. Am. Assoc. Cancer Res. *25*, 5787–5798. 10.1158/1078-0432.CCR-19-0070.

71. Huh, W.K., Brady, W.E., Fracasso, P.M., Dizon, D.S., Powell, M.A., Monk, B.J., Leath, C.A., Landrum, L.M., Tanner, E.J., Crane, E.K., et al. (2020). Phase II study of axalimogene filolisbac (ADXS-HPV) for platinum-refractory cervical carcinoma: An NRG oncology/gynecologic oncology group study. Gynecol. Oncol. *158*, 562–569. 10.1016/j.ygyno.2020.06.493.

72. Drake, C.G., Pachynski, R.K., Subudhi, S.K., McNeel, D.G., Antonarakis, E.S., Bauer, T.M., Lauer, P., Brockstedt, D., Patricia, D., Wade, M., et al. (2022). Safety and preliminary immunogenicity of JNJ-64041809, a live-attenuated, double-deleted Listeria monocytogenes-based immunotherapy, in metastatic castration-resistant prostate cancer. Prostate Cancer Prostatic Dis. *25*, 219–228. 10.1038/s41391-021-00402-8.

73. Stein, M.N., Fong, L., Tutrone, R., Mega, A., Lam, E.T., Parsi, M., Vangala, S., Gutierrez, A.A., and Haas, N.B. (2022). ADXS31142 Immunotherapy ± Pembrolizumab Treatment for Metastatic Castration-Resistant Prostate Cancer: Open-Label Phase I/II KEYNOTE-046 Study. The Oncologist *27*, 453–461. 10.1093/oncolo/oyac048.

74. Castillo, J.G., Fernandez, S., Campbell, T., Williams, J., Gonzalez-Ventura, D., Ybarra, J., Hernandez, N.F., Wells, E., Portnoy, D.A., and DuPage, M. (2024). Cellular mechanisms underlying beneficial versus detrimental effects of bacterial antitumor immunotherapy. Preprint, 10.1101/2024.02.15.580555 10.1101/2024.02.15.580555.

75. Meningitis - Symptoms and causes Mayo Clin. https://www.mayoclinic.org/diseases-conditions/meningitis/symptoms-causes/syc-20350508.

76. Ghosh, P., Halvorsen, E.M., Ammendolia, D.A., Mor-Vaknin, N., O'Riordan, M.X.D., Brumell, J.H., Markovitz, D.M., and Higgins, D.E. (2018). Invasion of the Brain by Listeria monocytogenes Is Mediated by InlF and Host Cell Vimentin. mBio *9*, e00160-18. 10.1128/mBio.00160-18.

77. Antal, E.-A., Løberg, E.M., Bracht, P., Melby, K.K., and Mæhlen, J. (2001). Evidence for Intraaxonal Spread of Listeria Monocytogenes from the Periphery to the Central Nervous System. Brain Pathol. *11*, 432–438. 10.1111/j.1750-3639.2001.tb00411.x.

78. Otter, A., and Blakemore, W.F. (1989). Observation on the presence of Listeria monocytogenes in axons. Acta Microbiol. Hung. *36*, 125–131.

79. Dons, L., Jin, Y., Kristensson, K., and Rottenberg, M.E. (2007). Axonal transport of Listeria monocytogenes and nerve-cell-induced bacterial killing. J. Neurosci. Res. *85*, 2529–2537. 10.1002/jnr.21256.

80. Gilman, J., Walls, L., Bandiera, L., and Menolascina, F. (2021). Statistical Design of Experiments for Synthetic Biology. ACS Synth. Biol. *10*, 1–18. 10.1021/acssynbio.0c00385.

81. Hullahalli, K., Dailey, K.G., and Waldor, M.K. (2023). Innate immune responses yield tissue-specific bottlenecks that scale with pathogen dose. BioRxiv Prepr. Serv. Biol., 2023.06.09.543079. 10.1101/2023.06.09.543079.

82. Wincott, C.J., Sritharan, G., Benns, H.J., May, D., Gilabert-Carbajo, C., Bunyan, M., Fairweather, A.R., Alves, E., Andrew, I., Game, L., et al. (2022). Cellular barcoding of protozoan pathogens reveals the within-host population dynamics of Toxoplasma gondii host colonization. Cell Rep. Methods *2*, 100274. 10.1016/j.crmeth.2022.100274.

83. Zhang, T., Sasabe, J., Hullahalli, K., Sit, B., and Waldor, M.K. (2021). Increased Listeria monocytogenes Dissemination and Altered Population Dynamics in Muc2-Deficient Mice. Infect. Immun. *89*, e00667-20. 10.1128/IAI.00667-20.

84. Gaillard, J.L., Berche, P., and Sansonetti, P. (1986). Transposon mutagenesis as a tool to study the role of hemolysin in the virulence of Listeria monocytogenes. Infect. Immun. *52*, 50–55. 10.1128/iai.52.1.50-55.1986.

85. Bou Ghanem, E.N., Myers-Morales, T., and D'Orazio, S.E.F. (2013). A mouse model of foodborne Listeria monocytogenes infection. Curr. Protoc. Microbiol. *31*, 9B.3.1-9B.3.16. 10.1002/9780471729259.mc09b03s31.

86. Rebhun, W.C. (1987). Listeriosis. Vet. Clin. North Am. Food Anim. Pract. *3*, 75–83. 10.1016/S0749-0720(15)31180-4.

87. March, P.A. (2006). Diseases of the Brain and Cranial Nerves. Saunders Man. Small Anim. Pract., 1249–1276. 10.1016/B0-72-160422-6/50128-5.

88. Cugurra, A., Mamuladze, T., Rustenhoven, J., Dykstra, T., Beroshvili, G., Greenberg, Z.J., Baker, W., Papadopoulos, Z., Drieu, A., Blackburn, S., et al. (2021). Skull and vertebral bone marrow are myeloid cell reservoirs for the meninges and CNS parenchyma. Science *373*, eabf7844. 10.1126/science.abf7844.

89. Lai, N.Y., Mills, K., and Chiu, I.M. (2017). Sensory neuron regulation of gastrointestinal inflammation and bacterial host defence. J. Intern. Med. *282*, 5–23. 10.1111/joim.12591.

90. Debray, R., Herbert, R.A., Jaffe, A.L., Crits-Christoph, A., Power, M.E., and Koskella, B. (2022). Priority effects in microbiome assembly. Nat. Rev. Microbiol. *20*, 109–121. 10.1038/s41579-021-00604-w.

91. Sprockett, D., Fukami, T., and Relman, D.A. (2018). Role of priority effects in the early-life assembly of the gut microbiota. Nat. Rev. Gastroenterol. Hepatol. *15*, 197–205. 10.1038/nrgastro.2017.173.

92. Lee, S.M., Donaldson, G.P., Mikulski, Z., Boyajian, S., Ley, K., and Mazmanian, S.K. (2013). Bacterial colonization factors control specificity and stability of the gut microbiota. Nature *501*, 426–429. 10.1038/nature12447.

93. Senay, T.E., Ferrell, J.L., Garrett, F.G., Albrecht, T.M., Cho, J., Alexander, K.L., Myers-Morales, T., Grothaus, O.F., and D'Orazio, S.E.F. (2020). Neurotropic Lineage III Strains of Listeria monocytogenes Disseminate to the Brain without Reaching High Titer in the Blood. mSphere *5*, e00871-20. 10.1128/mSphere.00871-20.

94. Bou Ghanem, E.N., Jones, G.S., Myers-Morales, T., Patil, P.D., Hidayatullah, A.N., and D'Orazio, S.E.F. (2012). InlA promotes dissemination of Listeria monocytogenes to the mesenteric lymph nodes during food borne infection of mice. PLoS Pathog. *8*, e1003015. 10.1371/journal.ppat.1003015.

95. Taur, Y., and Pamer, E.G. (2013). The Intestinal Microbiota and Susceptibility to Infection in Immunocompromised Patients. Curr. Opin. Infect. Dis. *26*, 332–337. 10.1097/QCO.0b013e3283630dd3.

96. Harty, J.T., and Bevan, M.J. (1999). Responses of CD8+ T cells to intracellular bacteria. Curr. Opin. Immunol. *11*, 89–93. 10.1016/S0952-7915(99)80016-8.

97. Lara-Tejero, M., and Pamer, E.G. (2004). T cell responses to Listeria monocytogenes. Curr. Opin. Microbiol. *7*, 45–50. 10.1016/j.mib.2003.12.002.

98. Bancroft, G.J., Bosma, M.J., Bosma, G.C., and Unanue, E.R. (1986). Regulation of macrophage Ia expression in mice with severe combined immunodeficiency: induction of Ia expression by a T cell-independent mechanism. J. Immunol. *137*, 4–9. 10.4049/jimmunol.137.1.4.

99. Guide for the Care and Use of Laboratory Animals: Eighth Edition | The National Academies Press https://nap.nationalacademies.org/catalog/12910/guide-for-the-care-and-use-of-laboratory-animals-eighth.

100. Bécavin, C., Bouchier, C., Lechat, P., Archambaud, C., Creno, S., Gouin, E., Wu, Z., Kühbacher, A., Brisse, S., Pucciarelli, M.G., et al. (2014). Comparison of widely used Listeria monocytogenes strains EGD, 10403S, and EGD-e highlights genomic variations underlying differences in pathogenicity. mBio *5*, e00969-00914. 10.1128/mBio.00969-14.

101. Rae, C.S., Geissler, A., Adamson, P.C., and Portnoy, D.A. (2011). Mutations of the Listeria monocytogenes Peptidoglycan N-Deacetylase and O-Acetylase Result in Enhanced Lysozyme Sensitivity, Bacteriolysis, and Hyperinduction of Innate Immune Pathways. Infect. Immun. *79*, 3596–3606. 10.1128/iai.00077-11.

102. Stahl, E.C., Sabo, J.K., Kang, M.H., Allen, R., Applegate, E., Kim, S.E., Kwon, Y., Seth, A., Lemus, N., Salinas-Rios, V., et al. (2023). Genome editing in the mouse brain with minimally immunogenic Cas9 RNPs. Mol. Ther. *31*, 2422–2438. 10.1016/j.ymthe.2023.06.019.

103. Cavalli-Sforza, L.L., and Edwards, A.W.F. (1967). Phylogenetic analysis. Models and estimation procedures. Am. J. Hum. Genet. *19*, 233–257.

104. Fay, K.T., Klingensmith, N.J., Chen, C.-W., Zhang, W., Sun, Y., Morrow, K.N., Liang, Z., Burd, E.M., Ford, M.L., and Coopersmith, C.M. (2019). The gut microbiome alters immunophenotype and survival from sepsis. FASEB J. *33*, 11258–11269. 10.1096/fj.201802188R.

105. Villarino, N.F., LeCleir, G.R., Denny, J.E., Dearth, S.P., Harding, C.L., Sloan, S.S., Gribble, J.L., Campagna, S.R., Wilhelm, S.W., and Schmidt, N.W. (2016). Composition of the gut microbiota modulates the severity of malaria. Proc. Natl. Acad. Sci. *113*, 2235–2240. 10.1073/pnas.1504887113.

106. Stough, J.M.A., Dearth, S.P., Denny, J.E., LeCleir, G.R., Schmidt, N.W., Campagna, S.R., and Wilhelm, S.W. (2016). Functional Characteristics of the Gut Microbiome in C57BL/6 Mice Differentially Susceptible to Plasmodium yoelii. Front. Microbiol. *7*, 1520. 10.3389/fmicb.2016.01520.

107. Al Nabhani, Z., and Eberl, G. (2020). Imprinting of the immune system by the microbiota early in life. Mucosal Immunol. *13*, 183–189. 10.1038/s41385-020-0257-y.

108. Robertson, S.J., Lemire, P., Maughan, H., Goethel, A., Turpin, W., Bedrani, L., Guttman, D.S., Croitoru, K., Girardin, S.E., and Philpott, D.J. (2019). Comparison of Co-housing and Littermate Methods for Microbiota Standardization in Mouse Models. Cell Rep. *27*, 1910-1919.e2. 10.1016/j.celrep.2019.04.023.

109. Chevée, V., Hullahalli, K., Dailey, K.G., Güereca, L., Zhang, C., Waldor, M.K., and Portnoy, D.A. (2024). Temporal and spatial dynamics of Listeria monocytogenes central nervous system infection in mice. Proc. Natl. Acad. Sci. U. S. A. *121*, e2320311121. 10.1073/pnas.2320311121.

110. Dunham, N.W., and Miya, T.S. (1957). A note on a simple apparatus for detecting neurological deficit in rats and mice. J. Am. Pharm. Assoc. Am. Pharm. Assoc. *46*, 208–209. 10.1002/jps.3030460322.

111. Deacon, R.M.J. (2013). Measuring Motor Coordination in Mice. J. Vis. Exp. JoVE, 2609. 10.3791/2609.

112. Ireland, D.D.C., Manangeeswaran, M., Lewkowicz, A.P., Engel, K., Clark, S.M., Laniyan, A., Sykes, J., Lee, H.-N., McWilliams, I.L., Kelley-Baker, L., et al. (2020). Long-term persistence of infectious Zika virus: Inflammation and behavioral sequela in mice. PLOS Pathog. *16*, e1008689. 10.1371/journal.ppat.1008689.

113. Firouzeh, N., Ziaali, N., Sheibani, V., Doustimotlagh, A.H., Afgar, A., Zamanpour, M., Keshavarz, H., Shojaee, S., Shafiei, R., Esmaeilpour, K., et al. (2021). Chronic Toxoplasma gondii Infection Potentiates Parkinson's Disease Course in Mice Model. Iran. J. Parasitol. *16*, 527–537. 10.18502/ijpa.v16i4.7863.

114. Lee, S.H., Jung, B.-K., Song, H., Seo, H.G., Chai, J.-Y., and Oh, B.-M. (2020). Neuroprotective Effect of Chronic Intracranial Toxoplasma gondii Infection in a Mouse Cerebral Ischemia Model. Korean J. Parasitol. *58*, 461–466. 10.3347/kjp.2020.58.4.461.

115. Bellantuono, I., de Cabo, R., Ehninger, D., Di Germanio, C., Lawrie, A., Miller, J., Mitchell, S., Navas-Enamorado, I., Potter, P., Tchkonia, T., et al. (2020). A toolbox for the longitudinal assessment of healthspan in ageing mice. Nat. Protoc. *15*, 540–574. 10.1038/s41596-019-0256-1.

116. Kawai, T., and Akira, S. (2010). The role of pattern-recognition receptors in innate immunity: update on Toll-like receptors. Nat. Immunol. *11*, 373–384. 10.1038/ni.1863.

117. Burdette, D.L., Monroe, K.M., Sotelo-Troha, K., Iwig, J.S., Eckert, B., Hyodo, M., Hayakawa, Y., and Vance, R.E. (2011). STING is a direct innate immune sensor of cyclic di-GMP. Nature *478*, 515–518. 10.1038/nature10429.

118. Barker, J.R., Koestler, B.J., Carpenter, V.K., Burdette, D.L., Waters, C.M., Vance, R.E., and Valdivia, R.H. (2013). STING-dependent recognition of cyclic di-AMP mediates type I interferon responses during Chlamydia trachomatis infection. mBio *4*, e00018-00013. 10.1128/mBio.00018-13.

119. Watson, R.O., Bell, S.L., MacDuff, D.A., Kimmey, J.M., Diner, E.J., Olivas, J., Vance, R.E., Stallings, C.L., Virgin, H.W., and Cox, J.S. (2015). The Cytosolic Sensor cGAS Detects Mycobacterium tuberculosis DNA to Induce Type I Interferons and Activate Autophagy. Cell Host Microbe *17*, 811–819. 10.1016/j.chom.2015.05.004.

120. Auerbuch, V., Brockstedt, D.G., Meyer-Morse, N., O'Riordan, M., and Portnoy, D.A. (2004). Mice Lacking the Type I Interferon Receptor Are Resistant to Listeria monocytogenes. J. Exp. Med. *200*, 527–533. 10.1084/jem.20040976.

121. Carrero, J.A., Calderon, B., and Unanue, E.R. (2004). Type I Interferon Sensitizes Lymphocytes to Apoptosis and Reduces Resistance to Listeria Infection. J. Exp. Med. *200*, 535–540. 10.1084/jem.20040769.

122. O'Connell, R.M., Saha, S.K., Vaidya, S.A., Bruhn, K.W., Miranda, G.A., Zarnegar, B., Perry, A.K., Nguyen, B.O., Lane, T.F., Taniguchi, T., et al. (2004). Type I Interferon Production Enhances Susceptibility to Listeria monocytogenes Infection. J. Exp. Med. *200*, 437–445. 10.1084/jem.20040712.

123. Abe, T., and Barber, G.N. (2014). Cytosolic-DNA-Mediated, STING-Dependent Proinflammatory Gene Induction Necessitates Canonical NF-κB Activation through TBK1. J. Virol. *88*, 5328–5341. 10.1128/jvi.00037-14.

124. Gui, X., Yang, H., Li, T., Tan, X., Shi, P., Li, M., Du, F., and Chen, Z.J. (2019). Autophagy induction via STING trafficking is a primordial function of the cGAS pathway. Nature *567*, 262–266. 10.1038/s41586-019-1006-9.

125. Chen, H., Sun, H., You, F., Sun, W., Zhou, X., Chen, L., Yang, J., Wang, Y., Tang, H., Guan, Y., et al. (2011). Activation of STAT6 by STING Is Critical for Antiviral Innate Immunity. Cell *147*, 436–446. 10.1016/j.cell.2011.09.022.

126. Jia, T., Serbina, N.V., Brandl, K., Zhong, M.X., Leiner, I.M., Charo, I.F., and Pamer, E.G. (2008). Additive roles for MCP-1 and MCP-3 in CCR2-mediated recruitment of inflammatory monocytes during Listeria monocytogenes infection. J. Immunol. Baltim. Md 1950 *180*, 6846–6853. 10.4049/jimmunol.180.10.6846.

127. Serbina, N.V., and Pamer, E.G. (2006). Monocyte emigration from bone marrow during bacterial infection requires signals mediated by chemokine receptor CCR2. Nat. Immunol. *7*, 311–317. 10.1038/ni1309.

128. Jones, G.S., and D'Orazio, S.E.F. (2017). Monocytes Are the Predominant Cell Type Associated with Listeria monocytogenes in the Gut, but They Do Not Serve as an Intracellular Growth Niche. J. Immunol. *198*, 2796–2804. 10.4049/jimmunol.1602076.

129. Bakardjiev, A.I., Stacy, B.A., and Portnoy, D.A. (2005). Growth of Listeria monocytogenes in the Guinea Pig Placenta and Role of Cell-to-Cell Spread in Fetal Infection. J. Infect. Dis. *191*, 1889–1897. 10.1086/430090.

130. Burdette, D.L., and Vance, R.E. (2013). STING and the innate immune response to nucleic acids in the cytosol. Nat. Immunol. *14*, 19–26. 10.1038/ni.2491.

131. Jin, L., Getahun, A., Knowles, H.M., Mogan, J., Akerlund, L.J., Packard, T.A., Perraud, A.-L., and Cambier, J.C. (2013). STING/MPYS mediates host defense against Listeria monocytogenes infection by regulating Ly6C(hi) monocyte migration. J. Immunol. Baltim. Md 1950 *190*, 2835–2843. 10.4049/jimmunol.1201788.

132. Pitts, M.G., Myers-Morales, T., and D'Orazio, S.E.F. (2016). Type I interferon does not promote susceptibility to foodborne Listeria monocytogenes. J. Immunol. Baltim. Md 1950 *196*, 3109–3116. 10.4049/jimmunol.1502192.

133. Yamashiro, L.H., Wilson, S.C., Morrison, H.M., Karalis, V., Chung, J.-Y.J., Chen, K.J., Bateup, H.S., Szpara, M.L., Lee, A.Y., Cox, J.S., et al. (2020). Interferon-independent STING signaling promotes resistance to HSV-1 in vivo. Nat. Commun. *11*, 3382. 10.1038/s41467-020-17156-x.

134. Margolis, S.R., Wilson, S.C., and Vance, R.E. (2017). Evolutionary Origins of cGAS-STING Signaling. Trends Immunol. *38*, 733–743. 10.1016/j.it.2017.03.004.

135. Motwani, M., Pesiridis, S., and Fitzgerald, K.A. (2019). DNA sensing by the cGAS-STING pathway in health and disease. Nat. Rev. Genet. *20*, 657–674. 10.1038/s41576-019-0151-1.

136. Chevée, V., Hullahalli, K., Dailey, K.G., Güereca, L., Zhang, C., Waldor, M.K., and Portnoy, D.A. (2024). Temporal and spatial dynamics of Listeria monocytogenes central nervous

system infection in mice. Proc. Natl. Acad. Sci. *121*, e2320311121. 10.1073/pnas.2320311121.

137. Carter, A.M. (2007). Animal Models of Human Placentation – A Review. Placenta *28*, S41–S47. 10.1016/j.placenta.2006.11.002.

138. de Rijk, E.P.C.T., and Van Esch, E. (2008). The Macaque Placenta—A Mini-Review. Toxicol. Pathol. *36*, 108S-118S. 10.1177/0192623308326095.

139. McCarthy, E.F. (2006). The Toxins of William B. Coley and the Treatment of Bone and Soft-Tissue Sarcomas. Iowa Orthop. J. *26*, 154–158.

140. Kaufmann, S.H.E. (2019). Immunology's Coming of Age. Front. Immunol. *10*, 684. 10.3389/fimmu.2019.00684.

141. Jiang, S., and Redelman-Sidi, G. (2022). BCG in Bladder Cancer Immunotherapy. Cancers *14*, 3073. 10.3390/cancers14133073.

142. Chávez-Arroyo, A., and Portnoy, D.A. (2020). Why is Listeria monocytogenes such a potent inducer of CD8+ T-cells? Cell. Microbiol. *22*, e13175. 10.1111/cmi.13175.

143. Deng, W., Lira, V., Hudson, T.E., Lemmens, E.E., Hanson, W.G., Flores, R., Barajas, G., Katibah, G.E., Desbien, A.L., Lauer, P., et al. (2018). Recombinant Listeria promotes tumor rejection by CD8+ T cell-dependent remodeling of the tumor microenvironment. Proc. Natl. Acad. Sci. *115*, 8179–8184. 10.1073/pnas.1801910115.

144. Kim, S.H., Castro, F., Gonzalez, D., Maciag, P.C., Paterson, Y., and Gravekamp, C. (2008). Mage-b vaccine delivered by recombinant Listeria monocytogenes is highly effective against breast cancer metastases. Br. J. Cancer *99*, 741–749. 10.1038/sj.bjc.6604526.

145. Bruhn, K.W., Craft, N., and Miller, J.F. (2007). Listeria as a vaccine vector. Microbes Infect. *9*, 1226–1235. 10.1016/j.micinf.2007.05.010.

146. Pan, Z.K., Ikonomidis, G., Lazenby, A., Pardoll, D., and Paterson, Y. (1995). A recombinant Listeria monocytogenes vaccine expressing a model tumour antigen protects mice against lethal tumour cell challenge and causes regression of established tumours. Nat. Med. *1*, 471–477. 10.1038/nm0595-471.

147. Nguyen, D.-H., Chong, A., Hong, Y., and Min, J.-J. (2023). Bioengineering of bacteria for cancer immunotherapy. Nat. Commun. *14*, 3553. 10.1038/s41467-023-39224-8.

148. Le, D.T., Wang-Gillam, A., Picozzi, V., Greten, T.F., Crocenzi, T., Springett, G., Morse, M., Zeh, H., Cohen, D., Fine, R.L., et al. (2015). Safety and survival with GVAX pancreas prime and Listeria Monocytogenes-expressing mesothelin (CRS-207) boost vaccines for metastatic pancreatic cancer. J. Clin. Oncol. Off. J. Am. Soc. Clin. Oncol. *33*, 1325–1333. 10.1200/JCO.2014.57.4244.

149. Basu, P., Mehta, A., Jain, M., Gupta, S., Nagarkar, R.V., John, S., and Petit, R. (2018). A Randomized Phase 2 Study of ADXS11-001 Listeria monocytogenes-Listeriolysin O Immunotherapy With or Without Cisplatin in Treatment of Advanced Cervical Cancer. Int. J. Gynecol. Cancer Off. J. Int. Gynecol. Cancer Soc. *28*, 764–772. 10.1097/IGC.0000000000001235.

150. Binnewies, M., Roberts, E.W., Kersten, K., Chan, V., Fearon, D.F., Merad, M., Coussens, L.M., Gabrilovich, D.I., Ostrand-Rosenberg, S., Hedrick, C.C., et al. (2018). Understanding the tumor immune microenvironment (TIME) for effective therapy. Nat. Med. *24*, 541–550. 10.1038/s41591-018-0014-x.

151. Perry, C.J., Muñoz-Rojas, A.R., Meeth, K.M., Kellman, L.N., Amezquita, R.A., Thakral, D., Du, V.Y., Wang, J.X., Damsky, W., Kuhlmann, A.L., et al. (2018). Myeloid-targeted immunotherapies act in synergy to induce inflammation and antitumor immunity. J. Exp. Med. *215*, 877–893. 10.1084/jem.20171435.

152. Janssen, B., Debets, J., Leenders, P., and Smits, J. (2002). Chronic measurement of cardiac output in conscious mice. Am. J. Physiol.-Regul. Integr. Comp. Physiol. *282*, R928–R935. 10.1152/ajpregu.00406.2001.

153. Forster, J.C., Harriss-Phillips, W.M., Douglass, M.J., and Bezak, E. (2017). A review of the development of tumor vasculature and its effects on the tumor microenvironment. Hypoxia *5*, 21–32. 10.2147/HP.S133231.

154. Lauer, P., Chow, M.Y.N., Loessner, M.J., Portnoy, D.A., and Calendar, R. (2002). Construction, characterization, and use of two Listeria monocytogenes site-specific phage integration vectors. J. Bacteriol. *184*, 4177–4186. 10.1128/JB.184.15.4177-4186.2002.

155. Jones, S., and Portnoy, D.A. (1994). Characterization of Listeria monocytogenes pathogenesis in a strain expressing perfringolysin O in place of listeriolysin O. Infect. Immun. *62*, 5608–5613. 10.1128/iai.62.12.5608-5613.1994.

156. Juliano, S.A. (2007). Population Dynamics. J. Am. Mosq. Control Assoc. *23*, 265–275.

157. Brockstedt, D.G., Giedlin, M.A., Leong, M.L., Bahjat, K.S., Gao, Y., Luckett, W., Liu, W., Cook, D.N., Portnoy, D.A., and Dubensky, T.W. (2004). Listeria-based cancer vaccines that segregate immunogenicity from toxicity. Proc. Natl. Acad. Sci. *101*, 13832–13837. 10.1073/pnas.0406035101.

158. Furness, J.B., Callaghan, B.P., Rivera, L.R., and Cho, H.-J. (2014). The Enteric Nervous System and Gastrointestinal Innervation: Integrated Local and Central Control. In Microbial Endocrinology: The Microbiota-Gut-Brain Axis in Health and Disease, M. Lyte and J. F. Cryan, eds. (Springer), pp. 39–71. 10.1007/978-1-4939-0897-4_3.